January 2009

Colloidal CdSe quantum nanowires: Synthesis, photo-induced photoluminescence enhancement and fabrication of core/shell, water-dispersible structures

Rui Tang
Washington University in St. Louis

WASHINGTON UNIVERSITY

Department of Chemistry

Dissertation Examination Committee:

William E. Buhro, Chair
Richard A. Loomis
Sophia E. Hayes
Patrick C. Gibbons
Richard Mabbs
Viktor Gruev

COLLOIDAL CADMIUM SELENIDE QUANTUM NANOWIRES: SYNTHESIS, PHOTO-INDUCED PHOTOLUMINESCENCE ENHANCEMENT, AND FABRICATION OF CORE/SHELL, WATER-DISPERSIBLE STRUCTURES

by

Rui Tang

A dissertation presented to the
Graduate School of Arts and Sciences
of Washington University in
partial fulfillment of the
requirements for the degree
of Doctor of Philosophy

August 2009

Saint Louis, Missouri

ABSTRACT OF THIS DISSERTATION

COLLOIDAL CADMIUM SELENIDE QUANTUM NANOWIRES: SYNTHESIS, PHOTO-INDUCED PHOTOLUMINESCENCE ENHANCEMENT, AND FABRICATION OF CORE/SHELL, WATER-DISPERSIBLE STRUCTURES

by

Rui Tang

Doctor of Philosophy in Chemistry

Washington University in St. Louis, 2009

Professor William E. Buhro, Chair

The goal of this project is to apply the solution-liquid-solid (SLS) mechanism developed in our group to optimize the growth of colloidal CdSe semiconductor nanowires (NWs) with rationally controlled composition, diameter, structure, and morpology. Bi nanoparticles are used to catalyze the CdSe nanowire growth in the coordinating solvent tri-*n*-octylphosphine oxide (TOPO). The availability of high quality CdSe quantum wires with both good morphology control and emission efficiency allow us to investigate the quantum-confinement effect in one dimensional (1D) semiconductor quantum structures.

High quality wurtzite CdSe quantum nanowires have been successfully synthesized with controlled diameters in the range of 5-16 nm. The best synthetic conditions are determined by varying precursors, amounts, ratios, and beneficial additives. The diameter control of the CdSe NWs is achieved by choosing different Bi nanoparticle

sizes and reaction temperatures. The size dependence of the effective bandgaps in the CdSe quantum wires are determined from the absorption spectra.

The impurities in different batches of commercial TOPO significantly influence the rates of nanocrystal formation, the nanocrystal morphologies, and the reproducibilities of CdSe nanowire syntheses. By studying the effects of the different impurities on the syntheses of the CdSe NWs, the important beneficial impurity dioctylphosphinic acid (DOPA) is proven to be critical for high quality nanowire formation. Now the use of purified TOPO with controlled amounts of specific additives will allow rational and reproducible nanocrystal syntheses.

The as-prepared CdSe quantum wires dispersed in organic solvents undergo a photo-induced photoluminescence enhancement when illuminated under fluorescent lighting. This process is investigated with different light intensities, various additives, and various solvents. The partial reversibility of the photo-enhancement effect is observed. The quantum yields of CdSe NWs are carefully calculated. The PL quantum yield of photo-enhanced NWs is improved to ~ 10% from the original 0.2%.

Type I CdSe/CdS and CdSe/ZnS core/shell nanowires are successfully fabricated via epitaxial growth. The optical properties of the core/shell structures are investigated. The PL quantum yield of the core/shell structures is enhanced to ~ 10%. Water-dispersible CdSe quantum wires, such as PEI-coated, PEG-phosphine-oxide coated and CdSe/SiO_2 core/shell structures, are also successfully synthesized. These structures will allow the applications of semiconductor quantum wires in biological systems.

ACKNOWLEDGEMENTS

Foremost, I would like to express my sincere gratitude to my advisor Prof. William E. Buhro for the continuous support of my Ph.D study and research, for his patience, motivation, enthusiasm, and immense knowledge. His guidance helped me in all the time of research and writing of this thesis. I could not have imagined having a better advisor and mentor for my Ph.D study.

I also thank the members of my dissertation committee, Professor Richard A. Loomis, Professor Sophia E. Hayes, Professor Richard Mabbs, Professor Patrick C. Gibbons, and Professor Daniel Giamar for taking time from their busy schedules to accommodate me.

Professor Loomis provided training in optical properties study and contributed to many useful and pleasant discussions. Professor Patrick C. Gibbons provided training in all aspects of electron microcopy.

I would also like to thank my friends in the Buhro group and Loomis group for their assistance. Special thanks go to Dr. Fudong Wang and Dr. John J. Glennon,

My final and very special thanks go to my wife, Yanan Duan, who always provides much moral and emotional support.

TABLE OF CONTENTS

LIST OF FIGURES

Introduction

Chapter 1

Chapter 2.

Chapter 3.

Chapter 4.

LIST OF TABLES

Introduction

This dissertation reports an optimized low-temperature solution-liquid-solid (SLS) process for synthesizing diameter-controlled single-crystalline semiconductor nanowires of CdSe (Chapter 1). By identifying and studying the effects of various impurities in commercial tri-*n*-octylphosphine oxide (TOPO), the essential beneficial impurity di-*n*-octylphosphinic acid (DOPA) was identified. Adding DOPA as a reagent in the synthesis resolved the irreproducibility in the formation of high-quality CdSe quantum-wires (Chapter 2). When the as-prepared CdSe nanowires with poor photoluminescence (PL) quantum efficiency were illuminated under fluorescent light, a proposed photo-induced surface reconstruction occurred spontaneously. This photo-induced PL enhancement process improved the PL quantum yield of CdSe nanowires up to 10% (Chapter 3). The syntheses of CdSe/CdS, CdSe/ZnS type-I core/shell structures with improved PL quantum yield are reported (Chapter 4). The syntheses of water-dispersible PEI (hyperbranched polyethylenimine) or PEG [poly(ethylene glycol)]-phosphine oxide polymer-coated CdSe nanowires and CdSe/SiO_2 core/shell structures are also reported (Chapter 4).

Nanoscience and technology is a field that is focused on: 1) the development of synthetic methods and surface analytical tools for building structures and materials on the sub-100 nanometer scale, 2) the identification and the improvement of the chemical and physical properties of these structures and materials, and 3) the use of such properties in the development of novel and functional devices and applications. Dimensionality plays a critical role in determining the properties of nanomaterials due to, for example, the different

ways that electrons interact in three-dimensional, two-dimensional (2D), and one-dimensional (1D) structures. The study of dimensionality has a long history in chemistry and physics.

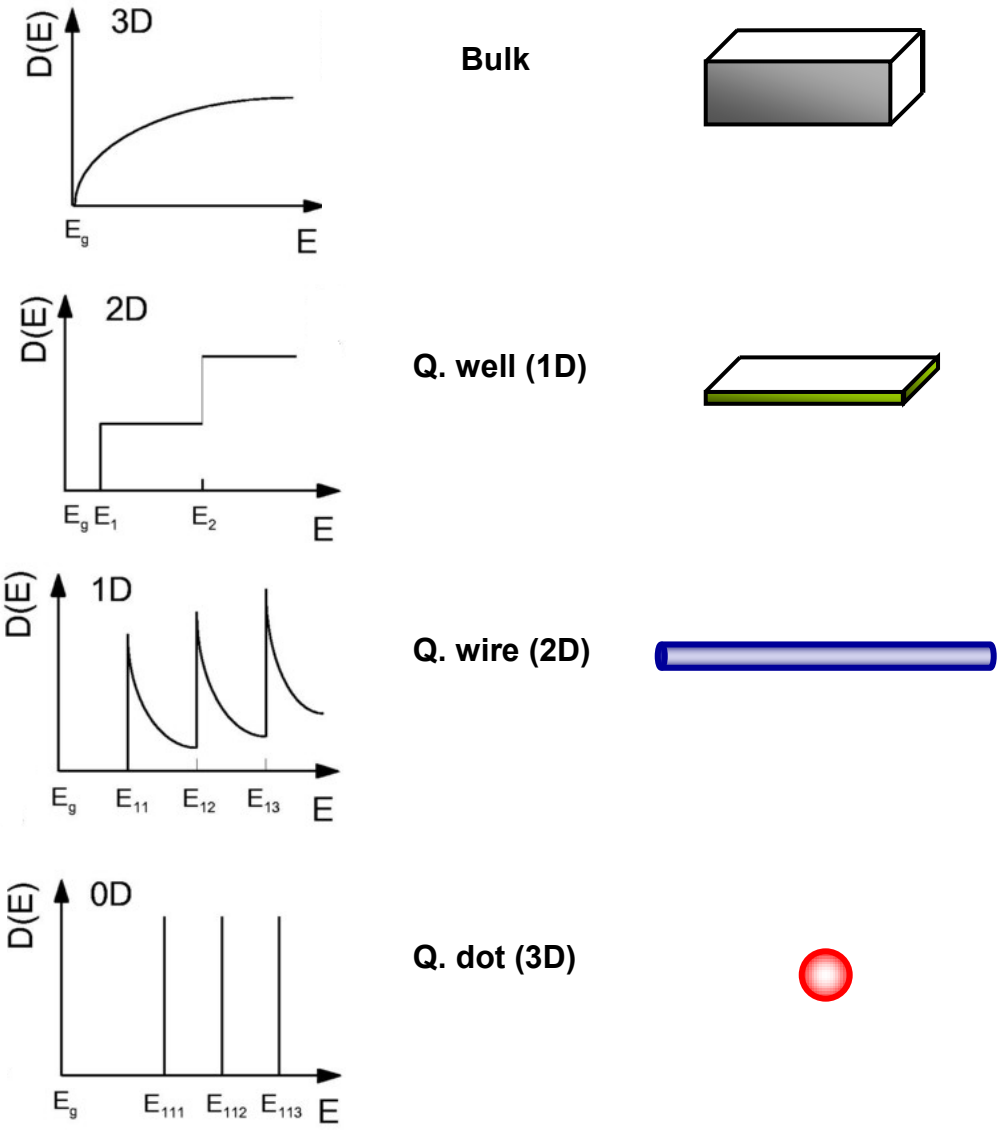

Figure I-1. The dimesionality of confinement and its effects on the density of states.

The quantum-confinement effect in semiconductors results from the geometric confinement of electrons and holes.[1] The normal size of an exciton in a large (bulk) crystal, expressed as an exciton Bohr radius, provides an approximate dimension for onset of quantum confinement effects.[1] When an electron-hole pair is squeezed into a nanocrystal with one or more dimensions approaching the bulk exciton Bohr radius, the effective bandgap of the semiconductor increases. The smaller the nanocrystal, the larger the effective bandgap, and the greater the energy of optical emission resulting from electron-hole recombination. However, the degree of the band-gap increases with reduced size is different for quantum wells, quantum wires, and quantum dots. As is shown in Figure I-1, the density of states changes from being continuous at all energies for a bulk material to discrete energy levels for a quantum dot.

The ΔE_g, the increase in the effective band gap over the bulk value, in quantum dots, quantum wires and quantum wells can be experessed by the following equations, respectively:

Quantum dot: $\Delta E_g = (4h^2/8d^2)[1/m_e+1/m_h]$ (1)

Quantum wire: $\Delta E_g = (2.34h^2/8d^2)[1/m_e+1/m_h]$ (2)

Quantum well: $\Delta E_g = (h^2/8d^2)[1/m_e+1/m_h]$ (3)

Where d is the diameter or thickness of the quantum nanostructure, h is Planck's constant, and m_e and m_h are the effective masses of the electron and hole in the semiconductor material. According to these equations, at a given size, the 3D-confined quantum dots show the largest ΔE_g, whereas the 2D-confined quantum wires show less confinement, and the 1D-confined quantum wells show the least

confinement due to the loss of the other two confinement dimensions. The quantum-confinement comparisons of the quantum wells, quantum dots, quantum rods, and quantum wires of the various semiconductor materials have been extensively studied by our group.[2-10]

Optimized synthesis of the SLS growth of CdSe nanowires. Fluorescent semiconductor nanowires (NWs) can lead to devices with efficient emission across the entire visible spectrum.[11-14] Cadmium selenide, as the most intensively studied semiconductor material, is a type II-VI ionic semiconductor. It can exist as wurtzite, zinc blende, or rock-salt phases, which are found at atmospheric pressure, thin film, and higher pressures, respectively.[15] The CdSe nanowires synthesized via the solution-liquid-solid (SLS) mechanism exhibit the wurtzite structure.

Many factors affect the morphology control and the optical properties of the CdSe nanowires. Carefully choosing suitable precursors, varying the ratios of the precursors, and adding beneficial additives are all important to achieve well-controlled colloidal CdSe nanowires with good emission efficiency. In Chapter 1, I report the optimized synthetic conditions for CdSe nanowires via testing different cadmium and selenium precursors, varying the cadmium-to-selenium precursor ratio and adding extra trioctylphosphine (TOP) and hexadecylamine (HDA) into the reaction system. The growth of the CdSe quantum wires is catalyzed by Bi nanoparticles. At the reaction temperature (240 -300 ^{o}C), the low-melting-point nanoparticles are in a molten-droplet state, which effectively

catalyzes the decomposition of precursors and initiates the growth of CdSe quantum wires.[3] Additionally, the quantum-wire diameter is dependent on the Bi-nanoparticle diameter (Figure I-2). Thus, by controlling the Bi-nanoparticle diameter and diameter distribution, control of the diameter and diameter distribution of the CdSe quantum wires is achieved.

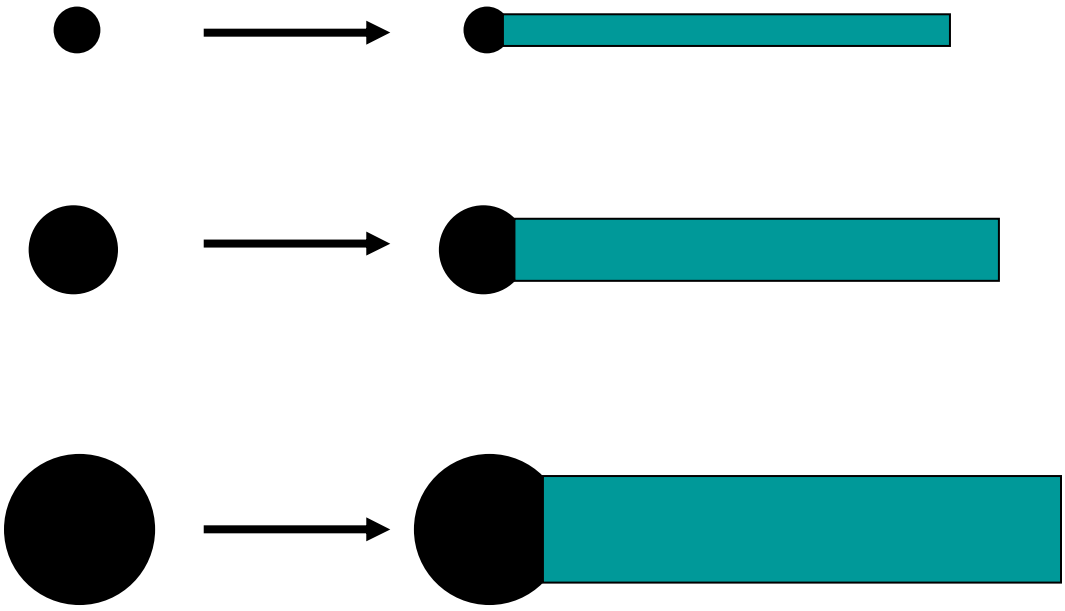

Figure I-2. Schematic representation of Bi-nanoparticle-diameter-dependent SLS growth of CdSe nanowires.

The reaction temperature also influences the diameter control of the CdSe nanowires, as reported in Chapter 1. The lengths of the CdSe nanowires are difficult to control, but minimizing the amount of Bi-nanoparticles used in the reaction system can achieve long CdSe nanowires up to ~ 10 μm in length.

The roles of the impurities in TOPO in CdSe quantum-wire growth. Tri-*n*-octylphosphine oxide (TOPO) is the most commonly used solvent for the synthesis of colloidal nanocrystals. The use of different batches of commercially obtained TOPO solvent introduces significant variability into the outcomes of CdSe quantum-wire syntheses. This irreproducibility is attributed to varying amounts of phosphorus-containing impurities in the different TOPO batches.[16, 17]

In Chapter 2, I report the synthetic results of adding different TOPO impurities during the CdSe quantum-wire synthesis. By comparing the morphology and optical properties, combined with ^{31}P NMR studies, various TOPO impurities are identified and their beneficial, harmful, or negligible effects on quantum-wire growth are determined. The impurity di-*n*-octylphosphinic acid (DOPA) is found to be the important beneficial TOPO impurity for the reproducible growth of high-quality CdSe quantum wires. DOPA is shown to beneficially modify precursor reactivity through ligand substitution. The use of purified TOPO with controlled amounts of specific additives (DOPA) allows rational and reproducible CdSe quantum-wire syntheses.

Photo-induced photoluminescence enhancement of CdSe quantum wires. Enhancement of the photoluminescence (PL) of colloidal CdSe and (core)shell (CdSe)ZnS quantum dots has been observed when the dots are illuminated above the band-gap energy.[18] The effect occurs in dots suspended in a variety of organic or aqueous environments.[19] During periods of constant illumination, the exciton PL quantum yield was found to reach a value of up to 60 times that of the solution

of as-prepared quantum dots and, if illumination was continued, subsequently declined slowly because of photooxidation.[18] It was postulated that the stabilization of surface trap states, lengthening their average lifetime, could occur by a light-activated rearrangement of surfactant molecules, thus increasing the probability of thermalization back to the lowest emitting exciton state and enhancing the quantum dot PL.[18]

In Chapter 3, I report a similar phenomenon observed when I illuminate CdSe quantum-wire suspensions under fluorescent lamps. The illumination of CdSe colloidal quantum wires in chloroform or toluene solution is observed to increase their PL quantum yield from 0.2 to ~ 10 %. I investigate the photo-enhancement procedure with different light power, different solvents, various additives, and compare the samples with or without stirring during the illumination period. The partially reversible photobrightening process similar to the quantum-dot study is also observed in the CdSe quantum-wire samples. The addition of TDPA to the CdSe nanowire solution results in the acceleration and amplification of the photo-enhancement effect. In contrast to the quantum-dot study, the photo-induced PL enhancement of CdSe quantum-wire samples do not show a shrinking in diameter, or a blue shift in the absorption or photoluminescence spectra.

Fabrication of CdSe/CdS(ZnS) and water-dispersible CdSe quantum wires.

Semiconductor nanostructures with low toxicity and biocompatibility exhibit interesting and potentially useful size-dependent photophysical properties based

on quantum-confinement effects, and as such have become increasingly important to the applications of these nanomaterials in bio-medical systems.[20-27]

Chapter 4 describes the syntheses of CdSe/CdS, CdSe/ZnS type-I core/shell structures. Two preparation methods of the core CdSe nanowires are performed to achieve the inorganic shell growth. The CdSe/CdS(ZnS) core/shell structure show improved PL efficiency compared to the core-only CdSe quantum wires due to the reduction of the surface traps through surface passivation. The deconstruction of the core/shell nanowires after a period is also observed, due the strain caused by the lattice mismatch of the core and shell materials.

I also report the syntheses of water-dispersible PEI (hyperbranched polyethylenimine) or PEG [poly (ethylene glycol)]-phosphine oxide polymer-coated CdSe nanowires and CdSe/SiO_2 core/shell structure. The optical properties of these structures are also investigated in Chapter 4.

References:

1. Yoffe, A. D. *Advances in Physics* **1993,** 42, (2), 173-266.
2. Yu, H.; Li, J. B.; Loomis, R. A.; Wang, L. W.; Buhro, W. E. *Nature Materials* **2003,** 2, (8), 517-520.
3. Yu, H.; Li, J. B.; Loomis, R. A.; Gibbons, P. C.; Wang, L. W.; Buhro, W. E. *Journal of the American Chemical Society* **2003,** 125, (52), 16168-16169.
4. Wang, F. D.; Loomis, R. A.; Kirmaier, C.; Holten, D.; Buhro, W. E. *Abstracts of Papers of the American Chemical Society* **2005,** 230, U2266-U2266.
5. Wang, F. D.; Buhro, W. E. *Journal of the American Chemical Society* **2007,** 129, (46), 14381-14387.
6. Wang, F.; Yu, H.; Li, J.; Hang, Q.; Zemlyanov, D.; Gibbons, P. C.; Wang, L. W.; Janes, D. B.; Buhro, W. E. *Journal of the American Chemical Society* **2007,** 129, (46), 14327-14335.
7. Dong, A.; Yu, H.; Wang, F.; Buhro, W. E. *Journal of the American Chemical Society* **2008,** 130, (18), 5954-5961.
8. Sun, J.; Wang, L. W.; Buhro, W. E. *Journal of the American Chemical Society* **2008,** 130, (25), 7997-8005.
9. Sun, J. W.; Buhro, W. E.; Wang, L. W.; Schrier, J. *Nano Letters* **2008,** 8, (9), 2913-2919.
10. Wang, F. D.; Yu, H.; Jeong, S. H.; Pietryga, J. M.; Hollingsworth, J. A.; Gibbons, P. C.; Buhro, W. E. *ACS Nano* **2008,** 2, (9), 1903-1913.
11. Lee, J.; Govorov, A. O.; Dulka, J.; Kotov, N. A. *Nano Letters* **2004,** 4, (12), 2323-2330.
12. Lee, J.; Govorov, A. O.; Kotov, N. A. *Nano Letters* **2005,** 5, (10), 2063-2069.
13. Tang, Z. Y.; Kotov, N. A.; Giersig, M. *Science* **2002,** 297, (5579), 237-240.
14. Wang, Y.; Tang, Z. Y.; Tan, S. S.; Kotov, N. A. *Nano Letters* **2005,** 5, (2), 243-248.

15. Zakharov, O.; Rubio, A.; Cohen, M. L. *Physical Review B* **1995,** 51, (8), 4926-4930.

16. Wang, F. D.; Tang, R.; Buhro, W. E. *Nano Letters* **2008,** 8, (10), 3521-3524.

17. Wang, F.; Tang, R.; Kao, J. L. F.; Dingman, S. D.; Buhro, W. E. *Journal of the American Chemical Society* **2009,** 131, (13), 4983-4994.

18. Jones, M.; Nedeljkovic, J.; Ellingson, R. J.; Nozik, A. J.; Rumbles, G. *Journal of Physical Chemistry B* **2003,** 107, (41), 11346-11352.

19. Maenosono, S.; Eiha, N.; Yamaguchi, Y. *Journal of Physical Chemistry B* **2003,** 107, (12), 2645-2650.

20. Gerion, D.; Pinaud, F.; Williams, S. C.; Parak, W. J.; Zanchet, D.; Weiss, S.; Alivisatos, A. P. *Journal of Physical Chemistry B* **2001,** 105, (37), 8861-8871.

21. Jin, T.; Fujii, F.; Sakata, H.; Tamura, M.; Kinjo, M. *Chemical Communications* **2005**, (22), 2829-2831.

22. Palaniappan, K.; Xue, C. H.; Arumugam, G.; Hackney, S. A.; Liu, J. *Chemistry of Materials* **2006,** 18, (5), 1275-1280.

23. Liu, Y. C.; Kim, M.; Wang, Y. J.; Wang, Y. A.; Peng, X. G. *Langmuir* **2006,** 22, (14), 6341-6345.

24. Wang, X. Q.; Wu, J. F.; Li, F. Y.; Li, H. B. *Nanotechnology* **2008,** 19, (20),

25. Roy, M. D.; Herzing, A. A.; Lacerda, S. H. D. P.; Becker, M. L. *Chemical Communications* **2008**, (18), 2106-2108.

26. Xing, R. M.; Wang, X. Y.; Yan, L. L.; Zhang, C. L.; Yang, Z.; Wang, X. H.; Guo, Z. J. *Dalton Transactions* **2009**, (10), 1710-1713.

27. Fahmi, A.; Pietsch, T.; Appelhans, D.; Gindy, N.; Voit, B. *New Journal of Chemistry* **2009,** 33, (4), 703-706.

Chapter 1

Optimized solution-liquid-solid synthesis of high quality CdSe quantum wires

Introduction

The solution-liquid-solid (SLS) growth of semiconductors developed by our group has shown great success for the synthesis of II-VI (CdSe,[1] CdTe,[2] CdS,[3] ZnSe,[4] and ZnTe[4]), III-V (GaAs,[5, 6] InP,[7] and InAs[8]) and IV-VI (PbSe, PbS[3]) quantum wires. The SLS mechanism[9] provides many advantages for semiconductor quantum-nanostructure synthesis over other methods, which includes well-controlled diameters, optimized surface passivation, dispersibility, and environmental stability. Studies of the optical properties of these semiconductor quantum wires by varying their diameters have lead to a rich understanding of the size-dependent quantum-confinement effect in various dimensionalities.[1, 2, 6-8, 10]

Among these semiconductors, CdSe has, over the last 20 years, been one of the most intensively studied semiconductor systems in nanoscale form.[1, 11-13] Recent work, however, has emphasized the development of CdSe nanorods[11-15] and nanowires[1, 16-22] through the manipulation of reaction conditions, Cd-coordinating ligands, and/or growth kinetics. Such trends reflect the realization that the properties of one-dimensional nanoscale materials (nanowires) are influenced not only by size and length, but also by the surface ligands. Thus, CdSe nanowires have evolved as a model system through which the physical, optical, and electrical properties of 1D nanoscale materials can be studied.

Previously, Dr. Heng Yu from our group reported the successful synthesis of CdSe nanowires via the solution-liquid-solid (SLS) mechanism.[1] CdSe nanowires were formed from cadmium stearate and *n*-Bu_3P=Se in

trioctylphosphine oxide (TOPO) at 240-300 ^{o}C, using monodisperse Bi nanoparticles to catalyze the wire growth. However, the quality of the CdSe quantum wires prepared by Yu was not ideal and they exhibited poor photoluminescence (PL) efficiencies. These deficiencies limited the in-depth study of the size-dependent optical properties of 1D CdSe quantum nanostructures.

In this chapter, I report the optimized SLS growth of CdSe nanowires by varying the cadmium precursor, selenium precursor, and cadmium-to-selenium precursor ratio. The effects of the additives such as hexadecylamine (HDA), trioctylphosphine (TOP) are also discussed. Finally, the achievement of nanowire-length control via the amount of Bi catalyst employed is addressed.

Results and Discussion

Synthesis. CdSe nanowires were prepared from cadmium stearate (or cadmium oxide + oleic acid) as the cadmium precursor, and tri-*n*-butylphosphine selenide (or tri-*n*-octylphosphine selenide) as the selenium precursor, in trioctylphosphine oxide (TOPO) as the reaction solvent at 240-300 ^{o}C. Bismuth nanoparticles[23] were used to catalyze wire growth. A schematic for the SLS growth of CdSe nanowires is shown in Figure 1-1. The reaction time for nanowire formation is very short, varying from 1 ~ 2 min, suggesting the high effectiveness of the Bi-nanoparticle catalyst. The reaction was usually continued for as long as 5 minutes before cooling, allowing the surface of the CdSe nanowires to anneal at high temperature to achieve better ligand coverage and better photoluminescence

efficiency. Some beneficial additives were found to improve the quality and the PL efficiency of the nanowires, such as hexadecylamine (HDA), and additional tributylphosphine (TBP)/TOP. I give the details of these results in this chapter.

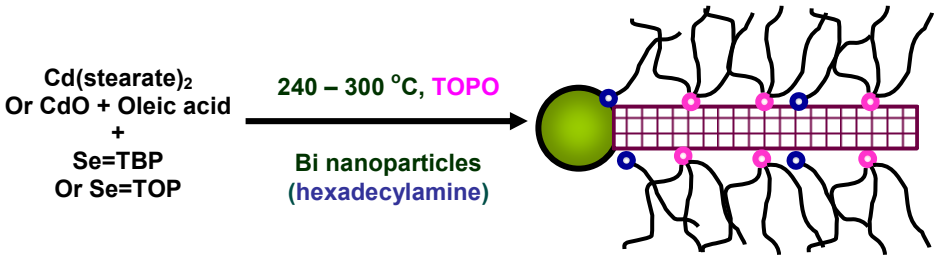

Figure 1-1 Schematic illustration of the SLS growth of CdSe nanowires.

Although the noncoordinating solvent 1-octadecene (ODE) produced great success for the synthesis of nanocrystals having various morphologies, including quantum dots, rods and tetrapods,[24] attempts to synthesize CdSe quantum wires in ODE were not very successful (Figure 1-2). Mixtures of dots, rods and tetrapods were observed in TEM images under various conditions. No Bi nanoparticles were found attached to the end of nanorods, suggesting that the nanorods were likely not grown via the SLS mechanism. The formation of nanodots, nanorods and tetrapods in ODE even in the presence of Bi catalyst suggests very high precursor reactivities in ODE, which favor the homogeneous nucleation and growth of morphologies like dots, rods and tetrapods instead of the SLS growth of the CdSe quantum wires.

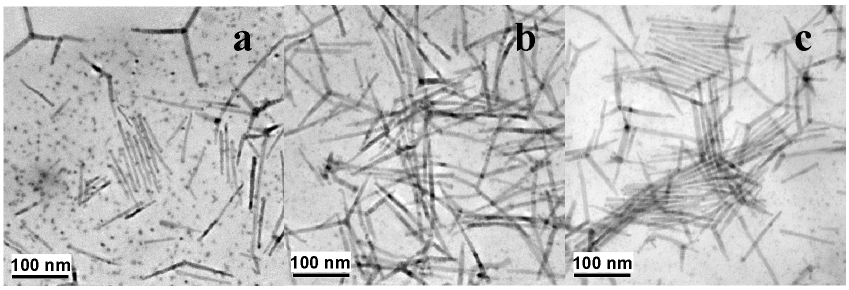

Figure 1-2. Representative TEM images of CdSe nanostructures synthesized in 1-octadecene (ODE). $Cd(OA)_2$ and TOP=Se were used as precursors. Bi nano-particles with a mean diameter of 8.8 nm were used as the catalyst. The reaction was conducted at 250 ^{o}C.

TOPO (tri-*n*-octylphosphine oxide) proved to be the best solvent for the SLS growth of CdSe quantum wires. High-quality CdSe quantum wires with narrow diameter distributions, good crystallinity (Figure 1-3), good morphologies (long and straight), and good surface passivation (high PL quantum yield) were prepared in this coordinating solvent. However, a problem for the CdSe quantum-wire synthesis in TOPO solvent was irreproducibility in the shape and quality of the nanowires resulting from variations in TOPO-impurity concentrations. I discuss in detail the resolution of this problem in Chapter 2.

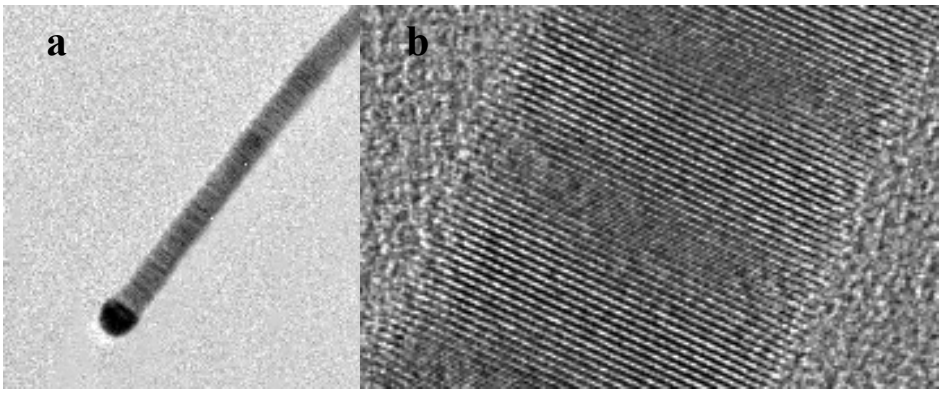

Figure 1-3. (a) A typical CdSe nanowire (diameter ~ 8 nm) grown via the SLS mechanism. Note the Bi catalyst attached to the end of the wire. (b) A high resolution TEM image of an 8 nm CdSe nanowire segment.

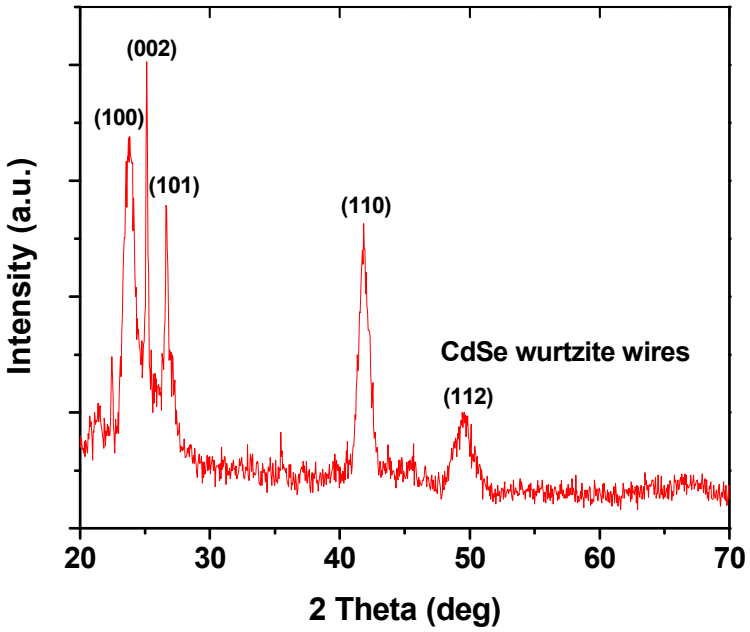

Figure 1-4. An x-ray diffraction pattern (Cu Kα radiation, λ = 1.542 Å) from a CdSe quantum-wire powder specimen (wire diameter ~ 8 nm).

Diameter control for CdSe quantum wires. Two major factors were found to be effective to control the diameter of the CdSe nanowires. The first is the diameter of the Bi catalyst seeds; the second is the reaction temperature, which can be altered by varying the temperature of the salt bath. The major diameter-control factor is the size of the Bi catalyst used. The nanoparticles attached to wire tips (Figure 1-3) confirmed that these CdSe nanowires were catalyzed by the Bi nanoparticles through the SLS growth mechanism. The diameter of CdSe nanowires could be easily tuned from ~5 nm to ~16 nm by using differently sized Bi-catalyst nanoparticles (Table 1-2 in experimental section). I found that the wire diameter is usually about 20% smaller than the size of the Bi nanoparticles from which it grows (Figure 1-3). For example, CdSe nanowires with a mean diameter ~4.95 nm were prepared from 6.20 nm Bi nanoparticles and CdSe nanowires with a mean diameter ~8.02 nm were prepared from 10.1 nm Bi nanoparticles.

For the cases when very small Bi nanoparticles were used (3 ~ 5 nm), the diameter control of the CdSe nanowires was usually poor, due to the aggregation of the small Bi nanoparticles at the high reaction temperature. The aggregation of Bi nanoparticles occurred soon after injection and before the SLS reaction took place, which broadened the size distribution of Bi catalyst particles. Therefore poor control of CdSe nanowire diameter resulted.

Figure 1-5 shows the absorption and photoluminescence spectra of the CdSe nanowires having diameters from 4.95 nm to 6.31 nm. The bulk band gap of

CdSe at room temperature is 1.74 eV (~712.6 nm),[25] which indicates our CdSe wires are in the quantum-confinement regime.

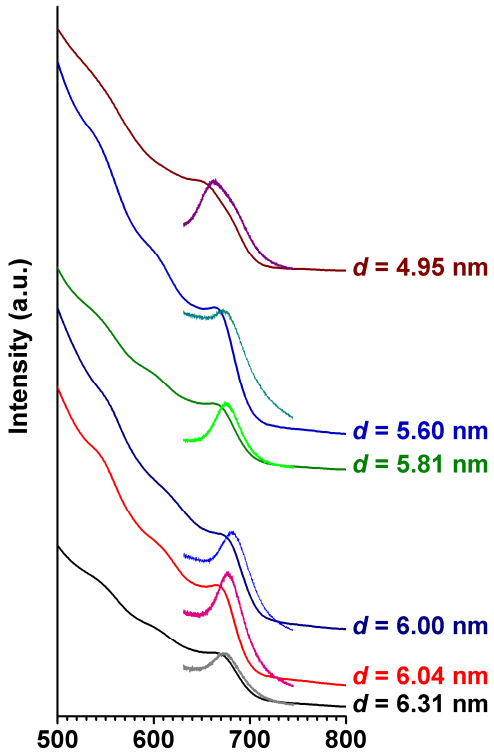

Figure 1-5. The absorption and photoluminescence spectra of CdSe nanowire samples having mean nanowire diameters from 4.95 nm to 6.31 nm.

All of the band-edge absorptions and the PL peaks of the CdSe quantum wires investigated show a blue shift relative to the bulk band-edge absorption at 1.74 eV (712.6 nm). In addition, as the diameter of the CdSe nanowires decreased, a systematic increase in the quantum-confinement energy was observed, indicating the expected size-dependent quantum-confinement effects. (See Table 1-1 below)

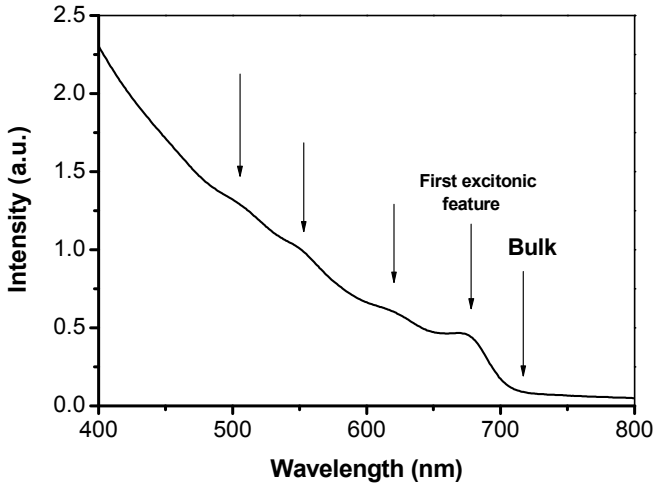

Figure 1-6. Representative absorption spectrum of CdSe quantum wires in toluene solution, showing possible absorption features indicated by black arrows.

A representative absorption spectrum of CdSe quantum wires having a mean diameter of 8.0 nm (Figure 1-6) shows several well-resolved absorption features. All the CdSe nanowires with high quality showed similar absorption features. In order to extract the exact position of the first excitonic feature of the absorption spectrum, we employed the fitting method reported previously by Yu.[1] Each spectrum was fit by several Gaussian functions, and the lowest-energy peak was extracted as a Gaussian from which the exact peak position was determined. A typical Gaussian function and its parameters are shown in Figure 1-7. A representative fitting of an absorption spectrum is shown in Figure 1-8.

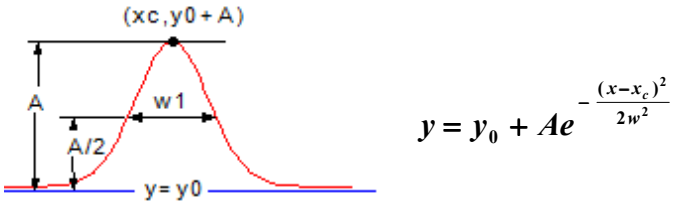

Figure 1-7. A Gaussian function to represent an absorption peak. A is the height of the peak, x_c is the peak position, W is the 2σ width.

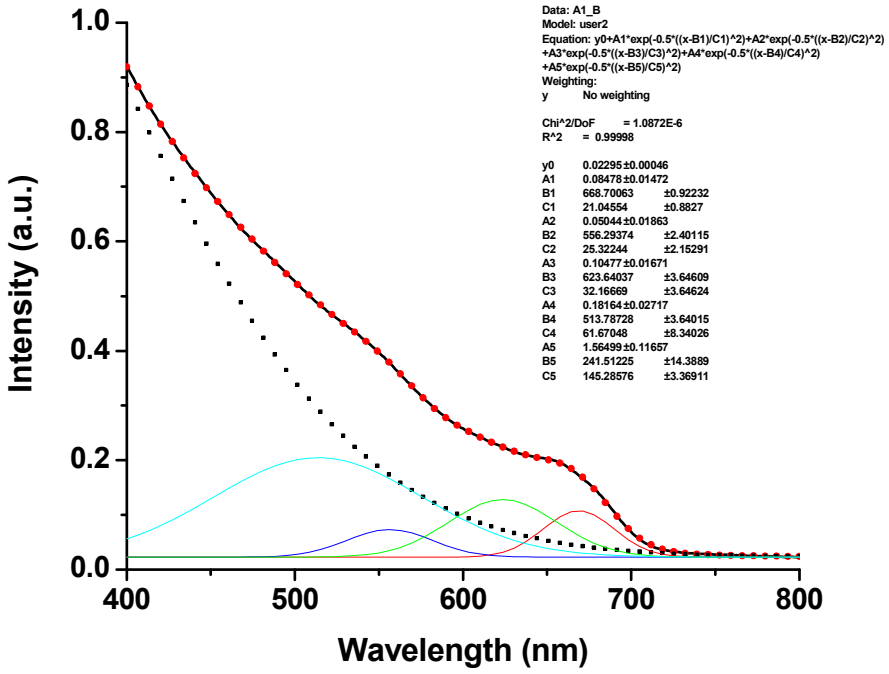

Figure 1-8. Representative fitting of an absorption spectrum of 5.60 nm CdSe nanowires. The black solid curve and the red dotted curve are the experimental spectrum and the fitted spectrum, respectively.

The fitted absorption (red dotted curve) is very close to the experimental data (black solid curve), which indicates the success of the fitting procedure. As shown from Figure 1-8, the fitting results give the lowest-energy peak position (excitonic feature) from which the band-gap and quantum-confinement energy (ΔE_g) are calculated. The determined band-gap and ΔE_g values for CdSe quantum wires of various diamters are shown in Table 1-1.

Table 1-1. Band-gap energies and quantum confinement energies (ΔE_gs) for CdSe quantum wires with different mean diameters from 4.95 to 12.1 nm.

$Diameter_{CdSe}$ (nm)	Band gap (eV)	Band gap (nm)	ΔE_g (eV)
4.95	1.893	655.1	0.153
5.20	1.879	660.1	0.139
5.60	1.854	668.7	0.114
6.04	1.851	669.9	0.111
8.02	1.833	676.5	0.093
9.05	1.800	688.9	0.060
10.2	1.786	694.4	0.046
12.1	1.768	701.2	0.028
Bulk	1.74	712.6	--

Cadmium precursor. Cadmium stearate was previously used as the cadmium precursor in our lab to replace the extremely toxic dimethylcadmium ($(CH_3)_2Cd$) precursor which had been used in the earlier years.[26] The mechanism of CdSe wire formation has been proposed to involve small clusters or oligomers formed from cadmium stearate and TBP=Se during the reaction, which are the growth nutrients.[1] The bismuth nanoparticles capture the *in-situ*-formed nutrients, catalyze the complete decomposition of them, dissolve the $(CdSe)_n$ fragments, and initiate the CdSe nanowire growth (Figure 1-9).[1] Recently CdO and oleic acid were used as the Cd precursor for the synthesis of high-quality CdSe quantum dots.[27-29] These quantum dots usually have better size control and better photoluminescence efficiency than those prepared from cadmium stearate.

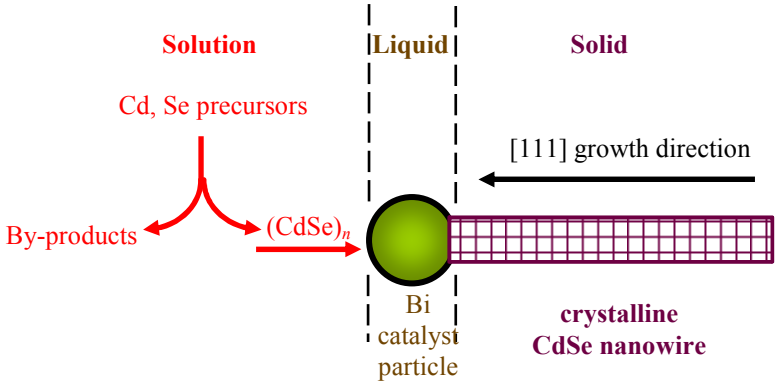

Figure 1-9. Schematic diagram illustrating CdSe nanowire growth via the SLS (solution-liquid-solid) mechanism from Bi-catalyst nanoparticles.

Stearic acid:

Oleic acid:

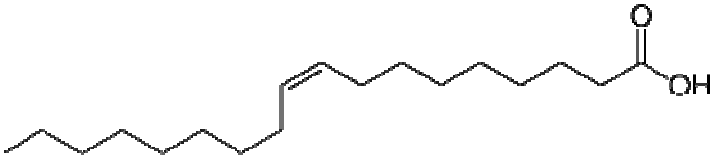

Figure 1-10. Structures of stearic acid and oleic acid

The success of CdO and oleic acid as the cadmium precursor in the CdSe quantum-dot system led us to adapt this combination to our nanowire synthesis. The initial reaction mixture containing CdO, oleic acid, TOPO, and HDA is dark brown. When the reaction tube is placed into the 320 ^{o}C salt bath for pre-heating, the reaction mixture becomes colorless, which indicates the formation of Cd(oleate)$_2$ in the TOPO solution. The pre-heating process usually takes about 10 min.

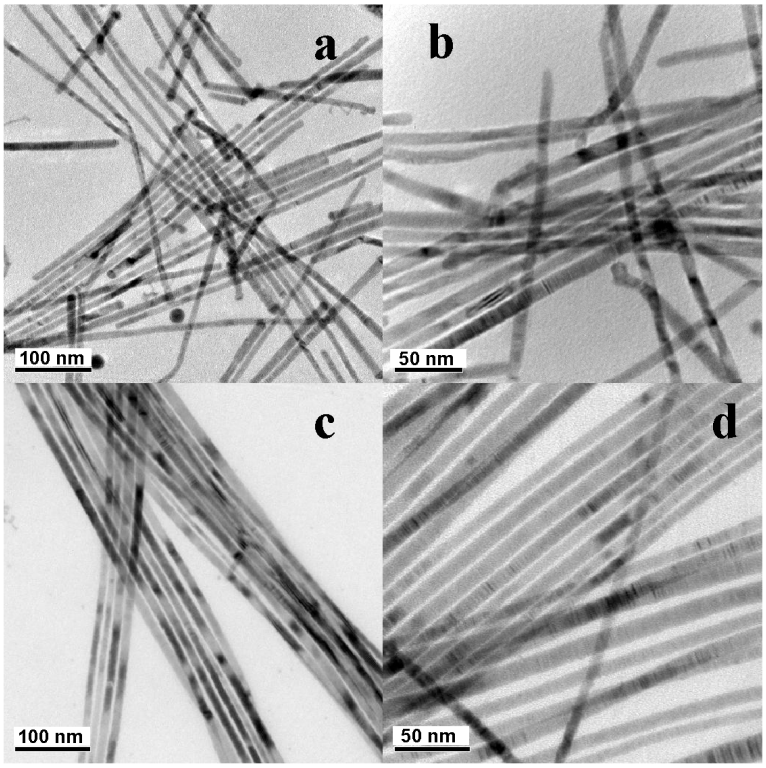

Figure 1-11. Representative TEM images of the CdSe nanowires synthesized using $Cd(stearate)_2$ as the Cd precursor (a and b), and using CdO + oleic acid as Cd precursor (c and d). All the other reaction conditions are same in these two cases.

In the TEM images (Figure 1-11), we can see CdSe nanowires prepared using CdO and oleic acid have better quality than the CdSe nanowires prepared using $Cd(stearate)_2$. CdSe nanowires from CdO and oleic acid usually show better diameter control, and are longer and straighter. This difference is proposed to result from the difference in the reactivities of $Cd(oleate)_2$ and $Cd(stearate)_2$. At the reaction temperature (250 ^{o}C), $Cd(oleate)_2$ is more reactive than $Cd(stearate)_2$ and reacts faster after injection into the hot reaction mixture, as evidenced by the color change observed. In the presence of Bi catalyst particles, all cadmium

precursors will thus promptly convert into CdSe-Bi alloy at an early stage in the process. Because the nucleation process is ended at early stage of the reaction, further wire growth can occur only via the SLS mechanism along the growth axis, which will lead to the better control of 1-D morphology, and preclude separate, homogeneous nucleation of dots and rods.

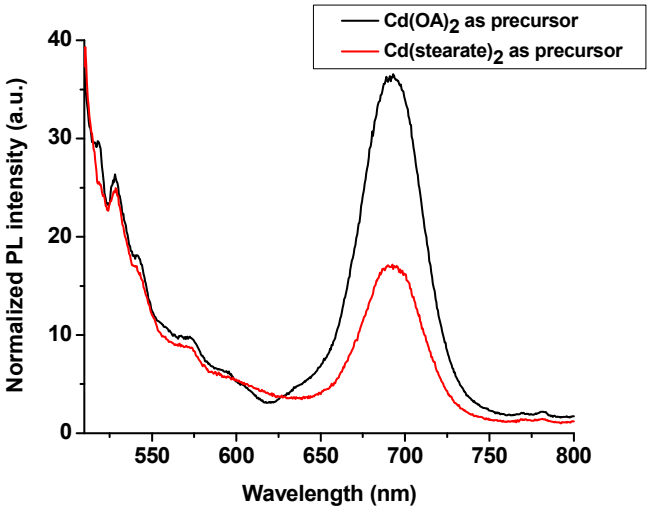

Figure 1-12. Normalized PL spectra of as-prepared CdSe nanowires (diameter = 8.0 nm) made from CdO + oleic acid and $Cd(stearate)_2$ as the Cd precursor. All the other synthetic conditions are the same.

The CdSe nanowires made from $Cd(oleate)_2$ also showed better emission efficiency than the nanowires made from $Cd(stearate)_2$ (Figure 1-12), which indicates better surface coverage for the nanowires prepared from $Cd(oleate)_2$. PL quantum yields are determined and discussed in Chapter 3. The difference between these two acids is the double bond in oleic acid (Figure 1-10). Because

oleic acid has a double bond, and is also presumed to be one of the surfactants on the CdSe nanowires, it may form some crosslinked structure at the surface of nanowires and therefore reduce the gaps in the surface passivation to minimize surface traps and improve the emission efficiency.

Additionally, the dispersibility of CdSe nanowires made from $Cd(oleate)_2$ is better than that of the nanowires made from $Cd(stearate)_2$, and they can retain their emission efficiency and dispersibility in organic solvents much longer than those from $Cd(stearate)_2$, presumably due to the better surface coverage to prevent the oxidation of the surface.

Se precusors. For CdSe nanocrystal synthesis, virtually all nonaqueous synthetic routes have employed tertiary alkylphosphine selenides as the selenium precursor because of their high solubility and reactivity in a range of organic solvents. It has been difficult to distinguish the effects of such reagents on crystal-growth dynamics and photoluminescence properties.

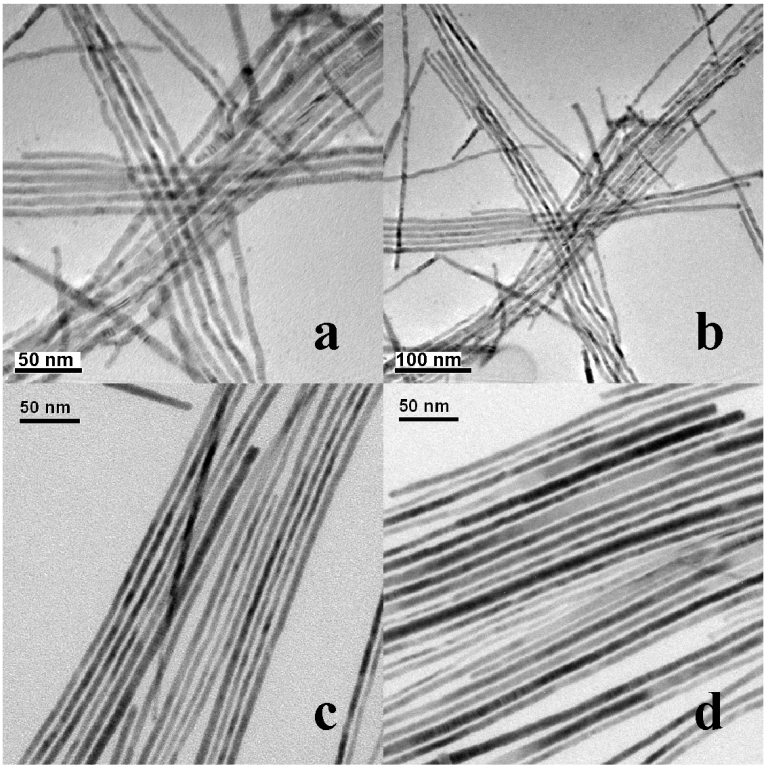

Figure 1-13. Representative TEM images synthesized using TBP=Se (a, b), and TOP=Se (c, d). All the other synthetic conditions are same in both experiments.

I now report that morphology control for CdSe nanowires prepared from TOP=Se is much better than that from TBP=Se (Figure 1-13). For the synthesis of binary semiconductor nanowires via the SLS mechanism from dual-source precursors, variations in the reactivity of the precursors can result in large differences in the quality of the product.[2, 3] I speculate that TOP=Se facilitates high-quality wire growth by moderating the rate at which molecular $(CdSe)_n$ clusters are generated. The mechanism for CdSe generation is shown in Figure 1-14.[30] In this mechanism, the R_3P=Se precursor is ultimately converted to R_3P=O. Because TOPO is the reaction solvent for CdSe nanowire growth, I argue that the rate of TOPO formation and therefore the rate of CdSe formation is suppressed.

We have shown that a moderate rate of CdSe formation is essential to the growth of high-quality CdSe nanowires.[22]

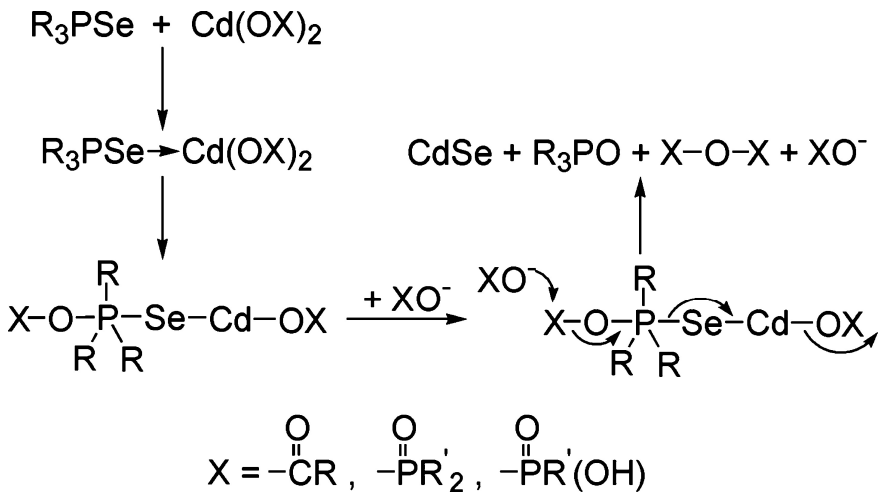

Figure 1-14. Mechanism of formation of CdSe and byproducts.[30]

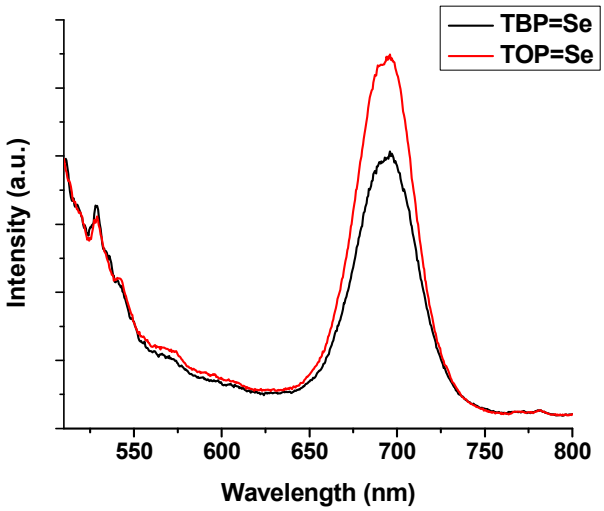

Figure 1-15. Normalized PL spectra of CdSe nanowires (diameter = 8.0 nm) made from TBP=Se and TOP=Se as the Se precursor. All the other synthetic conditions are the same.

Figure 1-15 shows that the photoluminescence of the CdSe nanowires made from TOP=Se is slightly better than the nanowires made from TBP=Se. Because TBP or TOP is also expected to be one of the surface ligands binding to the CdSe nanowires, TOP may be a better surfactant to remove trap sites. Therefore slightly better surface passivation of the CdSe nanowires is achieved.

HDA(hexadecylamine) as an additive to the reaction mixture. The use of primary amines in the surfactant mixtures have been shown to increase the PL efficiencies of CdSe quantum dots.[31-33] The chain length and the steric properties of the amine surfactant will affect the dispersibility of nanocrystals and their colloidal stability. Consequently, I have investigated several amine surfactants to optimize the passivation. Among the various amines (HDA, oleylamine, DOA (dioctylamine), TOA (trioctylamine)), HDA proved to be the best amine for controlling the morphology of CdSe nanowires (Figure 1-16).

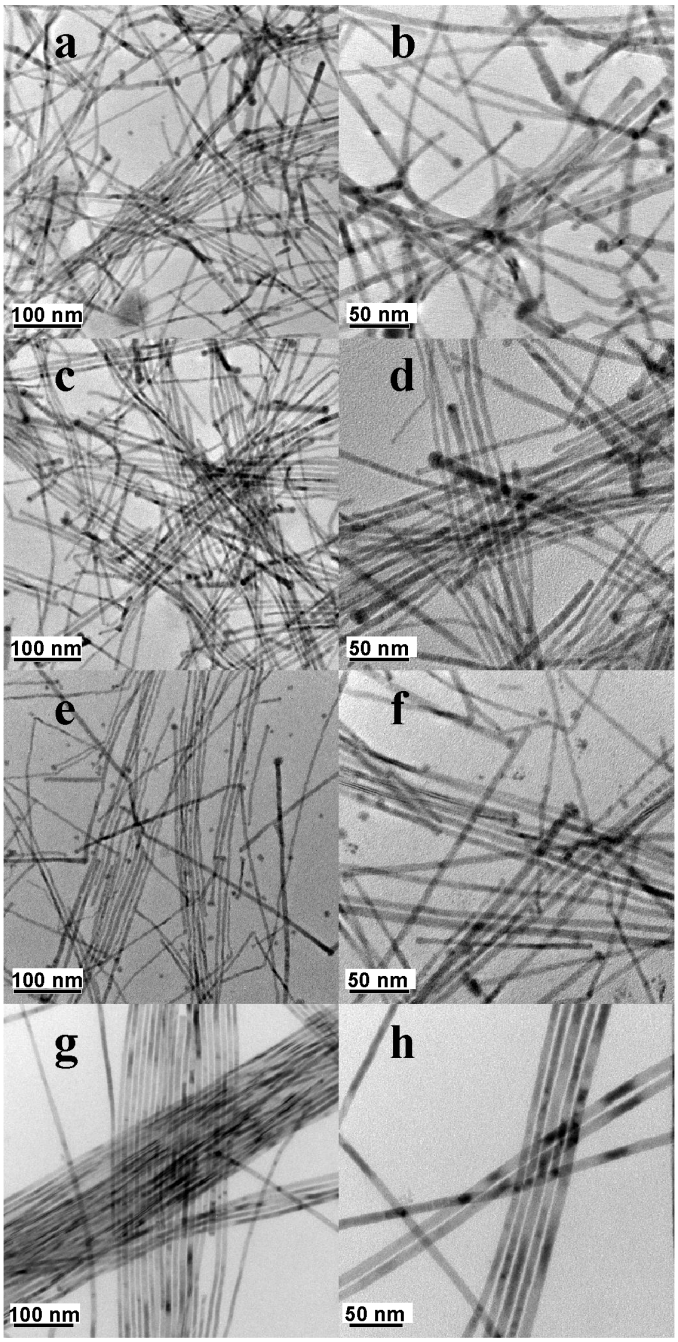

Figure 1-16. Representative TEM images of CdSe nanowires made with various amine surfactants. Dioctylamine (a, b), trioctylamine (c, d), oleylamine (e, f), and hexadecylamine (g, h). All the other synthetic conditions are the same.

Additionally, the use of HDA resulted in wires that exhibited detectable room-temperature PL. All the CdSe wires synthesized without HDA gave no or undetectable PL.

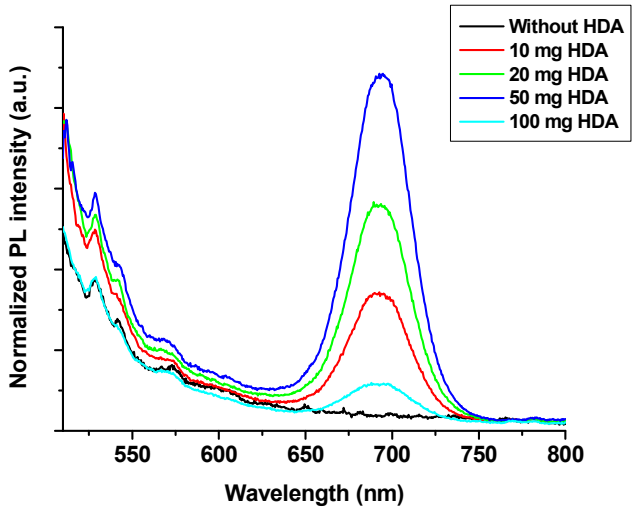

Figure 1-17. PL spectra from samples with different amounts of HDA added during synthesis. All the other experimental conditions were the same, and the absorption was adjusted to normalize the PL.

The amount of HDA added is also very important. Unlike the case for quantum dot synthesis, where HDA is typically used as a co-solvent, a large amount of HDA is harmful to the formation of high-quality CdSe nanowires. When HDA was used in co-solvent quantities, most of the product consisted of quantum dots, even with a sufficient amount of Bi catalysts. Additionally, more than 50 mg HDA in 5 g TOPO reduced the PL efficiency of the wires. (Figure 1-17) Although smaller amounts of HDA improved the optical properties of the CdSe quantum wires, 50 mg of HDA in 5 g of TOPO solvent proved to be the

best amount for CdSe nanowire synthesis, giving the best morphology control and achieving the best PL efficiency.

Additional TOP in the TOP=Se, Bi injection solution. In our CdSe nanowire synthesis, the selenium precursor is TOP=Se. This was a Se-saturated solution, which means all the TOP is bound to Se. Therefore, there was no free TOP in the injection solution. I found that additional TOP (about 100 mg) in the injection solution helped the wire growth and the optical properties of the CdSe nanowires.

There are two possible advantages to additional TOP in the reaction system. The first is that TOP may ligate the reaction precursors and give good passivation to the Bi catalyst[34] and CdSe-Bi alloy. Therefore a suitable precursor reactivity may be achieved. Also, TOP may act as another nanowire surfactant like HDA, leading to better surface passivation that reduces the surface traps on the CdSe nanowires.

Cd-to-Se precursor ratio. The influence of the initial ratio between the Cd and the Se precursors on the temporal evolution of the quality and the ensemble PL quantum yield of CdSe nanocrystals during their growth at 290 ^{o}C in a coordinating solvent has been investigated by Qu and Peng.[31] From this study, growth with an excess of Se monomer leads to the slowest growth rate and the smallest size polydispersity. Additionally, excess Cd precursors results in very low nanocrystal PL quantum yields; addition of an excess of Se monomer can revive the CdSe nanocrystal PL.[29] A large excess of cadmium precursor has been shown to be harmful to the formation of high-quality CdSe nanowires. Yu

observed dendritic nanowire products when the cadmium precursor was in large quantity, such as 200 mg in 5.0 g TOPO solution.[1] All these results from CdSe quantum dot and prior CdSe wire syntheses showed that a Se-rich precursor system is favorable for morphology control and optical-property optimization in the growth of CdSe nanostructures.

The Cd-to-Se ratio in our CdSe quantum wire synthesis was found to sensitively influence wire quality (Figure 1-17) and optical properties (Figure 1-18). I varied the Cd:Se precursor ratio in the wire syntheses to study the effect of precursor concentration and pursue the best precursor ratio. In the extreme cases, a large excess of Cd precursor (more than 500 mg in 5.0 g TOPO solution) led to precipitation of metallic Cd and uncontrolled growth of large CdSe crystals. However, the use of large amount TOP=Se did not have a significant harmful effect on the formation of well-controlled CdSe nanowires.

TEM images (Figure 1-18) in the Cd-rich cases always showed a "dirty" background, which may be fine Cd particles formed during the early stage of the reaction because of the high concentration of the Cd precursors. Also, the CdSe nanowires formed under these conditions usually exhibited poor diameter control. Upon increasing the amount of the Se precursor used, less particulate background was observed. Furthermore, the diameter and morphology control became progressively better. The growth under an excess of Se monomer led to the best diameter control in the CdSe quantum wires.

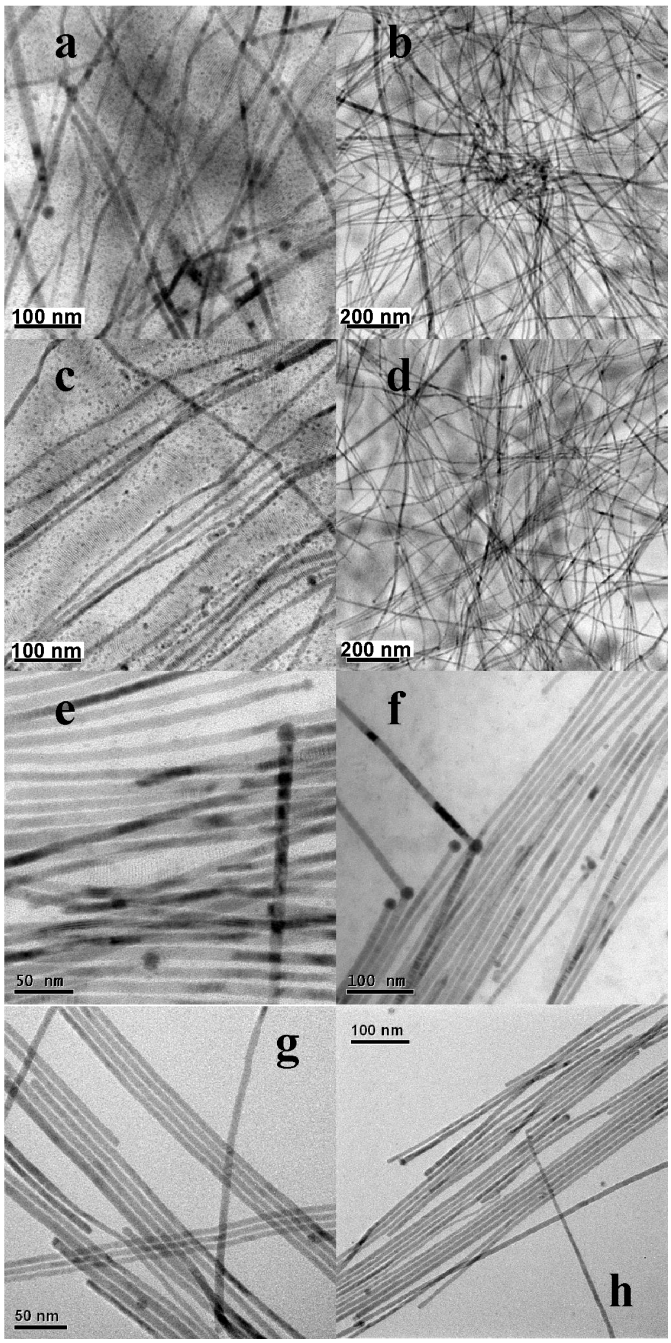

Figure 1-18. TEM images of CdSe nanowires synthesized with different Cd:Se precursor ratios: (a),(b) Cd:Se = 5:1 (c),(d) Cd:Se = 2:1 (e),(f) Cd:Se = 1:1 (g),(h) Cd:Se = 1:5

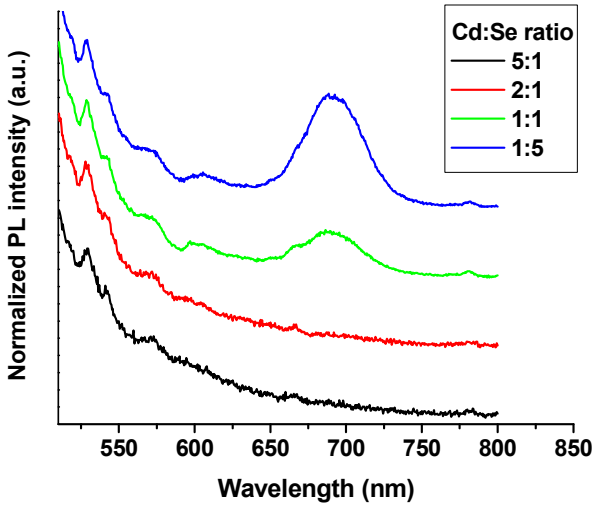

Figure 1-19. Photoluminescence spectra of CdSe nanowires synthesized at different Cd:Se precursor ratio from 5:1 to 1:5. All the other synthetic conditions were same in these experiments.

No PL was observed from CdSe nanowires synthesized from Cd-rich precursor ratios (Figure 1-19). Weak PL was observed in the Cd:Se = 1:1 synthetic condition, and even stronger PL from the more Se-rich system. Surface annealing under an excess of Se favors Se-rich facets and therefore reduces the amount of Cd dangling bonds.[35] Cd-Se nonpolar facets can undergo spontaneous surface reconstruction and polar Se facets are more effectively reconstructed than are the polar Cd facets.[35]

Amount of Bi catalyst. A suitable amount of Bi catalyst used in the CdSe nanowire synthesis is also very important to control morphology. The less Bi catalyst used, the fewer CdSe nanowires are formed; therefore longer CdSe nanowires are achieved. I found that about 23 mg (0.00092 mmol) Bi catalyst solution in 5.0 g of TOPO is the best amount for our system. It is the least amount of Bi we can use and still obtain high-quality CdSe quantum wires. Under the best synthetic conditions, with 23 mg of Bi catalyst solution, the length of the CdSe nanowires was up to 10 μm (Figure 1-20). Measuring the precise lengths of the CdSe nanowires is difficult because they are very long and bunched together on the TEM grid. Distinguishing the exact head or tail of the same nanowires in the low-resolution images was impossible.

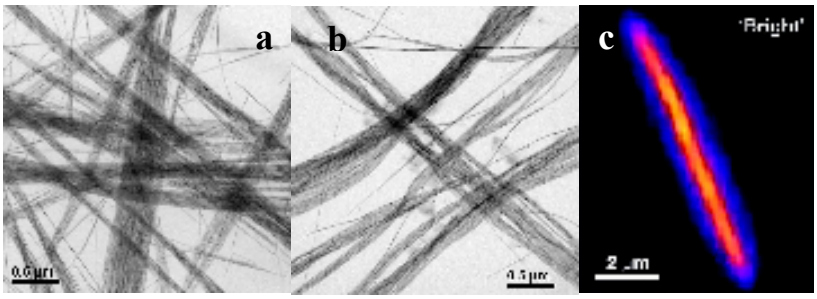

Figure 1-20. Representative low-resolution TEM images (a, b) and luminescent single-wire confocal image (c) of extremely long CdSe nanowires synthesized with 23 mg Bi catalyst. The length of the CdSe nanowires is up to 10 μm.

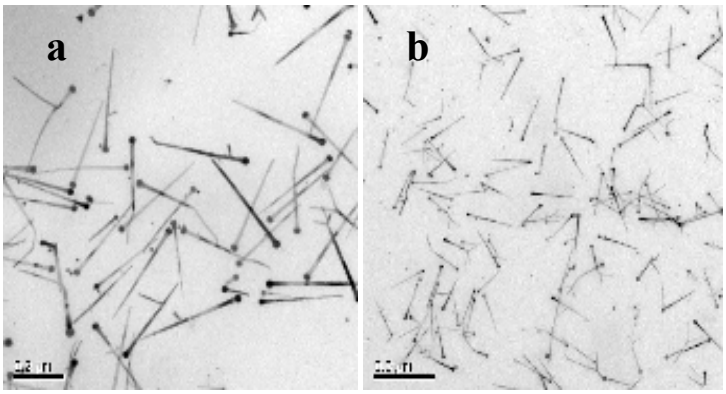

Figure 1-21. Representative TEM images of short CdSe nanowires synthesized with a large amount of Bi catalyst.

Attempts to vary the aspect ratio of the CdSe nanowires by varying the amount of Bi catalyst were not so successful. But a large amount of Bi catalyst (~500 mg per 5.0 g TOPO) produced very short CdSe nanowires (length ~ 200 nm, Figure 1-20). The Bi nanoparticles attached to the end of short CdSe nanowires confirmed the SLS growth mechanism. Note that the short nanowires have a tapered structure, which resulted from the big temperature change of the Bi nanoparticles after the injection. The longer wires synthesized under other conditions also have a tapered segment at the end where growth was initiated, opposite the catalyst particle.

Conclusion.

This chapter discussed all the synthetic parameters for the SLS growth of CdSe quantum wires. By varying precursors, amounts, ratios, and additives, I optimized the synthesis of CdSe nanowires for morphology control and photoluminescence efficiency. The best conditions for the SLS growth of CdSe nanowires uses $Cd(OA)_2$ and TOP=Se as the cadmium and selenium precursors, respectively. The injection solution should contain an excess amount of TOP=Se (500 mg, Cd:Se ratio ~ 1:30) and additional 100 mg TOP, along with 23 mg of Bi catalyst solution. The reaction mixture should contain $Cd(OA)_2$ precursor with 5 g of TOPO and 50 mg of HDA. The reaction temperature of the SLS growth can be varied from 240 - 280 ^{o}C. The diameter of the CdSe nanowires can be controlled by varying the size of the Bi nanoparticles used, and the reaction temperature (Table 1-2).

Experimental Section

Chemicals. Cadmium stearate (90%), Cadmium oxide (CdO, 99%), Oleic acid (OA, 90%), tri-n-octylphosphine oxide (TOPO, 99%), trioctylphosphine (TOP, 97%), selenium powder (Se, 100 mesh 99%), poly(1-hexadecen)$_{0.67}$-co-(1-vinylpyrrolidinone)$_{0.33}$, and Na[N(SiMe$_3$)$_2$] (1.0M solution in THF) were obtained from Aldrich and used as received. 1,3-diisopropylbenzene (DIPB, from Aldrich) was shaken with concentrated sulfuric acid to remove thiophene, washed with water, and distilled over Na.

Preparation of TOP=Se. A neat mixture of 4 g of elemental Se powder (0.051 mol) and 22 g TOP (0.059 mol) was loaded into a 100 ml storage bottle under dry, O_2-free N_2(g). The Se powder rapidly dissolved into the liquid mixture as heat was evolved. A second portion of 1 g of Se (0.013 mol) was added into the mixture to ensure the conversion of TOP to TOP=Se. The liquid fraction of the mixture was subsequently used.

Preparation of TBP=Se. A neat mixture of 4 g of elemental Se powder (0.051 mol) and 12 g of TBP (0.059 mol) was loaded into a 100 ml storage bottle under dry, O_2-free N_2(g). The Se powder rapidly dissolved into the liquid mixture as heat was evolved. A second portion of 1 g of Se (0.013 mol) was added into the mixture to ensure that all of the TBP had been converted to TBP=Se. The liquid fraction of the mixture was subsequently used.

Preparation of Bi-nanoparticle stock solutions. Monodispersed Bi nanoparticles were grown in DIPB solutions of poly(1-hexadecen) $_{0.67}$-co-(1-vinylpyrrolidinone) $_{0.33}$ and Na[N(SiMe$_3$)$_2$] at elevated temperatures (170-210 ^{o}C), following the procedure previously reported.[23] The diameter of Bi nanoparticles were tuned from 5 to 18 nm (std. deviation = 5-10% of the mean diameter) by varying reaction conditions, and the effective concentration of the dispersions was 0.04 mmol of Bi/g DIPB.

Bi-catalyzed growth of CdSe nanowires. In a typical synthesis of CdSe nanowires, 6 mg of CdO (0.047 mmol), 53 mg of oleic acid (0.19 mmol), 50 mg of hexadecylamine (0.21 mmol), and 5 g of trioctylphosphine oxide (13 mmol) were loaded into a 50 ml reaction tube, which was degassed on a Schlenk line and backfilled with N_2. The reaction mixture was heated at 320 ^{o}C in a salt bath ($NaNO_3$: KNO_3 ~ 1:1) until a clear solution was generated (~ 10 min). Then, the reaction tube was transferred to a 250 ^{o}C salt bath for wire growth. At this temperature, a mixed solution of 500 mg of TOP=Se (1.1 mmol), 100 mg of TOP (0.27 mmol) and 23 mg of Bi solution (0.00092 mmol) was rapidly injected into reaction tube.. After 5 min reaction, the reaction mixture was allowed to cool to room temperature.

1 ml aliquot of the reaction mixture was dissolved into 2 ml of toluene, the wires were precipitated with 6 ml of methanol and the sample was centrifuged and the supernatant was decanted. The precipitates were re-dispersed in 2 ml of toluene, precipitated with 6 ml of methanol, followed by centrifugation and

decanting the supernatant again. Then, the precipitates were re-dissolved in toluene for optical measurements.

The diameter of CdSe nanowires grown by this approach were varied by changing the reaction temperature from 240-280 ^{o}C and by choosing different-sized Bi nanoparticles as the catalyst seeds (Table 1-2).

Table 1-2. Synthetic conditions and results for CdSe nanowires.

CdO (mmol)	Oleic acid (mmol)	Se=TOP (mmol)	HDA/TOP (mmol)	TOPO (g)	Bi solution (mg)	Bi Nanoparticle size (nm)	Reaction T (^{o}C)	reaction time (min)	Diameter of the CdSe nanowires (nm)
0.047	0.19	1.1	0.21/0.27	5	23	6.1	240	5	4.76 (11.2%)
0.055	0.25	1.1	0.21/0.27	5	23	6.1	260	5	4.92 (10.33%)
0.047	0.21	1.1	0.21/0.27	5	23	6.1	280	5	5.01 (10.72%)
0.047	0.21	1.1	0.21/0.27	5	23	6.1	300	5	5.20 (10.20%)
0.055	0.25	1.1	0.21/0.27	5	23	8.1	240	5	6.90 (10.38%)
0.047	0.19	1.1	0.21/0.27	5	23	8.1	260	5	7.15 (10.79%)
0.047	0.21	1.1	0.21/0.27	5	23	8.1	280	5	7.35 (10.47%)
0.047	0.19	1.1	0.21/0.27	5	23	8.1	300	5	7.51 (11.12%)
0.055	0.25	1.1	0.21/0.27	5	23	10.2	240	5	8.02 (9.72%)
0.047	0.19	1.1	0.21/0.27	5	23	10.2	260	5	8.41 (10.53%)
0.047	0.21	1.1	0.21/0.27	5	23	10.2	280	5	8.61 (11.17%)
0.047	0.19	1.1	0.21/0.27	5	23	10.2	300	5	8.89 (12.10%)
0.047	0.22	1.1	0.21/0.27	5	46	17.4	240	5	13.35 (10.19%)
0.055	0.21	1.1	0.21/0.27	5	46	17.4	260	5	14.10 (9.38%)
0.055	0.24	1.1	0.21/0.27	5	46	17.4	280	5	15.01 (9.92%)
0.047	0.21	1.1	0.21/0.27	5	46	20.4	250	5	15.28 (9.34%)
0.047	0.21	1.1	0.21/0.27	5	46	20.4	280	5	15.92 (10.43%)
0.055	0.22	1.1	0.21/0.27	5	46	20.4	300	5	16.20 (12.29%)

Characterization. Samples for TEM analysis were prepared by dropping a dilute toluene solutions of NWs onto 300-mesh carbon-coated copper grids. TEM images were recorded using a JEOL 2000 FX microscope operating at 200 kV. The diameter distribution for each sample was determined using several TEM images at 500K magnification to ensure accurate measurement. The wire diameters were measured and recorded using Image-Pro Express software (version 4.5), and the distribution histograms were constructed from 400-500 diameter measurements for each specimen. HRTEM images were recorded on a JEOL JEM-2100F microscope operating at 200 kV. UV-visible absorption spectra were recorded on a Varian Cary 100E spectrophotometer at room temperature. The NW solution was prepared by diluting the purified NW sample with a certain amount of toluene in a 1-cm path-length quartz cuvette, and the baseline correction was performed prior to each measurement. Photoluminescence (PL) spectra were taken on a Varian Cary Eclipse fluorescence spectrophotometer at room temperature. Powder XRD scans were recorded on a Rigaku D-MAX/A diffractometer operating at 35 kV and 35 mA (Cu Kα irradiation, $\lambda = 1.542$ Å).

References:

1. Yu, H.; Li, J. B.; Loomis, R. A.; Gibbons, P. C.; Wang, L. W.; Buhro, W. E. *Journal of the American Chemical Society* **2003,** 125, (52), 16168-16169.

2. Sun, J.; Wang, L. W.; Buhro, W. E. *Journal of the American Chemical Society* **2008,** 130, (25), 7997-8005.

3. Sun, J. W.; Buhro, W. E. *Angewandte Chemie-International Edition* **2008,** 47, (17), 3215-3218.

4. Dong, A. G.; Wang, F. D.; Daulton, T. L.; Buhro, W. E. *Nano Letters* **2007,** 7, (5), 1308-1313.

5. Yu, H.; Buhro, W. E. *Advanced Materials* **2003,** 15, (5), 416-+.

6. Dong, A.; Yu, H.; Wang, F.; Buhro, W. E. *Journal of the American Chemical Society* **2008,** 130, (18), 5954-5961.

7. Wang, F.; Yu, H.; Li, J.; Hang, Q.; Zemlyanov, D.; Gibbons, P. C.; Wang, L. W.; Janes, D. B.; Buhro, W. E. *Journal of the American Chemical Society* **2007,** 129, (46), 14327-14335.

8. Wang, F. D.; Yu, H.; Jeong, S. H.; Pietryga, J. M.; Hollingsworth, J. A.; Gibbons, P. C.; Buhro, W. E. *Acs Nano* **2008,** 2, (9), 1903-1913.

9. Trentler, T. J.; Hickman, K. M.; Goel, S. C.; Viano, A. M.; Gibbons, P. C.; Buhro, W. E. *Science* **1995,** 270, (5243), 1791-1794.

10. Sun, J. W.; Buhro, W. E.; Wang, L. W.; Schrier, J. *Nano Letters* **2008,** 8, (9), 2913-2919.

11. Manna, L.; Scher, E. C.; Alivisatos, A. P. *Journal of the American Chemical Society* **2000,** 122, (51), 12700-12706.

12. Aruguete, D. M.; Marcus, M. A.; Li, L. S.; Williamson, A.; Fakra, S.; Gygi, F.; Galli, G. A.; Alivisatos, A. P. *Journal of Physical Chemistry C* **2007,** 111, (1), 75-79.

13. Li, L. S.; Alivisatos, A. P. *Physical Review Letters* **2003,** 90, (9), -.

14. Steiner, D.; Katz, D.; Millo, O.; Aharoni, A.; Kan, S.; Mokari, T.; Banin, U. *Nano Letters* **2004,** 4, (6), 1073-1077.

15. Millo, O.; Katz, D.; Steiner, D.; Rothenberg, E.; Mokari, T.; Kazes, M.; Banin, U. *Nanotechnology* **2004,** 15, (1), R1-R6.

16. Grebinski, J. W.; Hull, K. L.; Zhang, J.; Kosel, T. H.; Kuno, M. *Chemistry of Materials* **2004,** 16, (25), 5260-5272.

17. Protasenko, V. V.; Hull, K. L.; Kuno, M. *Advanced Materials* **2005,** 17, (24), 2942-+.

18. Protasenko, V.; Bacinello, D.; Kuno, M. *Journal of Physical Chemistry B* **2006,** 110, (50), 25322-25331.

19. Robel, I.; Bunker, B. A.; Kamat, P. V.; Kuno, M. *Nano Letters* **2006,** 6, (7), 1344-1349.

20. Wang, F. D.; Dong, A. G.; Sun, J. W.; Tang, R.; Yu, H.; Buhro, W. E. *Inorganic Chemistry* **2006,** 45, (19), 7511-7521.

21. Glennon, J. J.; Tang, R.; Buhro, W. E.; Loomis, R. A. *Nano Letters* **2007,** 7, (11), 3290-3295.

22. Wang, F. D.; Tang, R.; Buhro, W. E. *Nano Letters* **2008,** 8, (10), 3521-3524.

23. Wang, F. D.; Tang, R.; Yu, H.; Gibbons, P. C.; Buhro, W. E. *Chemistry of Materials* **2008,** 20, (11), 3656-3662.

24. Yu, W. W.; Wang, Y. A.; Peng, X. G. *Chemistry of Materials* **2003,** 15, (22), 4300-4308.

25. Majumder, F. A.; Swoboda, H. E.; Kempf, K.; Klingshirn, C. *Physical Review B* **1985,** 32, (4), 2407-2418.

26. Murray, C. B.; Norris, D. J.; Bawendi, M. G. *Journal of the American Chemical Society* **1993,** 115, (19), 8706-8715.

27. Qu, L. H.; Peng, Z. A.; Peng, X. G. *Nano Letters* **2001,** 1, (6), 333-337.

28. Peng, Z. A.; Peng, X. G. *Journal of the American Chemical Society* **2002,** 124, (13), 3343-3353.

29. Qu, L. H.; Peng, X. G. *Journal of the American Chemical Society* **2002,** 124, (9), 2049-2055.

30. Liu, H. T.; Owen, J. S.; Alivisatos, A. P. *Journal of the American Chemical Society* **2007,** 129, (2), 305-312.

31. Talapin, D. V.; Rogach, A. L.; Kornowski, A.; Haase, M.; Weller, H. *Nano Letters* **2001,** 1, (4), 207-211.

32. Hines, M. A.; Guyot-Sionnest, P. *Journal of Physical Chemistry B* **1998,** 102, (19), 3655-3657.

33. Norris, D. J.; Vlasov, Y. A. *Advanced Materials* **2001,** 13, (6), 371-376.

34. Li, Z.; Kornowski, A.; Myalitsin, A.; Mews, A. *Small* **2008,** 4, (10), 1698-1702.

35. Donega, C. D.; Hickey, S. G.; Wuister, S. F.; Vanmaekelbergh, D.; Meijerink, A. *Journal of Physical Chemistry B* **2003,** 107, (2), 489-496.

Chapter 2

Effects of TOPO impurities during the SLS growth of the CdSe quantum wires

Introduction

Chemical modification of nanocrystal surfaces is fundamentally important to their assembly, their implementation in biology and medicine, and greatly impacts their electrical and optical properties.[1] However, it remains a major challenge owing to a lack of analytical tools to directly determine nanoparticle surface structures.[2] The nature and strength of the interaction between the ligands and the surface atoms of nanocrystals determine the stability of the nanocrystal-ligand complexes. The stability of nanocrystal-ligand complexes has become a focus of study in recent years because several promising applications of nanocrystals, such as biomedical labeling, and light-emitting diodes using semiconductor nanocrystals, seem to be limited by their stability.[1, 3]

Our successful SLS synthesis gives the best morphology control and photoluminescence efficiency of 1-D CdSe nanowires.[4, 5] Tri-*n*-octylphosphine oxide (TOPO) is the major reaction solvent for our CdSe nanowire syntheses, and it is one of the surface ligands of the quantum wires as described in Chapter 1. I found significant irreproducibility problems in the synthesis of CdSe nanowires upon using different batches of commercial TOPO (Figure 2-1). These problems were ultimately traced to the presence of adventitious impurities in the TOPO,[6] as detailed in this chapter.

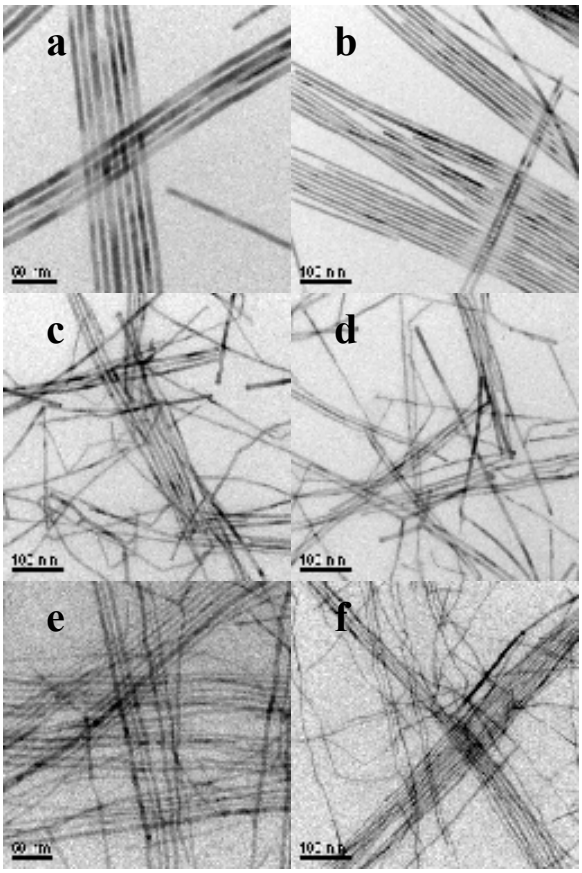

Figure 2-1. Representative TEM images of CdSe quantum wires grown in TOPO A (a and b),TOPO F (c and d), and distilled TOPO F (e and f)

From the TEM images, the original CdSe nanowires prepared using a good batch of TOPO (batch #00529CD, hereafter TOPO A) were long and straight with good morphology control (Figure 2-1a and b) and fairly good photoluminescence quantum efficiency. When I changed to a new batch of TOPO (batch #03003CE, hereafter TOPO F), the quality of the CdSe nanowires was greatly reduced. The wires synthesized in TOPO F were short, with large diameter distributions (Figure 2-1c and d), and poor quantum efficiency compared to the nanowires synthesized

in TOPO A. Such TOPO-induced irreproducibility could have three possible origins. (1) Essential, beneficial impurities may be present in good TOPO, in which high-quality nanowires may be prepared, but absent in other batches. (2) Harmful impurities may be present in bad TOPO, but absent in good TOPO. (3) Batch-to-batch variations in the concentrations of either beneficial or harmful impurities may be responsible for the synthetic irreproducibility. I purified TOPO F and used it to synthesize the CdSe nanowires. However, the nanowires synthesized in distilled TOPO F did not show improved quality (Figure 2-1e, f). This result eliminated the possibility of harmful impurities in TOPO F. There must be some beneficial impurities in TOPO A that were helping the morphology control of the CdSe nanowires.

TOPO has long been used for acetic-acid recovery[7] and metal-ion extraction.[8] It is currently available under the trade name CYANEX 921 for these purposes. In the 1980s, the synthesis of semiconductor nanoparticles in reverse micelles was introduced.[9-16] During that early synthetic era, the Bell Laboratories group discovered that poorly crystalline CdSe nanoparticles prepared in reverse micelles could be ripened and recrystallized in *n*-Bu_3P/*n*-Bu_3PO mixtures.[17, 18] The phosphine-oxide component was found necessary to the process. Shortly thereafter, Murray, Norris, and Bawendi introduced an organometallic synthesis of CdE nanocrystals (E=S, Se and Te) using *n*-$octyl_3P$ (TOP)/TOPO solvent mixtures,[19] which constituted a breakthrough in the preparation of semiconductor nanocrystals. Subsequently, TOP and TOPO mixtures were employed as solvents in a wide range of nanocrystal syntheses.[20-55] More recently, "greener" syntheses

of quantum dots and quantum rods employing non-coordinating solvents have emerged.[56-60] However, TOPO remains an important option for the synthesis of semiconductor nanocrystals[1, 61-71].

The likely participation of adventitious TOPO impurities in nanocrystal growth has been recognized for many years.[29] TOPO is available from research-chemical suppliers in nominal 90%-purity (technical) and 99%-purity grades. In 2000, Alivisatos and coworkers reported that CdSe quantum rods grew at a slower rate and with better shape control in 90%-purity-grade TOPO than in 99%-purity-grade TOPO, apparently as a result of impurities present in the 90%-purity-grade solvent.[29] The active impurities were presumed to be alkylphosphonic and/or alkylphosphinic acids. Purposeful addition of hexylphosphonic acid (HPA) to 99%-purity-grade TOPO allowed the synthesis of CdSe quantum rods in a more controlled and reproducible manner,[29] initiating extensive subsequent research activities and interest in semiconductor quantum rods. A separate study by Alivisatos and coworkers found that the growth kinetics and morphologies of hyperbranched nanocrystals varied when using 99%-purity-grade TOPO from different batches and/or suppliers.[72] A related synthetic reproducibility problem was also reported for the growth of CdSe quantum dots, but attempts to analyze the influential TOPO impurities were unsuccessful.[73] Similarly, we have experienced significant synthetic-irreproducibility problems in the growth of CdSe quantum wires[5, 74] using various batches of 99%-purity-grade TOPO.[6]

Unfortunately, only a few of the phosphinic and phosphonic acids are commercially available. The initial attempts to gain morphology control were

performed by adding commercially available tetradecylphosphonic acid (TDPA) and diphenylphosphinic acid (DPPA) into the reaction system with a new batch of TOPO (batch #08716AH, hereafter TOPO C) used (Figure 2-2). Neither result was satisfactory. The sample with TDPA did not show impoved morphology control, but did show the improvement in optical properties, which I will discuss in Chapter 3. The sample with DPPA showed improvement in the length of the CdSe nanowires, but the wires contained bends and exhibited a broad diameter distribution.

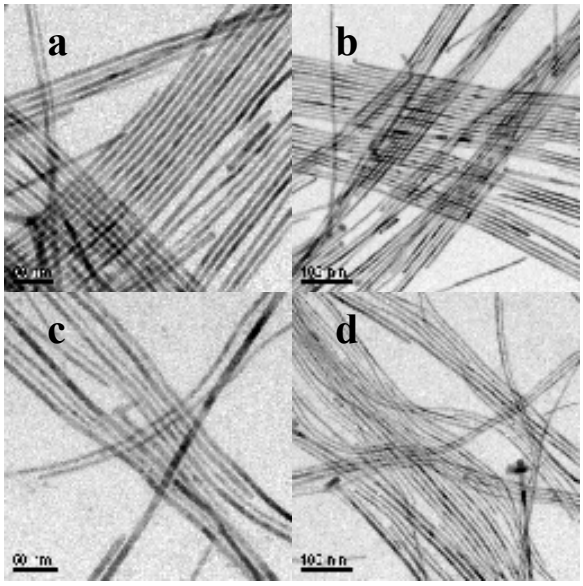

Figure 2-2. Representative TEM images of CdSe QWs grown in TOPO C with additional TDPA (a and b), and additional DPPA (c and d).

The 90%-purity-grade TOPO is known to contain a variety of phosphorus-containing impurities (Figure 2-3): *n*-octylphosphonic acid (OPA), mono-*n*-octylphosphinic acid (MOPA), di-*n*-octylphosphine oxide (DOPO), di-*n*-octylphosphinic acid (DOPA), and *n*-octyl di-*n*-octylphosphinate (ODOP).[75] The 99%-purity-grade TOPO contains some of the same impurities, in smaller amounts.[6, 69] Although such impurities were believed to influence the quality, morphology, and growth kinetics of quantum dots and quantum rods,[27, 29, 73] the active impurities had not been specifically identified until recent work from our group.[6]

In this Chapter, I will compare the results of CdSe nanowire syntheses in different batches of commercially obtained TOPO to the results obtained by adding possible impurities into the reaction system. The various batches and impurities are analyzed by ^{31}P NMR spectroscopy. The results establish the influences of individual TOPO impurities on CdSe quantum wire growth. In this work, DOPA is proven to be the essential impurity for the synthesis of high-quality CdSe quantum wires.

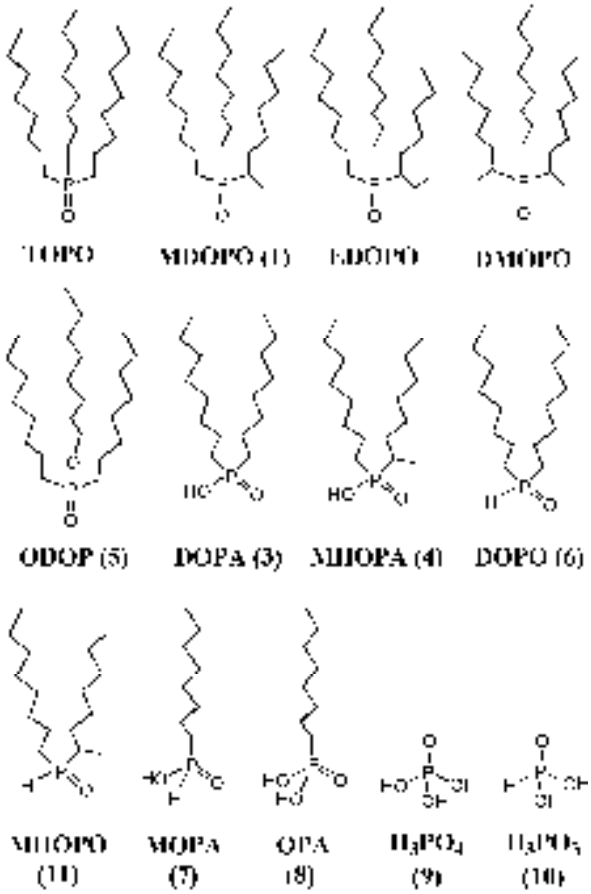

Figure 2-3. The structures of various TOPO impurities or suspected impurities. EDOPO and DMOPO are not found in commercial TOPO samples

Results

Synthesis of CdSe quantum wires in various batches of TOPO and with different additives

I compared the synthetic utility of three batches of 99%-purity-grade and several batches of 90%-purity-grade TOPO. I am labeling the three 99%-purity specimens TOPO A, TOPO F, and TOPO C, corresponding to the excellent, failed, and intermediate synthetic results achieved in each of these specimens, respectively. The Aldrich batch numbers for the 99% and 90%-purity specimens employed are listed in the Experimental Section.

The synthetic procedure for the SLS growth of CdSe nanwires was described in Chapter 1. As mentioned above, high-quality CdSe nanowires were not reproducibly synthesized in the various 99%-purity TOPO batches. The nanowires grown in TOPO A were long (> 5 μm) and straight, with uniform diameters along their lengths and narrow diameter distributions (Figure 2-1a and b). In contrast, the nanowires grown in TOPO F were short (<1 μm), and exhibited kinks, branches, diameter fluctuations, and wide diameter distributions (Figure 2-1c and d). The quality of the nanowires grown in TOPO C (Figure 2-4a and b) was clearly improved over those from TOPO F; however, it was less than that of the nanowires grown in TOPO A. This indicated some beneficial impurity is present in TOPO C that is not in TOPO F. However, the concentration of the impurity or impurities in TOPO A and TOPO C is different.

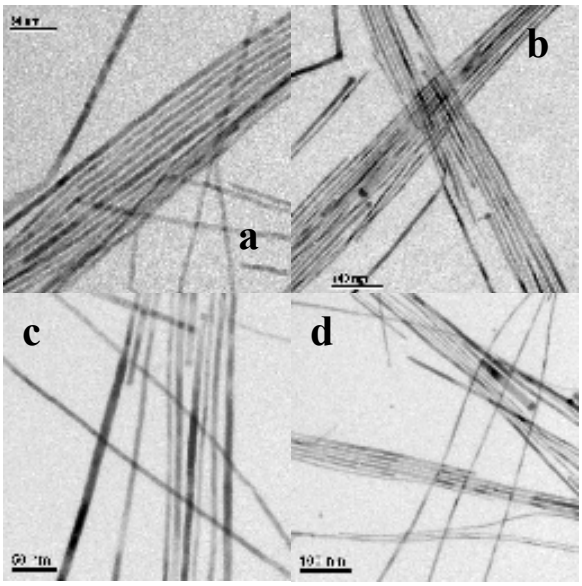

Figure 2-4. Representative TEM images of CdSe nanowires made from TOPO C (#08716AH) (a, b) and purified TOPO C (c, d)

The purified TOPO C (Figure 2-4c and d) did not produce good diameter control, further proving the lack of some beneficial impurity.

The varying qualities of these nanowire specimens were also evident in the absorption spectra (Figure 2-5). The first four excitonic features were sharper and better resolved for nanowires grown in good TOPO as compared to those grown in TOPO C or TOPO F.

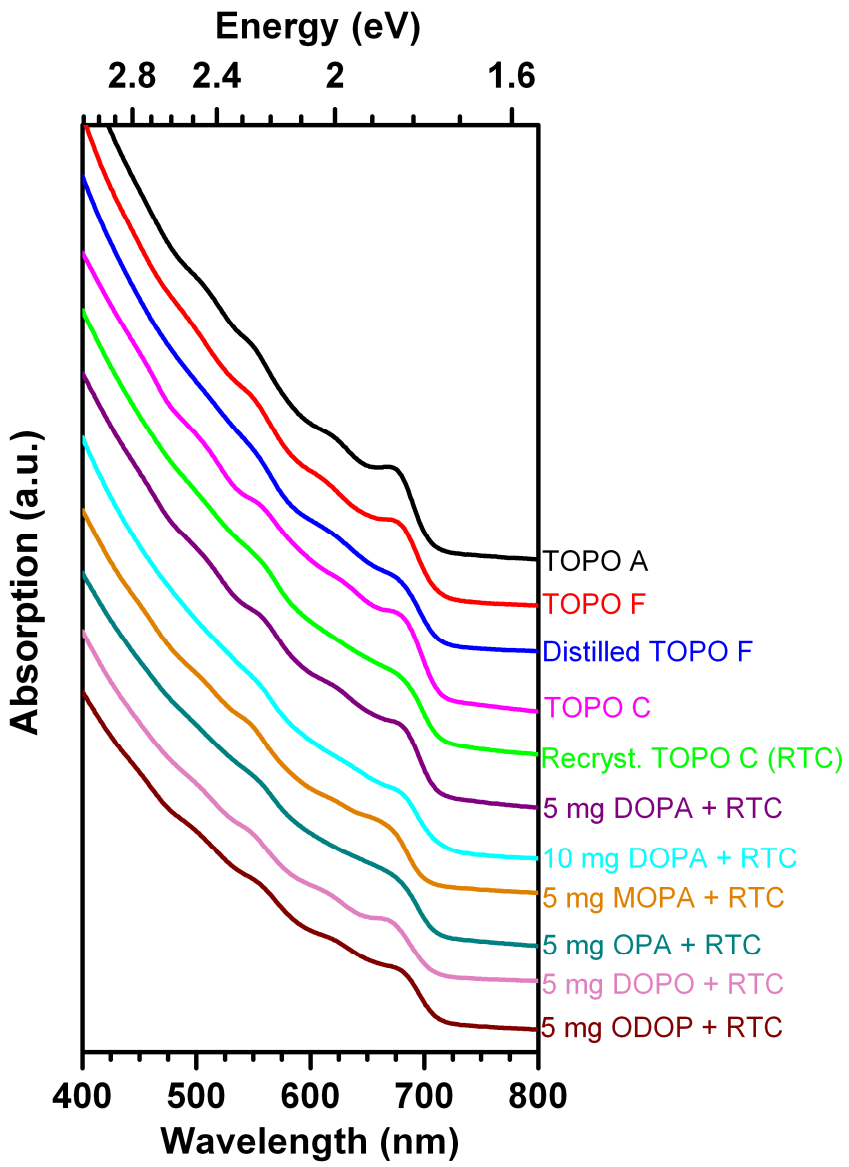

Figure 2-5. Absorption spectra of CdSe QWs grown in various TOPO batches in the presence of additives. The absorption spectra are offset for clarity.

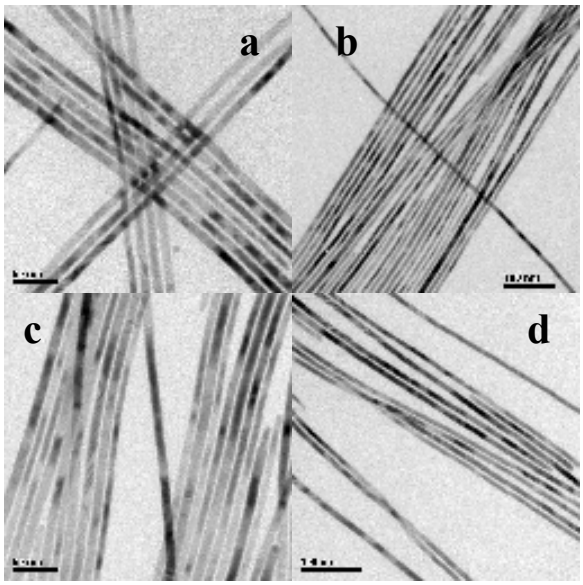

Figure 2-6. Representative TEM images of CdSe nanowires made from TOPO F + 10 mg of DOPA (a, b), and + 20 mg of DOPA (c, d)

Figure 2-6 shows representative TEM images of CdSe nanowires synthesized in the TOPO F with added DOPA (Figure 2-3). The nanowires grown with DOPA showed greatly improved morphology control compare to those grown in TOPO F only samples (Figure 2-1c and d). The CdSe nanowires were straight, long, and uniform in diameter along the length. Kinks and branches observed when using TOPO F alone were not found under this reaction condition.

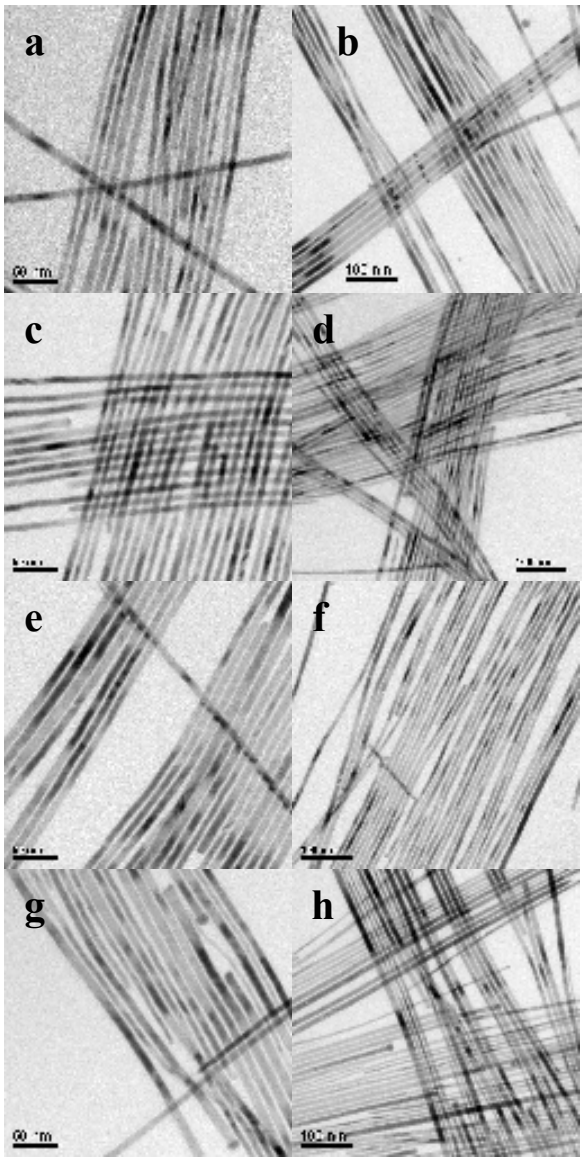

Figure 2-7. Representative TEM images of CdSe nanowires made from TOPO C + 5 mg of DOPA (a, b), + 10 mg of DOPA (c, d), + 20 mg of DOPA (e, f), and + 100 mg of DOPA (g, h).

Figure 2-7 shows representative TEM images of CdSe nanowires synthesized in TOPO C with added DOPA. These nanowires were straighter, much longer, and exhibited narrower distributions and more-uniform diameters

along their length than did those grown in TOPO C only (Figure 2-4a and b). However, too much added DOPA was harmful to the morphology control of the CdSe nanowires. Addition of 100 mg of DOPA into the reaction system caused nanowire precipitation after 2 min of reaction time. Although there were CdSe nanowires in the precipitates, the diameter and length control were not good (Figure 2-7g and h).

Figure 2-8 shows representative TEM images of CdSe nanowires synthesized in purified TOPO C with added DOPA. Similar results were obtained as with adding DOPA into TOPO F or TOPO C described above. The CdSe nanowires were straight, long, and with good diameter control, showing significant improvement from the nanowires synthesized without DOPA (Figure 2-4c and d). As above, increasing the amount of DOPA did not further improve the quality of the nanowires. For example, 20 mg of DOPA in purified TOPO C gave poorer quality compared to 5 mg and 10 mg of added DOPA. The best amount seems to be 5 mg of DOPA in 5 g of TOPO. This result can be seen in all the 3 cases in which I added DOPA (Figure 2-6, 2-7 and 2-8).

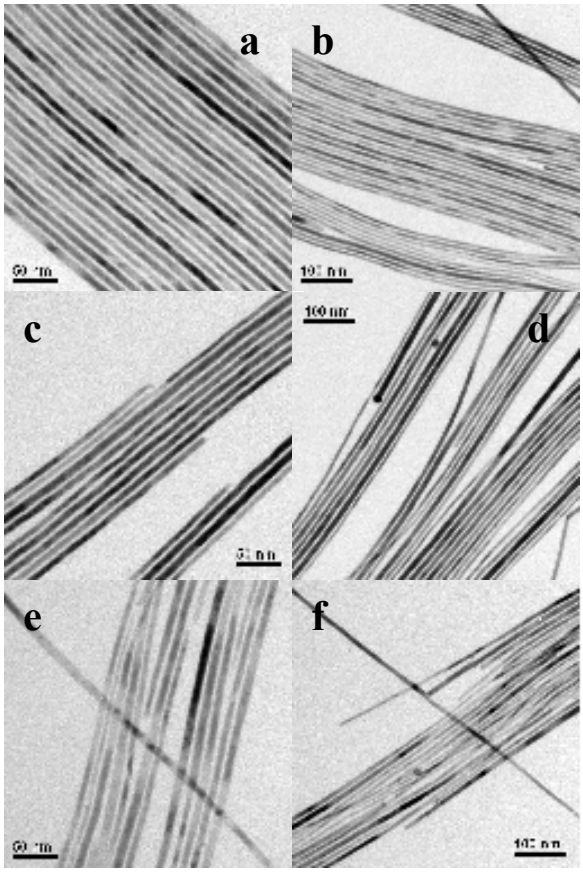

Figure 2-8. Representative TEM images of CdSe nanowires made from purified TOPO C + 5 mg of DOPA (a, b), + 10 mg of DOPA (c,d), and + 20 mg of DOPA (e, f)

The additives MOPA and OPA were similarly found to have beneficial effects on CdSe nanowires growth, but less than those achieved with DOPA. Figure 2-9 shows representative TEM images of CdSe nanowires synthesized in TOPO F with added OPA and MOPA. Both experiments showed improved straightness and diameter distribution of the nanowires relative to the sample without the additives (Figure 2-1c and d). But the length of the CdSe nanowires was less satisfactory, and usually less than 2 μm. I also observed a small amount

of CdSe quantum dots forming in these syntheses, which are also evident in the TEM images.

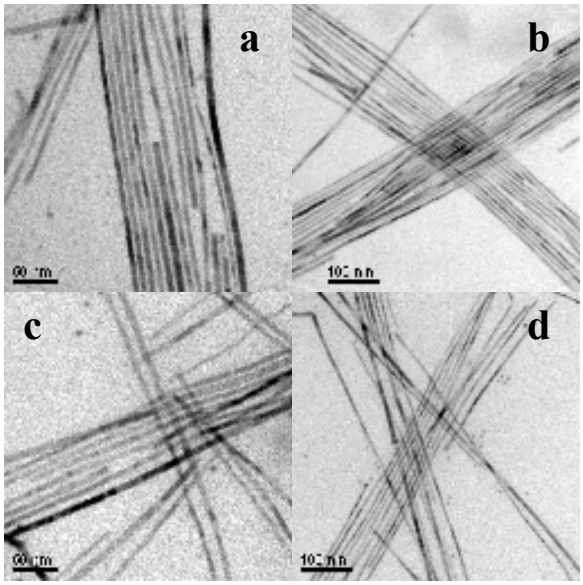

Figure 2-9. Representative TEM images of CdSe nanowires made from TOPO F + 10 mg OPA (a, b), + 12 mg MOPA (c, d),

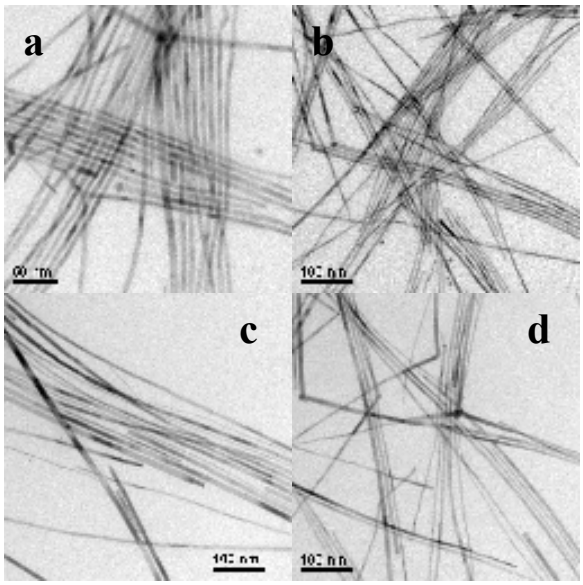

Figure 2-10. Representative TEM images of CdSe nanowires made from TOPO C + 12 mg of MOPA (a, b), + 33 mg of MOPA (c, d).

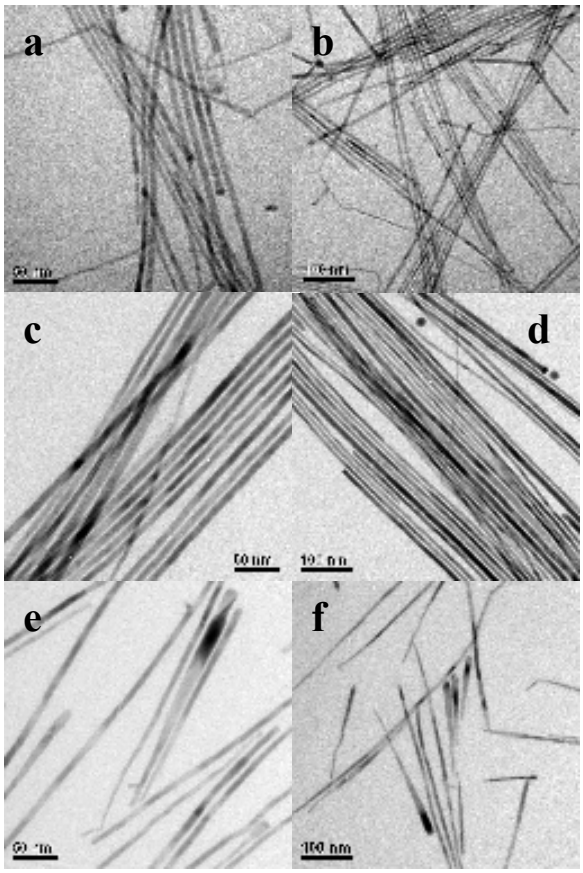

Figure 2-11. Representative TEM images of CdSe nanowires made from purified TOPO C + 5 mg of MOPA (a, b), + 12 mg of MOPA (c,d), and + 24 mg of MOPA (e, f).

Figure 2-10 and 2-11 show representative TEM images of CdSe nanowires synthesized in TOPO C and purified TOPO C with different amounts of added MOPA. The wire quality was slightly improved, but not as satisfactory as that achieved by adding DOPA. Furthermore, an increased amount of MOPA resulted in shorter wires. The length of the nanowires produced was less than 500 nm, and the wires were observed to be tapered (Figure 2-11 e and f).

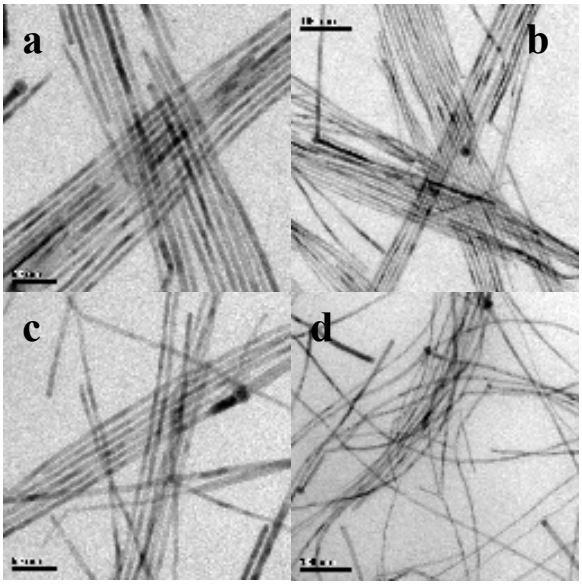

Figure 2-12. Representative TEM images of CdSe nanowires made from TOPO C + 10 mg of OPA (a, b), and 30 mg of OPA (c, d)

Figure 2-12 and 2-13 show representative TEM images of CdSe nanowires synthesized from TOPO C and purified TOPO C with different amounts of added OPA. Straight nanowires having lengths of < 2 μm and uniform diameters along their lengths were grown in the presence of a small amount of OPA (Figure 2-13a and b). Larger amount of OPA induced short (< 1 μm), bent (Figure 2-12d), and branched (Figure 2-12c) wires, with poorer diameter control and diameter fluctuations along the wire. From these results, neither MOPA nor OPA could reproduce the optimal results obtained with DOPA.

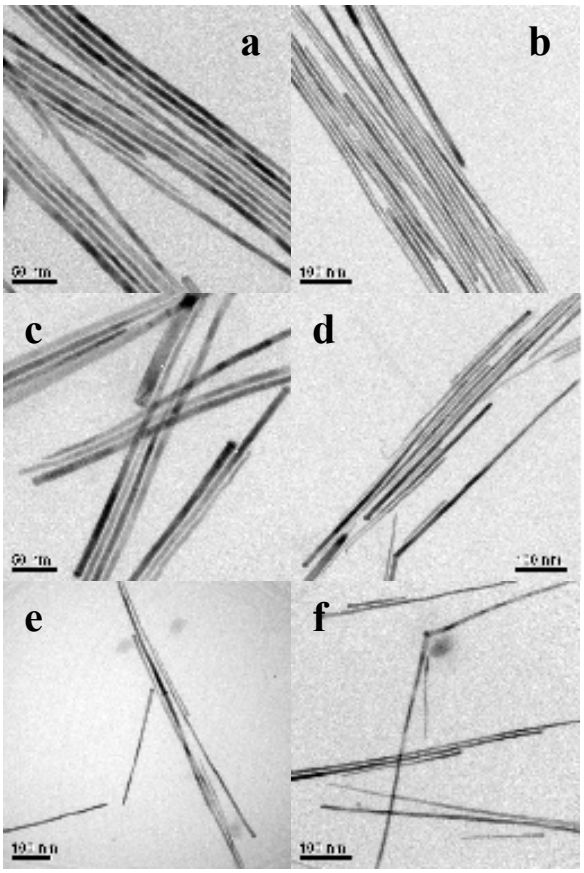

Figure 2-13. Representative TEM images of CdSe nanowires made from purified TOPO C + 5 mg of OPA (a, b), + 10 mg of OPA (c, d) and + 20 mg of OPA (e, f).

Other additives were found to have deleterious effects on CdSe nanowire growth. Figure 2-14 and 2-15 show the representative TEM images of CdSe nanowires synthesized from TOPO C and purifed TOPO C with different amounts of DOPO added. Even in a small amount (i.e. 5 mg, 0.1 mol %), DOPO induced the growth of CdSe quantum dots (Figure 2-15a and b), while the nanowire quality was not improved. In larger amount, even more quantum dots were

formed (Figure 2-14c and d). When 1 g of DOPO (20% of the reaction solution) was used, almost no CdSe nanowires were formed. The majority of the product was CdSe quantum dots (Figure 2-14e and f).

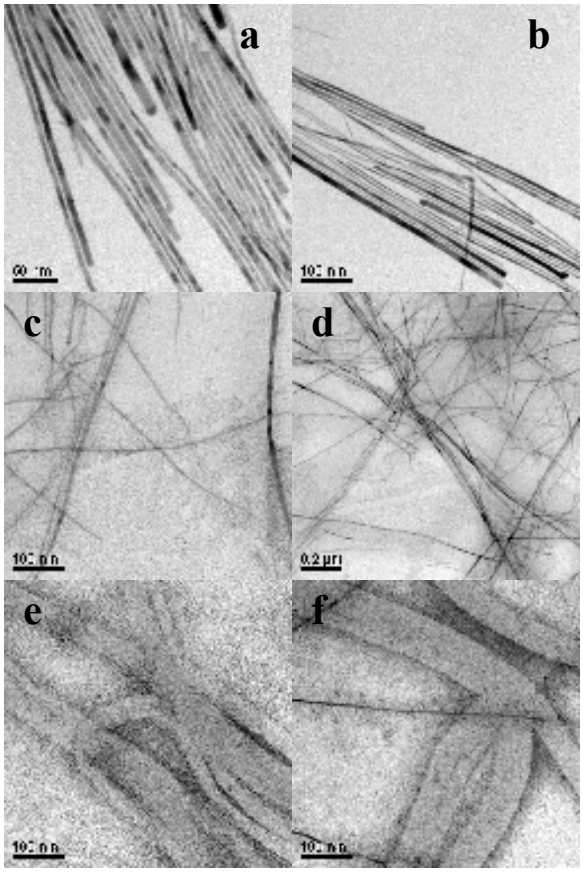

Figure 2-14. Representative TEM images of CdSe nanowires made from TOPO C + 10 mg of DOPO (a, b), + 100 mg of DOPO (c,d), and +1 g of DOPO (e, f).

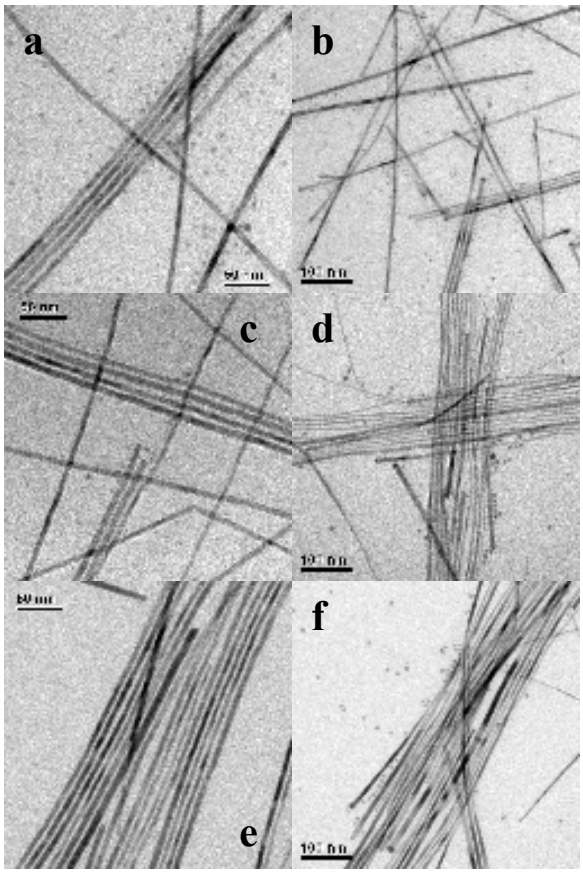

Figure 2-15. Representative TEM images of CdSe nanowires made from purifed TOPO C + 5 mg of DOPO (a, b), 10 mg of DOPO (c, d) and 20 mg of DOPO (e, f).

Figure 2-16 shows representative TEM images of CdSe nanowires synthesized in purified TOPO C with different amounts of added ODOP. These nanowires were short (< 1 μm), with kinks and branching (Figure 2-16e and f).

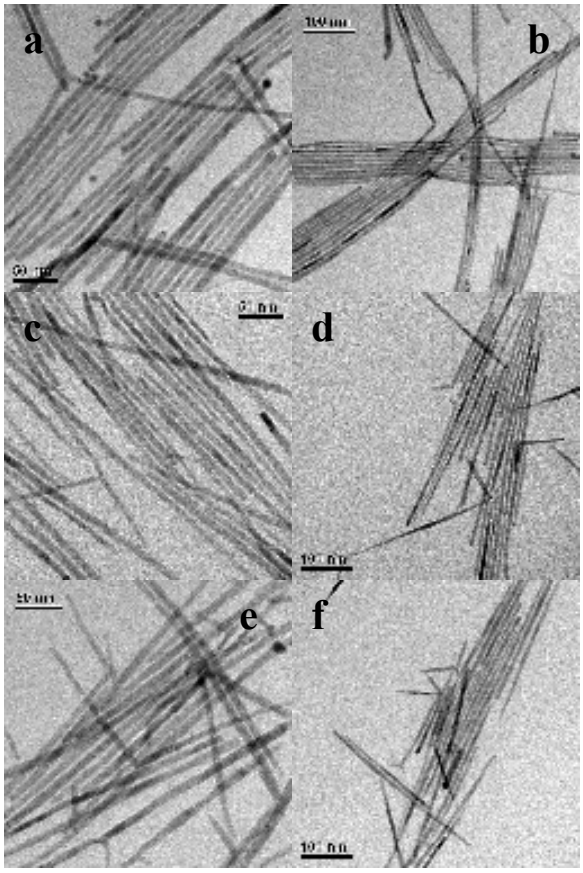

Figure 2-16. Representative TEM images of CdSe nanowires made from purifed TOPO C + 5 mg of ODOP (a, b), 10 mg of ODOP (c, d) and 20 mg of ODOP (e, f)

The syntheses of the CdSe nanowires with added H_3PO_3 (4 mg, 0.4 mol %) and H_3PO_4 (5 mg, 0.4mol %) were not successful. Insoluble white suspensions were generated when H_3PO_3 or H_3PO_4 combined with precursor mixtures containing CdO, oleic acid (OA), HDA, and TOPO. No nanowires or other CdSe nanostructures were subsequently produced from the corresponding reaction mixtures.

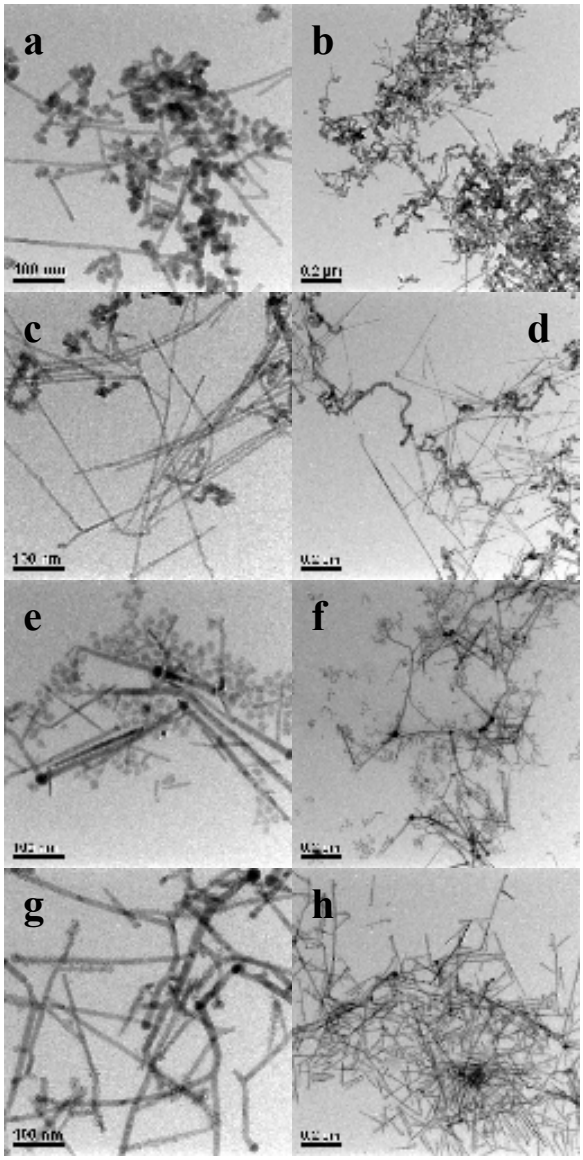

Figure 2-17. Representative TEM images of CdSe nanowires made from various 90% TOPO samples: 04220MB (a, b), 08506DD (c, d), 06520ED (e, f) and 04301BA (g, h).

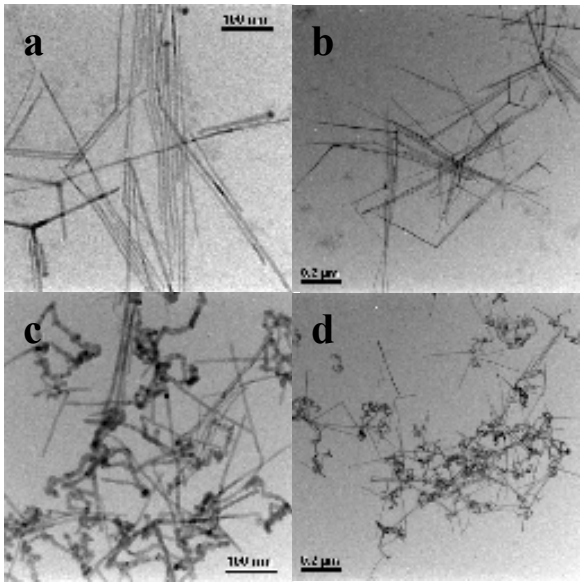

Figure 2-18. Representative TEM images of CdSe nanowires made from various 90% TOPO samples: 06820CH (a, b), and distilled 04220MB

The quality of the CdSe nanowires grown in 90% TOPO samples was even lower than that of nanowires grown in the 99% TOPO samples. Poorly formed wires, other irregularly shaped nanocrystals, and the occasional presence of dots indicated poor control over wire growth, which we attributed to the presence of impurities in the TOPO samples (Figure 2-17 and 2-18). Notably, a single recrystallization or distillation of 90% TOPO was insufficient to completely remove all harmful impurities, and such samples may also lack the beneficial impurity of DOPA (Figure 2-18 c and d).

We demonstrated the growth of high-quality CdSe nanowires from the initially unsuccessful 99% TOPO specimens (TOPO F, TOPO C and purified TOPO C), by adding to them the beneficial impurity DOPA. The straightness and diameter uniformity of the nanowires were dramatically improved over those achieved in TOPO F, TOPO C or purified TOPO C only. Very narrow size distributions were obtained (Figure 2-19 and Table 2-1).

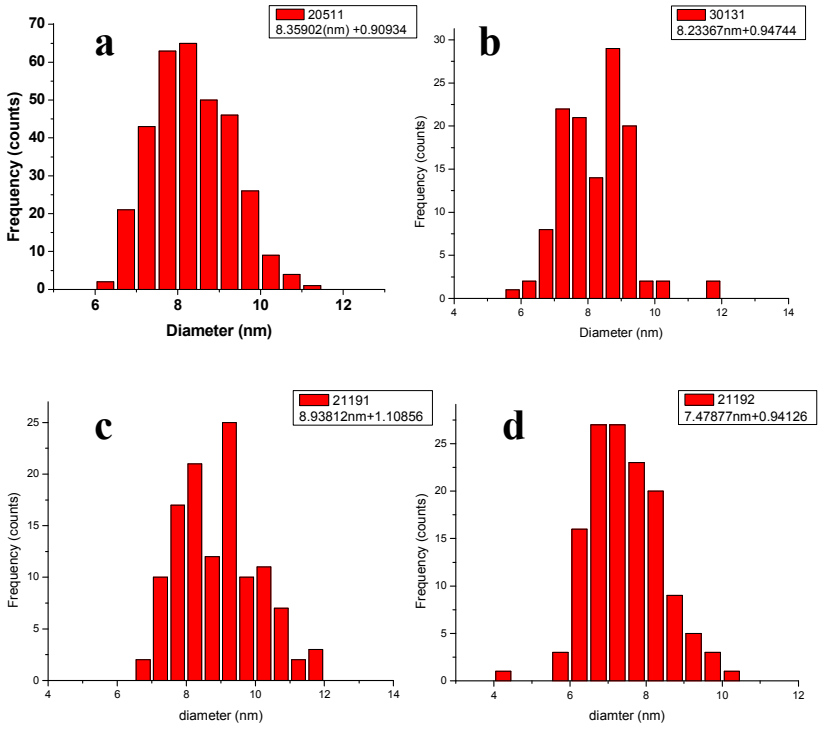

Figure 2-19. Representative histograms of the size of CdSe nanowires made from TOPO C (a), purified TOPO C+ 5 mg of DOPA (b), TOPO F + 10 mg of DOPA (c), and TOPO C + 10 mg of DOPA (d).

Table 2-1 . Diameter of the CdSe nanowires synthesized under different conditions

Sample	#	size
TOPO A	20511	8.4 ± 0.9nm (11%)
TOPO F	20212	7.6 ± 1.0nm (13%)
TOPO C	2109	7.9 ± 1.1nm (14%)
Purified TOPO C (PTC)	30251	8.7 ± 1.9nm (22%)
Purified TOPO F	20431	7.0 ± 1.5nm (21%)
Purified TOPO F #2	30512	7.8 ± 1.6nm (21%)
PTC + 5 mg DOPA	30131	8.2 ± 0.9nm (11%)
PTC + 10 mg DOPA	30151	8.3 ± 0.9nm (11%)
PTC + 20 mg DOPA	30212	8.8 ± 1.0nm (11%)
TOPO F + 10 mg DOPA	21191	8.9 ± 1.1nm (12%)
TOPO F + 12 mg MOPA	21311	7.5 ± 1.1nm (15%)
TOPO F + 10 mg OPA	21071	7.5 ± 1.3nm (17%)
TOPO C + 10 mg DOPA	21192	7.5 ± 0.9nm (12%)
TOPO C + 12 mg MOPA	21352	7.1 ± 1.3nm (18%)
TOPO C + 10 mg OPA	2113	7.5 ± 1.3nm (17%)
PTC + 5 mg MOPA	30312	7.6 ± 1.2nm (16%)
PTC + 12 mg MOPA	30111	8.4 ± 1.2nm (14%)
PTC + 5 mg OPA	30132	7.6 ± 1.5nm (20%)
PTC + 10 mg OPA	30112	8.3 ± 2.1nm (25%)

The results above established that small impurity concentrations dramatically influenced the synthesis of CdSe nanowires. MOPA, OPA and especially DOPA were beneficial at low concentrations, whereas larger amounts were detrimental to the quality of the wires. DOPO, ODOP, H_3PO_3 and H_3PO_4 were deleterious at all concentrations studied. 99% TOPO specimens are sufficiently free of deleterious impurities that only an appropriate concentration of DOPA is required to produce excellent synthetic results. That is, 99% TOPO can probably be used without further purification.

Although the various beneficial and harmful impurities were influential at comparatively low concentrations in TOPO, we note that they were present in molar quantities comparable to those of precursor species such as $Cd(oleate)_2$. For example, a typical, optimized nanowire synthesis employed 0.047 mmol of CdSe and 0.034 mmol of DOPA. Therefore, the impurity levels in the commercially obtained 90% and 99% TOPO specimens, and the optimal levels of beneficial additives to purified TOPO, were stoichiometrically significant.

Discussion

Origins of TOPO impurities. TOPO is manufactured by the sequential radical addition of 1-octene to PH_3, followed by oxidation of the P(III) center (black branch of Figure 2-20). The varying numbers of alkyl chains, oxygen contents, and structures of the chains in the typical TOPO impurities (Figure 2-2) are consistent with this manufacturing process. Figure 2-2 impurities have 0-3 alkyl substituents corresponding to the number of 1-octene addition steps that occur prior to oxidation. Thus, phosphoric acid (**9**) and phosphorous acid (**10**) are derived from oxidation of residual PH_3, MOPA (**7**) and OPA (**8**) from (*n*-octyl)PH_2, and DOPO (**6**) and DOPA (**3**) from (*n*-octyl)$_2$PH (blue branches of Figure 2-20).

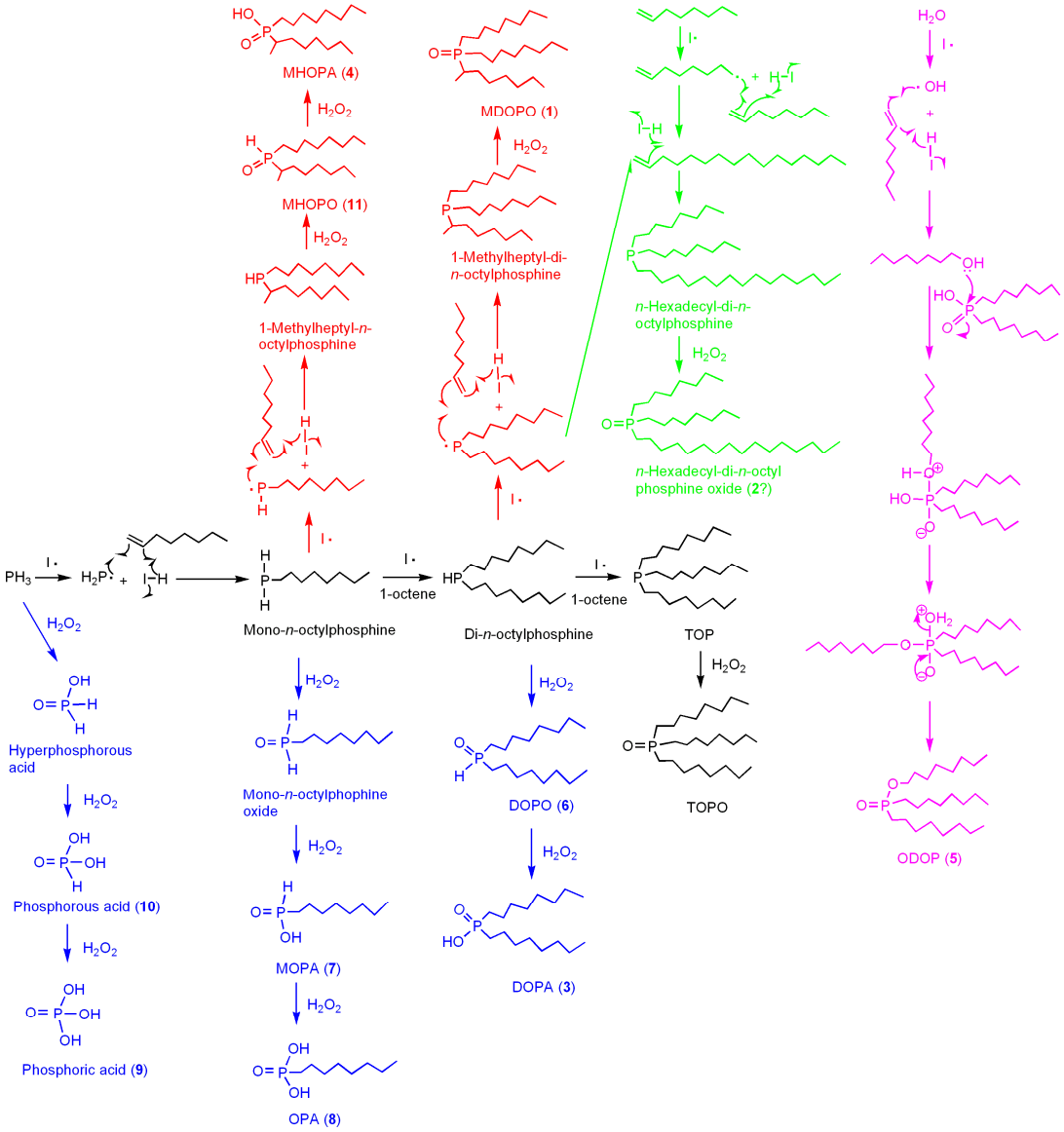

Figure 2-20. Synthetic pathway for the manufacture of TOPO, and proposed pathways for the formation of the common TOPO impurities. The symbol I· represents a radical initiator.

Occasionally, the radical addition occurs with reversed regiochemistry, resulting in a bond between P and C_2 (rather than C_1) of 1-octene. Such reversed additions are responsible for the branched-chain isomers MHOPO (**11**), MHOPA (**4**), and MDOPO (**1**), the predominant TOPO impurity (red branches of Figure 2-20). We propose that ODOP (**5**) results from small amounts of 1-octanol formed in a side reaction (magenta branch of Figure 2-20). Finally, we speculate that the unknown impurity **2** may be a TOPO analog having one hexadecyl chain replacing an octyl chain (green branch of Figure 2-20). This compound may form by radical dimerization of 1-octene to 1-hexadecene, followed by its addition to (*n*-octyl)$_2$PH, and subsequent oxidation of the resulting tertiary phosphine. Although most of these impurities are typically present in sub-percentage quantities, the amounts are stoichiometrically significant for nanocrystal syntheses conducted in TOPO, as noted above.

^{31}P NMR spectroscopic analysis of TOPO impurities. ^{31}P NMR analysis of the impurities preset in commercial TOPO was critically important to this study. These analyses were conducted by Dr. Fudong Wang, whom I thank. I am placing these results in the discussion to emphasize that they are not my own. The ^{31}P{^{1}H} NMR spectra for TOPO specimens used in this study are shown in Figures 2-21. The TOPO resonance appeared at $\delta \approx$ 44.5–46.5 ppm, along with many small resonances arising from impurities. 7–12 impurity peaks were found

in 99% TOPO, whereas over 16 impurity peaks were found in 90% TOPO. The purities of the various TOPO specimens were determined by calibrated integration of the ^{31}P NMR spectra, and were found to vary from 93 to 98 mol % for 99% TOPO, and from 87 to 95 mol % for 90% TOPO.

The impurity species in Figure 2-21 were arbitrarily assigned the compound labels **1**–**16**. TOPO A and TOPO F differed by the presence of impurities **2**, **3**, **4**, **5**, and **11** and a larger amount of impurity **1** in TOPO A (Figure 2-20). The remaining impurities in TOPO A and TOPO F were present in similar amounts, and thus were unlikely to be significantly beneficial or harmful impurities. TOPO C and TOPO F differed by the presence of impurity **6** and larger amounts of impurities **1** and **12** in TOPO F. Comparisons of the amount of impurity **1** present in these three TOPO specimens (3.1 mol % in A, 2.1 mol % in F, and 1.7 mol % in C) suggested that impurity **1** was unlikely a beneficial or harmful impurity. Additionally, the nanowires synthesized in TOPO C before and after recrystallization were of similar quality. We will show below that recrystallization of 99% TOPO reduced all impurity levels, including **1** and **12**, below our ^{31}P NMR detection limit, indicating that impurities **1** and **12**–**16**, which were present in TOPO C, were not significantly influential to the wire growth.

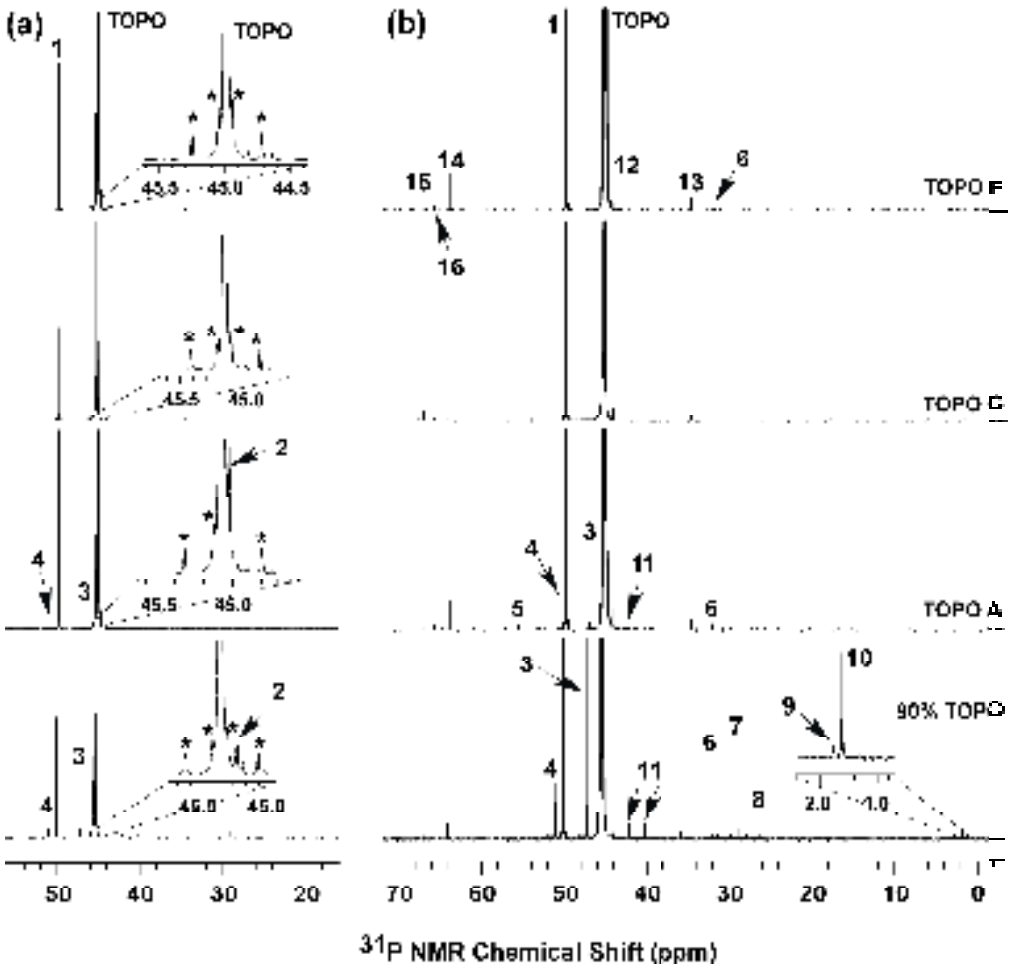

Figure 2-21 . ^{31}P $\{^{1}H\}$ NMR spectra of TOPO F (03008CE), TOPO C (08716AH), TOPO A (00529CD), and 90% TOPO (06520ED) collected in d_6-acetone. The peak intensities for TOPO (~ 45 ppm) were normalized and the impurities were arbitrarily labeled with compound numbers. (a) The TOPO peak intensities were decreased to a lower value to show impurity **1**. Insets: magnified view of the TOPO peaks to show impurity **2** and the ^{13}C satellites (*). (b) The TOPO peak intensities were increased to a higher value to show all the impurity peaks. Inset: magnified view of impurities **9** and **10** in the 90% TOPO (06520ED).

The above reasoning suggested that impurity **6** may have been a harmful impurity in TOPO F, and that impurities **2**, **3**, **4**, **5**, and **11** may have been beneficial impurities in TOPO A. Our next task was thus to identify impurities **2**, **3**, **4**, **5**, **6**, and **11** among the Figure 2-21 substances. Therefore, each of the Figure 2-21 compounds was either obtained commercially or independently synthesized by adapting literature procedures. These independent specimens were used to identify compounds **3**, **4**, **5**, **6**, and **11** by ^{31}P NMR, as described below. Compound **2** has not been positively identified, but is not necessary to the growth of high-quality CdSe nanowires.

Impurity **3** was identified as DOPA by measuring the ^{31}P NMR spectrum of DOPA (d_6-acetone) in the presence and absence of TOPO. Like many Figure 2-21 compounds, DOPA exhibited a concentration-dependent chemical shift in mixtures with TOPO, due to hydrogen bonding. DOPA exhibited a chemical shift of 58.6 ppm in the absence of TOPO (Figure 2-22). However, when a small concentration of DOPA (0.5 mol %) was added to TOPO A, the resonance for impurity **3** was enhanced and shifted to 47.0 ppm (Figure 2-22), slightly downfield of its position in TOPO A and significantly upfield of the chemical shift of "pure" DOPA (in d_6-acetone). As the amount of DOPA added to TOPO A was increased, the impurity-**3** resonance was further enhanced and progressively shifted downfield, towards the position of "pure" DOPA. Consequently, DOPA and **3** are the same substance, with a concentration of 0.44 mol % in TOPO A. DOPA was similarly identified as **3** in 90% TOPO, in which its concentration varied from 0.3–3 mol %.

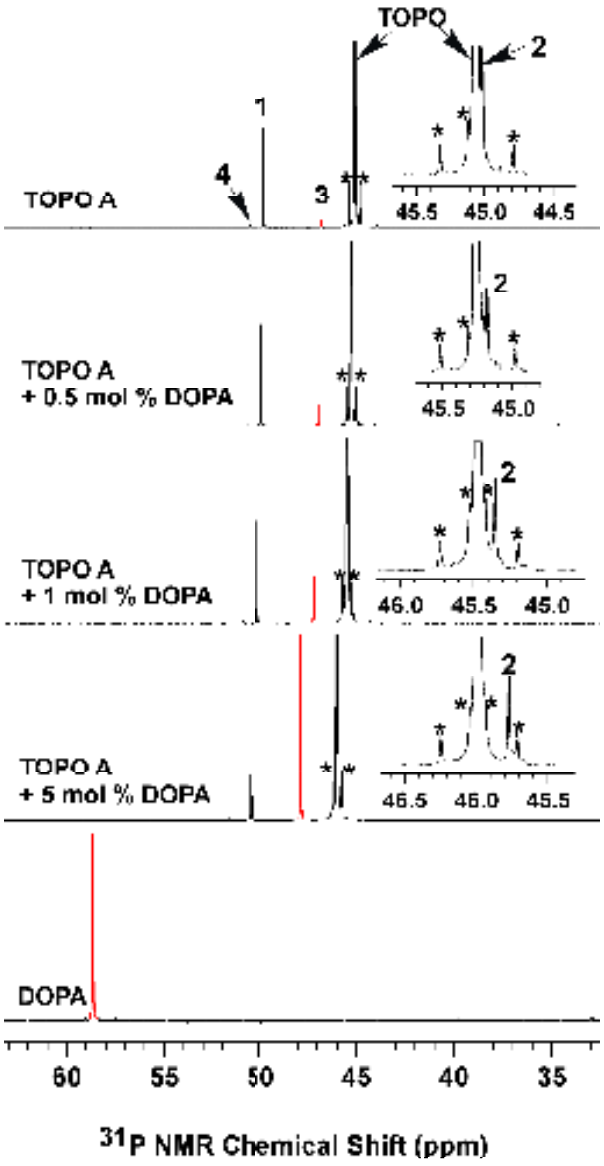

Figure 2-22. $^{31}P\{^{1}H\}$ NMR spectra for identifying DOPA in TOPO A (00529CD). The spectra were collected in d_6-acetone. The peak intensities for TOPO were normalized and the DOPA peaks labeled in red. Note the DOPA resonance in the mixtures shifted upfield from its pure form, whereas the resonance of TOPO and other impurities shifted downfield with increasing DOPA concentration. Insets: magnified view of the TOPO peaks to show the shifting of impurity **2**. The ^{13}C satellites (*) are labeled.

In the course of the DOPA identification, we observed that the impurity-**4** resonance remained a constant 3.8 ppm downfield of the DOPA resonance in TOPO (Figure 2-22), irrespective of the concentration of DOPA and therefore the absolute chemical shift of DOPA (Figures 2-21, and 2-22). Because of its similar spectroscopic behavior, we surmised that impurity **4** was possibly a DOPA isomer with a branched octyl (i.e., 1-methylheptyl) chain. This was confirmed by addition of the DOPA isomer MHOPA (Figure 2-20) into 90% TOPO, for which the MHOPA resonance merged with that of **4**.

Through related ^{31}P NMR experiments, seven additional TOPO impurities were identified as indicated by the compound numbers (labels) in Figure 2-20. The resonance for DOPO added to a 90%-TOPO sample superposed with that of impurity **6**, at 32.1 ppm. The proton-coupled ^{31}P NMR spectrum of DOPO matched that of impurity **6** in 90% TOPO, giving the expected doublet with a coupling constant of $^{1}J_{\text{H-P}}$ = 446 Hz. The most-prominent impurity in nearly all of the TOPO specimens, compound **1**, was confirmed to be the branched-chain TOPO isomer MDOPO. It is neither a harmful or beneficial impurity. Other significant impurities in the 90%-TOPO specimens (but not in the 99% specimens) were MOPA (**7**), OPA (**8**), phosphoric acid (H_3PO_4, **9**) and phosphorous acid (aka phosphonic acid, H_3PO_3, **10**).

As noted above, another prominent impurity, compound **2**, was not positively identified. The ^{31}P NMR chemical shift of **2** was very close to that of TOPO, such that it was always observed on the high-field shoulder of the TOPO resonance (Figure 2-21a). Because the chemical shift of **2** (relative to TOPO) was

unchanged after addition of NH_4OH (aq), it contained no acidic proton and therefore no P-OH group. We concluded that **2** was likely a trialkylphosphine oxide, like TOPO. The two likely branched-chain TOPO isomers EDOPO and DMOPO (Figure 2-20) were synthesized, but their chemical shifts were significantly *downfield* from that of TOPO, excluding them as significant impurities. We speculate that **2** is a trialkylphosphine oxide with two *n*-octyl groups and one longer-chain, *unbranched* substituent. As such its ^{31}P NMR chemical shift and chemical properties would be very similar to those of TOPO.

Conclusion

The solvent TOPO has been critically important to the development of colloidal nanoscience. In TOPO the first modern synthesis of semiconductor quantum dots was achieved. The adventitious impurities in TOPO were responsible for the discovery of semiconductor quantum rods. These impurities significantly influence the rates of nanocrystal formation, the nanocrystal morphologies, and the reproducibilities of nanocrystal syntheses in TOPO. In this Chapter, I have discussed the effects of various TOPO impurities on the synthesis of the CdSe quantum wires. Combined with the results from the ^{31}P NMR study, dioctylphosphinic acid (DOPA) proved to be the important beneficial impurity that helped the nucleation and growth of the CdSe nanowires. With a suitable amount of DOPA added to purified commercial TOPO, we can achieve the best morphology control over the CdSe nanowires. Now the use of purified TOPO with controlled amounts of specific additives will allow rational and reproducible nanocrystal syntheses.

Experimental Section

Materials. *n*-Octylphosphonic acid (OPA, 99%, Lancaster), tri-*n*-octylphosphine (TOP, 90%, Aldrich), oleic acid (OA, 90%, Aldrich), selenium (Se, 99.99%, Aldrich), cadmium oxide (CdO, 99.99%, Aldrich), and 1-octadecene (ODE, 90%, Aldrich) were used as received. *n*-Hexadecylamine (HDA, 90%, Aldrich) was vacuum distilled at 200 °C (~0.1 torr). Tri-*n*-octylphosphine oxide (TOPO, 90% and 99%) specimens were purchased from Aldrich, if not otherwise specified. The batch numbers for the 99% TOPO were 00529CD (TOPO A, for growth of high-quality CdSe quantum wires), 03008CE (TOPO F, resulting in poor-quality CdSe quantum wires), 08716AH (TOPO C, resulting in average-quality CdSe quantum wires). The batch numbers for the 90% TOPO were 04028DJ, 04220MB, 04301BA, 06520ED, 06820CH, 08506DD, B4751105 (Strem), and B1026024 (Strem). A CYANEX 921 sample (batch no. WE7060753B) was provided by Cytec Canada Inc. A 9.0-nm-diameter Bi-nanoparticle stock solution (containing 0.04 mmol Bi atoms/g solution) was prepared as previously described.[76] The TOPSe stock solution was prepared by dissolving Se (4 g, 0.051 mol) into TOP (22 g, 0.059 mol) at ~100 °C under dry, O_2-free N_2 (g). A second portion of Se (1 g, 0.013 mol) was added into the mixture to ensure all TOP had been converted to TOPSe. The liquid fraction of the mixture was subsequently used.

Purification of TOPO. Three TOPO samples were fractionally distilled under vacuum to decrease the concentrations of impurities. TOPO F (03008CE)

was purified by distillation, retaining the fraction transferred between 190–230 °C at 0.35 torr. 90% TOPO (04220MB) was purified by distillation, retaining the fraction transferred between 200–260 °C at 0.5 torr. The Strem 90% TOPO (B4751105) was purified by distillation, retaining the fraction transferred between 180–240 °C at 0.25 torr.

Purified TOPO (~80 g) was obtained via recrystallization of TOPO C (08716AH, 100 g) in acetonitrile (200 mL)[6]. In a similar manner, purified TOPO could be obtained from 90% TOPO by double recrystallization. Briefly, the 90% TOPO (500 g) was dissolved in acetonitrile (2 L) at ~80 °C. The solution was allowed to cool to room temperature to recrystallize the TOPO solute (1–2 days). The white solid isolated by suction filtration was redissolved in acetonitrile (1 L) at ~80 °C. The solution was allowed to cool to room temperature overnight to recrystallize the TOPO solute. Suction filtration yielded shiny, free flowing, needle-like crystals (~250-275 g, 50-55%). If the 90% TOPO appeared to be sticky and oily (i.e., Strem B4751105), a fractional distillation was performed, followed by a double recrystallization (with ~45% overall yield).

Syntheses of TOPO impurities. Syntheses of DOPA[76], MOPA[77], DOPO[77], and ODOP[78] were adapted from literature methods as described previously.

Synthesis of CdSe Nanowires. All synthetic procedures were conducted under dry, O_2-free N_2 (g), but the isolation and purification steps were conducted in the ambient atmosphere. In a typical preparation of high-quality CdSe

nanowires, CdO (6 mg, 0.047 mmol), OA (53 mg, 0.19 mmol), HDA (50 mg, 0.21 mmol), DOPA (10 mg, 0.034 mmol), and 99% or purified TOPO (5 g, 12.9 mmol) were loaded into a 50-mL Schlenk reaction tube. A Bi-nanoparticle stock solution (23 mg, 0.00092 mmol Bi atoms), TOPSe (500 mg, 1.1 mmol), and TOP (100 mg, 0.27 mmol) were combined in a separate vial, which was septum capped. The mixture of Bi nanoparticles and TOPSe was then loaded into a 3-mL syringe. The reaction mixture in the Schlenk tube was degassed under vacuum (0.01–0.1 torr) at 100 °C for 15 min, back-filled with N_2(g), and then inserted into a 320 °C salt bath ($NaNO_3$/KNO_3, 46:54 by weight) to achieve a clear solution. (The time required to dissolve CdO in 90% and 99% TOPO and the optical clarity of the resulting solutions are listed in Table 2-2). The Schlenk tube was switched to a 250 °C salt bath, and the mixture of Bi nanoparticles and TOPSe was quickly injected into the tube. A reddish to brown color resulted in about 5 s. The tube was withdrawn from the bath after 5 min and allowed to cool to room temperature.

The nanowires were isolated as a brown precipitate from a 1-mL aliquot of the reaction mixture (before its solidification, or upon gentle warming to melt the TOPO) by adding toluene (ca. 2 mL) and methanol (ca. 2 mL), followed by centrifugation (benchtop centrifuge) and decanting of the supernatant. The precipitate was redispersed in toluene to form a uniform and optically clear light-brown dispersion for spectroscopic analysis. For TEM analysis, the quantum wire precipitate was subjected to an additional dispersion-centrifugation cycle in a mixture of toluene (ca. 2 mL) and methanol (ca. 6 mL). The nanowires ultimately

were redispersed in toluene. Carbon-coated copper grids were dipped in the toluene solution of quantum wires and then immediately taken out to evaporate the solvent.

Table 2-2. Time required to dissolve CdO in 90% and 99% TOPO, optical clarity of the resulting solutions, and final products in the CdSe quantum wire synthesis.

TOPO samples (batch numbers)	**Time (min)***	Color/clarity of resulting solution	Product
TOPO A (00529	10	colorless/clear	Long (> 5 μm), straight, uniform wires with narrow diameter distributions
TOPO C (08716AH)	20	colorless/clear	Straight wires with broad diameter distributions and intermediate length (< 2 μm)
Recrystallized TOPO C	20	colorless/clear	Wires (similar as TOPO C)
TOPO F (03003CE)	20	slightly yellowish/clear	Short (< 1 μm), kinked, and branched wires with broad diameter distributions
Distilled TOPO F	15	colorless/clear	Wires (with length and straightness improved over TOPO F)
90% (06520ED)	30	whitish/a little opaque	Short, thick, branched, and kinked wires with broad diameter distributions, and nanocrystals
90% (08506DD)	25	slightly yellowish/clear	Short wires and irregularly shaped nanocrystals
90% (04301BA)	25	whitish/a little opaque	Short, thick, branched, and kinked wires with broad diameter distributions, and nanocrystals
90% (04028DJ)	20	whitish/opaque	Very short, branched, and kinked wires, and nanocrystals
90% (04220MB)	45	slightly yellowish/clear	Few short wires and many irregularly shaped nanocrystals
Distilled 04220MB	30	slightly yellowish/clear	Short wires and irregularly shaped nanocrystals
90% (Strem B1026024)	20	pale yellowish/clear	Short, thick, branched, and kinked wires with broad diameter distributions, and nanocrystals
90% (Strem B4751105)	30	whitish/opaque	No products could be isolated
Distilled Strem B4751105	30	whitish/opaque	No products could be isolated
Singly recrystallized 90% (06820CH)	50	grayish, whitish/ opaque	Short and straight wires with occasional branching and kinks, and nanocrystals

References:

1. Owen, J. S.; Park, J.; Trudeau, P. E.; Alivisatos, A. P. *Journal of the American Chemical Society* **2008,** 130, (37), 12279-+.

2. Alivisatos, A. P. *Journal of Physical Chemistry* **1996,** 100, (31), 13226-13239.

3. Munro, A. M.; Plante, I. J. L.; Ng, M. S.; Ginger, D. S. *Journal of Physical Chemistry C* **2007,** 111, (17), 6220-6227.

4. Trentler, T. J.; Hickman, K. M.; Goel, S. C.; Viano, A. M.; Gibbons, P. C.; Buhro, W. E. *Science* **1995,** 270, (5243), 1791-1794.

5. Wang, F. D.; Dong, A. G.; Sun, J. W.; Tang, R.; Yu, H.; Buhro, W. E. *Inorganic Chemistry* **2006,** 45, (19), 7511-7521.

6. Wang, F. D.; Tang, R.; Buhro, W. E. *Nano Letters* **2008,** 8, (10), 3521-3524.

7. Golob, J.; Grilc, V.; Zadnik, B. *Industrial & Engineering Chemistry Process Design and Development* **1981,** 20, (3), 433-435.

8. Flett, D. S. *Journal of Organometallic Chemistry* **2005,** 690, (10), 2426-2438.

9. Meyer, M.; Wallberg, C.; Kurihara, K.; Fendler, J. H. *Journal of the Chemical Society-Chemical Communications* **1984**, (2), 90-91.

10. Lianos, P.; Thomas, J. K. *Chemical Physics Letters* **1986,** 125, (3), 299-302.

11. Fendler, J. H. *Chemical Reviews* **1987,** 87, (5), 877-899.

12. Dannhauser, T.; Oneil, M.; Johansson, K.; Whitten, D.; Mclendon, G. *Journal of Physical Chemistry* **1986,** 90, (23), 6074-6076.

13. Petit, C.; Pileni, M. P. *Journal of Physical Chemistry* **1988,** 92, (8), 2282-2286.

14. Steigerwald, M. L.; Alivisatos, A. P.; Gibson, J. M.; Harris, T. D.; Kortan, R.; Muller, A. J.; Thayer, A. M.; Duncan, T. M.; Douglass, D. C.; Brus, L. E. *Journal of the American Chemical Society* **1988,** 110, (10), 3046-3050.

15. Kortan, A. R.; Hull, R.; Opila, R. L.; Bawendi, M. G.; Steigerwald, M. L.; Carroll, P. J.; Brus, L. E. *Journal of the American Chemical Society* **1990,** 112, (4), 1327-1332.

16. Steigerwald, M. L.; Brus, L. E. *Accounts of Chemical Research* **1990,** 23, (6), 183-188.

17. Bawendi, M. G.; Wilson, W. L.; Rothberg, L.; Carroll, P. J.; Jedju, T. M.; Steigerwald, M. L.; Brus, L. E. *Physical Review Letters* **1990,** 65, (13), 1623-1626.

18. Bawendi, M. G.; Carroll, P. J.; Wilson, W. L.; Brus, L. E. *Journal of Chemical Physics* **1992,** 96, (2), 946-954.

19. Murray, C. B.; Norris, D. J.; Bawendi, M. G. *Journal of the American Chemical Society* **1993,** 115, (19), 8706-8715.

20. Katari, J. E. B.; Colvin, V. L.; Alivisatos, A. P. *Journal of Physical Chemistry* **1994,** 98, (15), 4109-4117.

21. Micic, O. I.; Sprague, J. R.; Curtis, C. J.; Jones, K. M.; Machol, J. L.; Nozik, A. J.; Giessen, H.; Fluegel, B.; Mohs, G.; Peyghambarian, N. *Journal of Physical Chemistry* **1995,** 99, (19), 7754-7759.

22. Guzelian, A. A.; Katari, J. E. B.; Kadavanich, A. V.; Banin, U.; Hamad, K.; Juban, E.; Alivisatos, A. P.; Wolters, R. H.; Arnold, C. C.; Heath, J. R. *Journal of Physical Chemistry* **1996,** 100, (17), 7212-7219.

23. Peng, X. G.; Wickham, J.; Alivisatos, A. P. *Journal of the American Chemical Society* **1998,** 120, (21), 5343-5344.

24. Peng, Z. A.; Peng, X. G. *Journal of the American Chemical Society* **2001,** 123, (1), 183-184.

25. Qu, L. H.; Peng, Z. A.; Peng, X. G. *Nano Letters* **2001,** 1, (6), 333-337.

26. Qu, L. H.; Peng, X. G. *Journal of the American Chemical Society* **2002,** 124, (9), 2049-2055.

27. Mekis, I.; Talapin, D. V.; Kornowski, A.; Haase, M.; Weller, H. *Journal of Physical Chemistry B* **2003,** 107, (30), 7454-7462.

28. Qu, L. H.; Yu, W. W.; Peng, X. P. *Nano Letters* **2004,** 4, (3), 465-469.

29. Peng, X. G.; Manna, L.; Yang, W. D.; Wickham, J.; Scher, E.; Kadavanich, A.; Alivisatos, A. P. *Nature* **2000,** 404, (6773), 59-61.

30. Manna, L.; Scher, E. C.; Alivisatos, A. P. *Journal of the American Chemical Society* **2000,** 122, (51), 12700-12706.

31. Peng, Z. A.; Peng, X. G. *Journal of the American Chemical Society* **2001,** 123, (7), 1389-1395.

32. Li, L. S.; Hu, J. T.; Yang, W. D.; Alivisatos, A. P. *Nano Letters* **2001,** 1, (7), 349-351.

33. Hu, J. T.; Li, L. S.; Yang, W. D.; Manna, L.; Wang, L. W.; Alivisatos, A. P. *Science* **2001,** 292, (5524), 2060-2063.

34. Peng, Z. A.; Peng, X. G. *Journal of the American Chemical Society* **2002,** 124, (13), 3343-3353.

35. Manna, L.; Scher, E. C.; Li, L. S.; Alivisatos, A. P. *Journal of the American Chemical Society* **2002,** 124, (24), 7136-7145.

36. Mokari, T.; Banin, U. *Chemistry of Materials* **2003,** 15, (20), 3955-3960.

37. Kan, S.; Mokari, T.; Rothenberg, E.; Banin, U. *Nature Materials* **2003,** 2, (3), 155-158.

38. Kan, S. H.; Aharoni, A.; Mokari, T.; Banin, U. *Faraday Discussions* **2004,** 125, 23-38.

39. Talapin, D. V.; Nelson, J. H.; Shevchenko, E. V.; Aloni, S.; Sadtler, B.; Alivisatos, A. P. *Nano Letters* **2007,** 7, (10), 2951-2959.

40. Carbone, L.; Nobile, C.; De Giorgi, M.; Sala, F. D.; Morello, G.; Pompa, P.; Hytch, M.; Snoeck, E.; Fiore, A.; Franchini, I. R.; Nadasan, M.; Silvestre, A. F.; Chiodo, L.; Kudera, S.; Cingolani, R.; Krahne, R.; Manna, L. *Nano Letters* **2007,** 7, (10), 2942-2950.

41. Manna, L.; Milliron, D. J.; Meisel, A.; Scher, E. C.; Alivisatos, A. P. *Nature Materials* **2003,** 2, (6), 382-385.

42. Milliron, D. J.; Hughes, S. M.; Cui, Y.; Manna, L.; Li, J. B.; Wang, L. W.; Alivisatos, A. P. *Nature* **2004,** 430, (6996), 190-195.

43. Carbone, L.; Kudera, S.; Carlino, E.; Parak, W. J.; Giannini, C.; Cingolani, R.; Manna, L. *Journal of the American Chemical Society* **2006,** 128, (3), 748-755.

44. Trentler, T. J.; Denler, T. E.; Bertone, J. F.; Agrawal, A.; Colvin, V. L. *Journal of the American Chemical Society* **1999,** 121, (7), 1613-1614.

45. Green, M.; O'Brien, P. *Chemical Communications* **2000**, (3), 183-184.

46. Park, S. J.; Kim, S.; Lee, S.; Khim, Z. G.; Char, K.; Hyeon, T. *Journal of the American Chemical Society* **2000,** 122, (35), 8581-8582.

47. Puntes, V. F.; Krishnan, K. M.; Alivisatos, A. P. *Science* **2001,** 291, (5511), 2115-2117.

48. Puntes, V. F.; Zanchet, D.; Erdonmez, C. K.; Alivisatos, A. P. *Journal of the American Chemical Society* **2002,** 124, (43), 12874-12880.

49. Joo, J.; Yu, T.; Kim, Y. W.; Park, H. M.; Wu, F. X.; Zhang, J. Z.; Hyeon, T. *Journal of the American Chemical Society* **2003,** 125, (21), 6553-6557.

50. Perera, S. C.; Tsoi, G.; Wenger, L. E.; Brock, S. L. *Journal of the American Chemical Society* **2003,** 125, (46), 13960-13961.

51. Jun, Y. W.; Casula, M. F.; Sim, J. H.; Kim, S. Y.; Cheon, J.; Alivisatos, A. P. *Journal of the American Chemical Society* **2003,** 125, (51), 15981-15985.

52. Qian, C.; Kim, F.; Ma, L.; Tsui, F.; Yang, P. D.; Liu, J. *Journal of the American Chemical Society* **2004,** 126, (4), 1195-1198.

53. Park, J.; Koo, B.; Yoon, K. Y.; Hwang, Y.; Kang, M.; Park, J. G.; Hyeon, T. *Journal of the American Chemical Society* **2005,** 127, (23), 8433-8440.

54. Li, Y.; Malik, M. A.; O'Brien, P. *Journal of the American Chemical Society* **2005,** 127, (46), 16020-16021.

55. Samia, A. C. S.; Schlueter, J. A.; Jiang, J. S.; Bader, S. D.; Qin, C. J.; Lin, X. M. *Chemistry of Materials* **2006,** 18, (22), 5203-5212.

56. Yu, W. W.; Peng, X. G. *Angewandte Chemie-International Edition* **2002,** 41, (13), 2368-2371.

57. Battaglia, D.; Peng, X. G. *Nano Letters* **2002,** 2, (9), 1027-1030.

58. Li, J. J.; Wang, Y. A.; Guo, W. Z.; Keay, J. C.; Mishima, T. D.; Johnson, M. B.; Peng, X. G. *Journal of the American Chemical Society* **2003,** 125, (41), 12567-12575.

59. Yu, W. W.; Qu, L. H.; Guo, W. Z.; Peng, X. G. *Chemistry of Materials* **2003,** 15, (14), 2854-2860.

60. Xie, R.; Battaglia, D.; Peng, X. *Journal of the American Chemical Society* **2007,** 129, (50), 15432-+.

61. Yu, H.; Li, J. B.; Loomis, R. A.; Gibbons, P. C.; Wang, L. W.; Buhro, W. E. *Journal of the American Chemical Society* **2003,** 125, (52), 16168-16169.

62. Grebinski, J. W.; Hull, K. L.; Zhang, J.; Kosel, T. H.; Kuno, M. *Chemistry of Materials* **2004,** 16, (25), 5260-5272.

63. Dong, A. G.; Wang, F. D.; Daulton, T. L.; Buhro, W. E. *Nano Letters* **2007,** 7, (5), 1308-1313.

64. Wang, F.; Yu, H.; Li, J.; Hang, Q.; Zemlyanov, D.; Gibbons, P. C.; Wang, L. W.; Janes, D. B.; Buhro, W. E. *Journal of the American Chemical Society* **2007,** 129, (46), 14327-14335.

65. Wang, F. D.; Buhro, W. E. *Journal of the American Chemical Society* **2007,** 129, (46), 14381-14387.

66. Sun, J. W.; Buhro, W. E. *Angewandte Chemie-International Edition* **2008,** 47, (17), 3215-3218.

67. Dong, A.; Yu, H.; Wang, F.; Buhro, W. E. *Journal of the American Chemical Society* **2008,** 130, (18), 5954-5961.

68. Sun, J.; Wang, L. W.; Buhro, W. E. *Journal of the American Chemical Society* **2008,** 130, (25), 7997-8005.

69. Liu, H. T.; Owen, J. S.; Alivisatos, A. P. *Journal of the American Chemical Society* **2007,** 129, (2), 305-312.

70. Wang, W.; Banerjee, S.; Jia, S. G.; Steigerwald, M. L.; Herman, I. P. *Chemistry of Materials* **2007,** 19, (10), 2573-2580.

71. Kopping, J. T.; Patten, T. E. *Journal of the American Chemical Society* **2008,** 130, (17), 5689-5698.

72. Kanaras, A. G.; Sonnichsen, C.; Liu, H. T.; Alivisatos, A. P. *Nano Letters* **2005,** 5, (11), 2164-2167.

73. Kawa, M.; Morii, H.; Ioku, A.; Saita, S.; Okuyama, K. *Journal of Nanoparticle Research* **2003,** 5, (1-2), 81-85.

74. Yu, H.; Li, J. B.; Loomis, R. A.; Wang, L. W.; Buhro, W. E. *Nature Materials* **2003,** 2, (8), 517-520.

75. Kolosky, M.; Vialle, J.; Cotel, T. *Journal of Chromatography* **1984,** 299, (2), 436-444.

76. Wang, F. D.; Tang, R.; Yu, H.; Gibbons, P. C.; Buhro, W. E. *Chemistry of Materials* **2008,** 20, (11), 3656-3662.

77. Agustin, C. H.; Martinez, M. M. *Journal of Dispersion Science and Technology* **1988,** 9, (3), 209-221.

77. Williams, R. H.; Hamilton, L. A. *Journal of the American Chemical Society* **1952**, 74, 5418−5420.

78. Kosolapoff, G. M.; Watson, R. M. *Journal of the American Chemical Society* **1951**, 73, 4101−4102.

Chapter 3

Photo-induced photoluminescence enhancement of SLS-grown CdSe quantum wires and the measurement of photoluminescence quantum yield

Introduction

Nanometer-scale CdSe semiconductor quantum wires represent one-dimensional structures where the exciton wavefunction is confined in two dimensions. This property of quantum wires creates unique optical characteristics such as wavelength-tunable photoluminescence (PL). However, improvements in PL efficiencies are required before quantum wires may be used in applications. I report such improvement in this chapter.

The activation of quantum dots with UV or visible light is a powerful tool for increasing their photoluminescence after their preparation or further functionalization.[1, 2] Despite intense research into light-induced PL enhancement of semiconductor nanoparticles during recent years,[2-11] the mechanism of this process is not yet fully understood. This is because various parameters, such as oxygen, water, gaseous molecules, stabilizing agents, or the preparation history of the quantum dots can influence the photo-activation process.[2, 4-10, 12, 13] So far, four possible mechanisms for the photo-activation of quantum dots have been proposed:[12, 13] i) photon-induced passivation of surface states,[6, 14, 15] ii) photon-induced surface transformations,[5, 7, 14-16] iii) photoneutralization of local charge centers inside and outside the quantum dots,[17] and iv) photoelectrification, corresponding to photoionization of the quantum dots and subsequent trap filling by ejected charge carriers, leading to a suppression of the ionization probability of the remaining neutral quantum dots.[12, 18] The photon-induced passivation of surface states by physisorption of gaseous and solvent molecules is a reversible process, [6, 14, 16] whereas the photon-induced transformation of the particle surface

or the core/shell interface is an irreversible process.[5, 7, 14-16] Charge carriers, generated by irradiation with light, are postulated to interact with oxygen that is present in the environment, leading to the formation of O_2^- ions. The remaining holes on the quantum dots surfaces oxidize Se atoms on the surface of the particles yielding SeO_2.[4, 19] Subsequently, SeO_2 desorbs from the particles leading to a smoothing of the quantum dot surface. As a consequence, the non-radiative decay of excitons is reduced and thus the PL increases.

Further, it has to be considered that light irradiation of semiconductor nanoparticles may also cause photo-quenching. If the light intensity is low, photo-activation processes dominate.[11] An enhancement of the light intensity or an extension of the irradiation time leads to competition between activation and quenching processes and finally to a dominance of deactivation processes. Under these conditions, irradiation causes the destruction of bonds at the surface of the nanocrystals, as well as the creation of new defects, whose energy states are located inside the bandgap.[8] As a consequence, the probability of radiative electron-hole recombination decreases.

However, the photo-enhancement of semiconductor quantum wires has not been studied due to the lack of well-controlled nanowires with reasonable photoluminescence intensities. Our optimized synthesis of CdSe nanowires, described in Chapter 1, now allows us to study the photo-enhancement phenomenon in 2-D confined quantum nanostructures.

In this chapter, I discuss the photo-induced photoluminescence enhancement of colloidal CdSe nanowires. I have systematically investigated the

role of those parameters affecting the photo-activation of the CdSe quantum wires. Luminescent impurities in our colloidal CdSe quantum-wire system have been identified, therefore allowing reliable PL quantum yields for the CdSe nanowires to be determined.

Results and Discussion

Photo-induced PL enhancement.

The as-prepared CdSe nanowires generally exhibited poor photoluminescence efficiency even when they had good morphology control and were well suspended in toluene. The quantum yield of the as-prepared samples from the earlier synthesis (with no added phosphinic or phosphonic acid) was around 0.2%, which is low compared to the quantum yield of CdSe dots (generally > 20% as-prepared[20-22]). However, when the nanowire dispersions were allowed to stand in the fume hood under the illumination of fluorescent lights, the PL intensity and the quantum yield were observed to increase. Photoluminescence spectra were recorded over several days. The relative intensity of the excitonic features of the wire samples showed a significant enhancement after 3 - 4 days and reached a maxium after 6 - 7 days. The photo-induced PL enhancement of the CdSe nanowires followed a roughly exponential rise over the early days (Figure 3-1). In a fast rise at the early stage of the PL enhancement, the intensity of the PL peak increased by 50% of the total enhancement (1 - 2 days). Then the enhancement rate gradually slowed down, and reached the maximum intensity after 6 - 7 days. After that, the intensity of the photoluminescence began to decrease slowly. The decrease may due to the penetration of oxygen or water molecules through the network of surface ligands, therefore oxidizing some surface atoms to create surface traps.

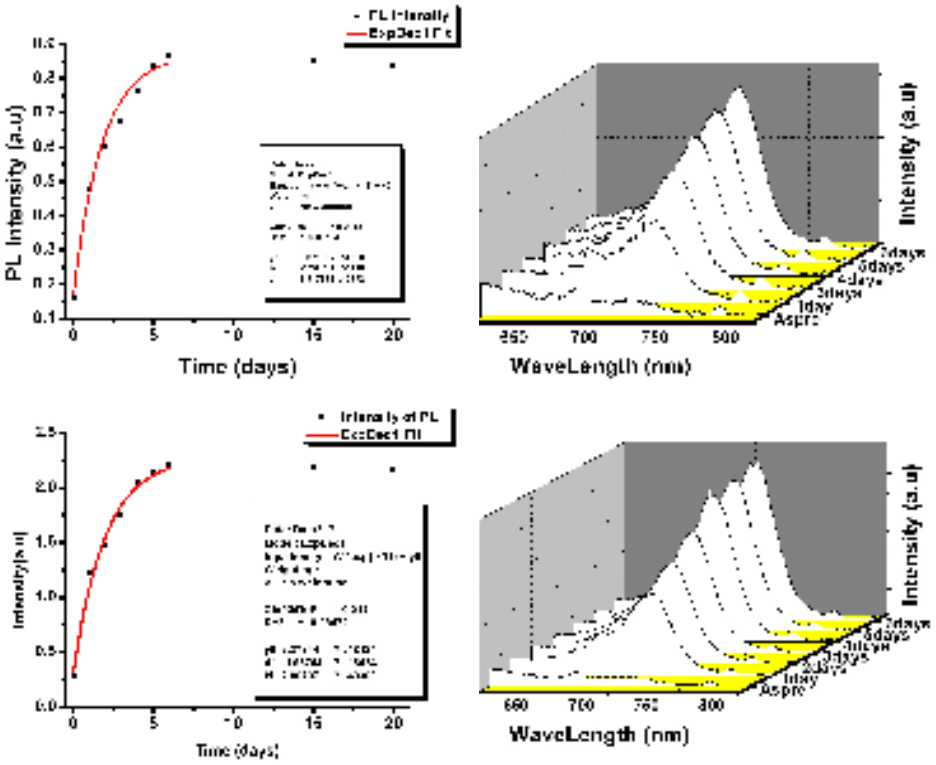

Figure 3-1. The evolution of the photoluminescence enhancement and the fitting of the intensity data of two samples. The diameter of the nanowires is ~10 nm.

The procedure for the photo-induced photoluminescence enhancement was very simple. The intensity of the fluorescent lights in the fume hood at the cuvette was 0.5 mW/cm^2. Under this condition, the enhancement process was slow and no damage was caused to the morphology of the CdSe nanowires (see below).

Measuring the PL quantum yield.

The band-edge emission from semiconductor nanocrystals has to compete with both radiative and non-radiative decay channels originating from surface electronic states. In colloidal 1-D CdSe nanostructures (nanorods and nanowires), there are additional factors that further reduce the luminescence when compared to spherical CdSe nanocrystals. In nanowires, the surface-to-volume ratio is higher than in spheres. This increases the occurrence of surface trap states, which reduce the luminescence.

Fluorescence intensity is proportional to the concentration of a species, its absorption cross section (or absorptivity) at the excitation wavelength, and its fluorescence quantum yield. The measurement of fluorescence quantum yields can often be difficult and troublesome, and the need for absolute care during every step cannot be over emphasized.

To get reliable quantum yields for the CdSe quantum wires, the following procedure needs to be carefully followed.

1) Selection of the standard

First of all, a standard sample is required for measurement of the quantum yield. The standard sample should be chosen to ensure it absorbs at the excitation wavelength of choice for the wire samples, and emits in a similar region as the wire samples. Freebase TPP (tetraphenylporphyrin, H_2TPP) is selected to be the best standard for our CdSe nanowire samples. It's well characterized and with the

best emission wavelength which is suitable for the quantum-yield measurements for our wire sample. The organic structure of freebase TPP is shown in Figure 3-2.

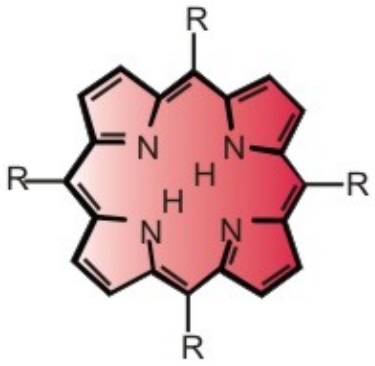

Figure 3-2. Structure of freebase TPP (tetraphenylporphyrin).

2) Determination of the correct concentration range.

In order to minimize re-absorption effects,[23] absorbance in the 10 mm fluorescence cuvette should be at a low value (< 0.15 A) at and above the excitation wavelength. Above this level, non-linear effects may be observed due to inner-filter effects, and the resulting quantum yield values may be unreliable.

The detail of this procedure is described in the experimental section.

3) Background correction.

In the absorption and photoluminescence spectra of the CdSe quantum wires, a rise to the higher energy of the PL peak, a "shoulder" or rising background is always observed (Figure 3-3). The PL feature from the wire excitonic emission should be a Guassian-like peak. The "shoulder" must be from other substances remaining in the CdSe quantum-wire sample.

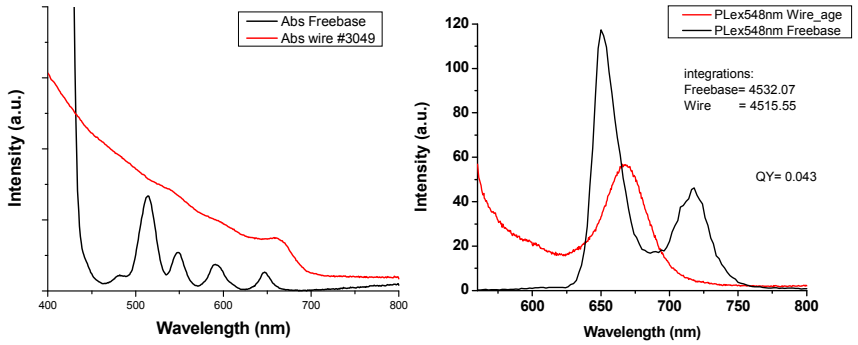

Figure 3-3. Typical absorption spectrum and photoluminescence spectrum of ensemble CdSe quantum wire sample and Freebase TPP.

The existence of this "shoulder" in the PL spectrum complicates quantum-yield measurement. This species absorbs at the excitation wavelength, and emits a feature that overlaps in the PL spectrum of CdSe quantum wires. Thus not all of the absorbance at the excitation wavelength is by CdSe quantum wires, and part of the integrated PL is not from CdSe quantum wires.

To solve this problem, I first needed to find out what substance was responsible for the emission of the "shoulder". Because several reagents were used during the synthesis of the CdSe quantum wires, many possibilities existed for emissive impurities.

We also observed green material by confocal microscopy of single CdSe wire. Presumably, this green material was responsible for the shoulder in the ensemble PL spectra (Figure 3-3). This impurity could not be removed by the purification procedure, but was bleached when illuminated with high power. To investigate which reagents contributed to the green material, control experiments

were performed. Various combinations of the reagents used in the nanowire synthesis were combined under the same conditions used for wire synthesis (duration, temperature, amount, etc.). These various combinations were placed in the confocal microscope to examine their appearance. These result are shown in Table 3-1.

Table 3-1. Observations of the different reagent combinations under the confocal microscope.

Component	**Phenomenon in microscope**
Bi + TBP	Green fluorescent pools
Bi	Small green speckles, initially very bright fluorescence/fades very quickly upon irradiation
TOPO + HDA + OA + Bi	Green fluorescent species
TOPO/HDA/OA	Fluorescent drops (green small dots) , very weak compared to Bi samples
TOPO/HDA	Very very weak fluorescence
HDA	Blinking 'species'
OA	Weak fluorescence drops/background fades quickly
TOPO	No fluorescence

From the results, only the Bi-related reagent combinations were observed to produce green material. This indicated that Bi was forming some complex with another reagent in the reaction that emits green light. Studies of solid-state compounds containing Bi have shown emission from Bi^{3+} in the green region at

2.40 eV (~ 517 nm).[24, 25] This result is similar to our observation. Thus, the Bi catalyst in the reaction system may form a Bi^{3+} complex with another reagent present.

To further investigate what compound was formed during the reaction, MALDI-MS (Matrix Assisted Laser Desorption Ionisation - Mass Spectrometry) was obtained from from CdSe quantum-wire samples (Figure 3-4).

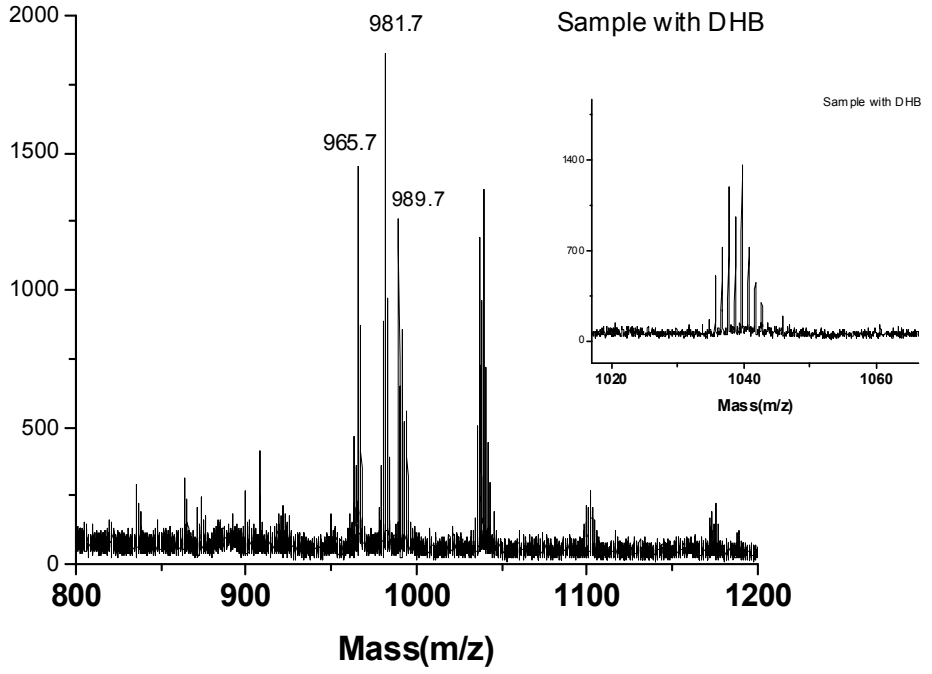

Figure 3-4. MALDI-MS out view of a CdSe quantum-wire sample in DHB (2, 5-Dihydroxy benzoic acid). The inset is the zoom view of the peaks around 1037.7 m/z.

Only 4 major signals were observed in the MALDI-MS experiment. The signal around 1037.7 m/z is a very complex 8-peak pattern. This signal is from Cd compounds due to the various natural isotopes of Cd. MS/MS (Tandem mass

spectrometry) experiments of the CdSe quantum wires were conducted to investigate the compositions corresponding to the first 3 signals.

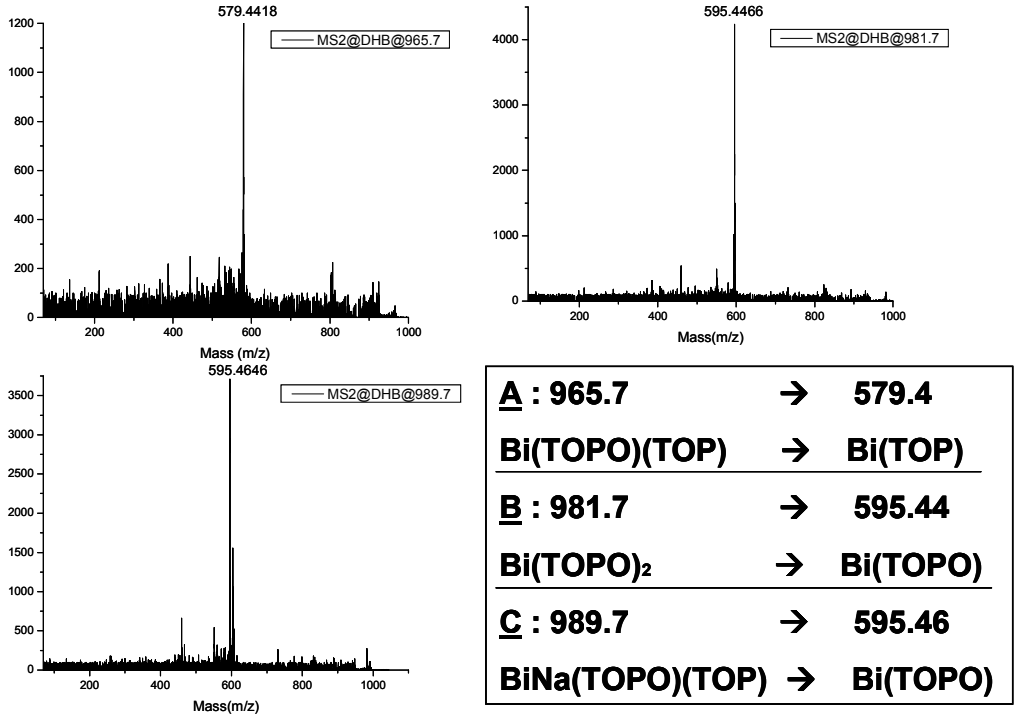

Figure 3-5. MS/MS spectra of fragments from a CdSe quantum-wire sample. (A) MS/MS at 965.7 m/z, (B) MS/MS at 981.7 m/z and (C) MS/MS at 989.7 m/z

All the MS/MS results were very simple and clear. The possible assignments are listed in Figure 3-5. The results indicate that the fragments all contain Bi, which is consistent with the observation under the microscope. The green material that emits at higher energy and contributes to the "shoulder" of the PL spectrum of CdSe quantum wire is a $Bi^{3+}(TOPO)_n(TOP)_m$ compound.

The next step was to synthesize this Bi^{3+} compound to calibrate the background of the PL spectrum of the CdSe quantum wires. Reactions of $BiCl_3$

and TOPO or TOP were conducted. Table 3-2 shows the appearance of the resulting mixtures.

Table 3-2. Color and appearance of $BiCl_3$ and reaction with TOP and TOPO

TOP	Clear colorless
$BiCl_3$	Gray-white powder
TOPO	White powder
TOP+$BiCl_3$ before heat	Clear brown solution
TOPO+$BiCl_3$ Heat@ 240 ^oC	Cannot dissolve
TOP+$BiCl_3$ heat @ 240 ^oC	Clear yellowish-green solution

From the color, a $Bi^{3+}(TOP)_m$ compound is the green material formed at the reaction temperature. The formation of the $Bi^{3+}(TOP)_m$ compound was further proven by a NMR study, which is shown in Figure 3-6.

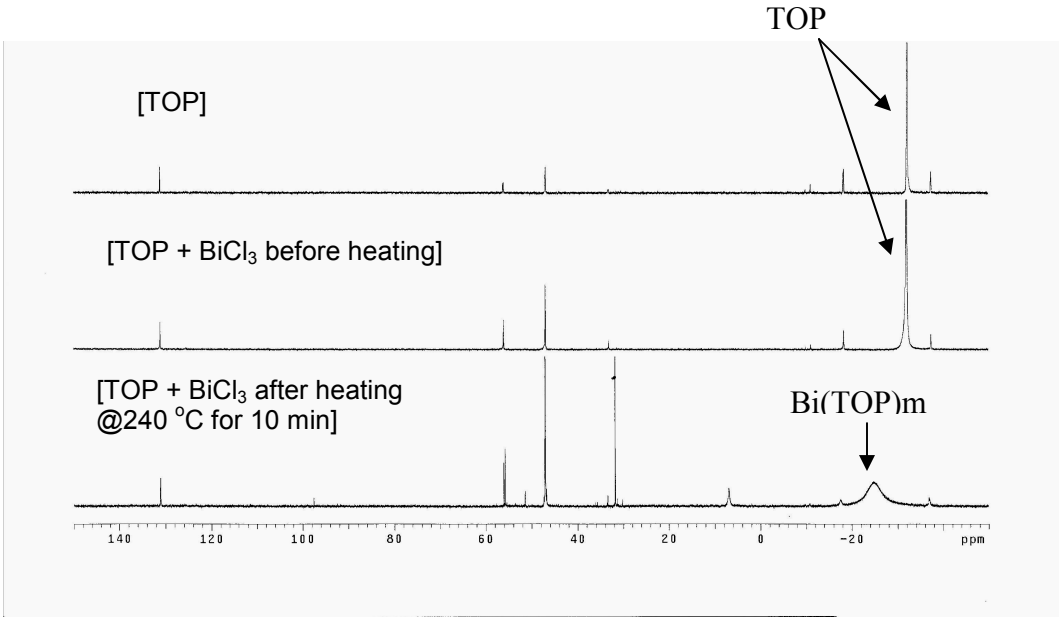

Figure 3-6. NMR spectra of TOP alone, TOP + $BiCl_3$ before heating and TOP + $BiCl_3$ after heating at 240 ^oC for 10 min.

The shift and broadening of the TOP peak from -32.5 ppm to -24.5 ppm revealed a reaction between Bi^{3+} and TOP, forming a coordination compound that emitted green light upon illumination. The absorption and PL spectra of this compound are shown in Figure 3-7.

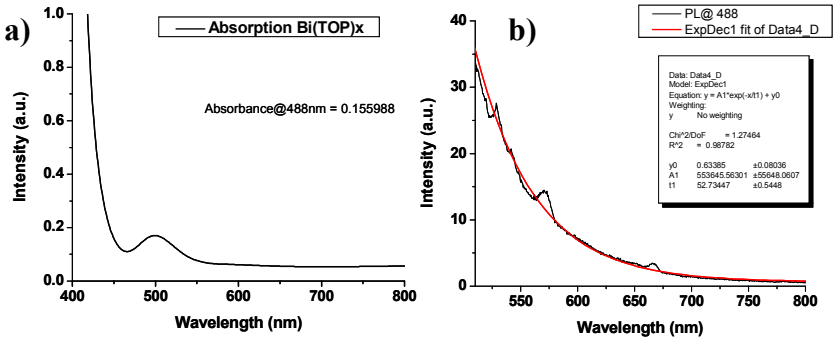

Figure 3-7. (a) Absorption and (b) photoluminescence spectra of the $Bi^{3+}(TOP)_m$ compound. The red curve in PL spectrum is the exponential fit of the PL.

The low-energy edge of the PL peak from $Bi^{3+}(TOP)_m$ matched the "shoulder" in the PL spectra of the CdSe quantum wires. This result further proved the formation of the $Bi^{3+}(TOP)_m$ compound during the wire synthesis. Furthermore, overheating this compound destroyed the yellowish-green color, which also matched the bleaching of the green material under the microscope with long-time laser irradiation.

Analysis of CdSe quantum-wire spectra by subtraction of the $Bi^{3+}(TOP)_m$ feature.

With the PL spectrum of the green material, this feature can be fit and subtracted from the CdSe quantum-wire PL spectra, therefore allowing determination of reliable PL quantum yields for the CdSe quantum wires.

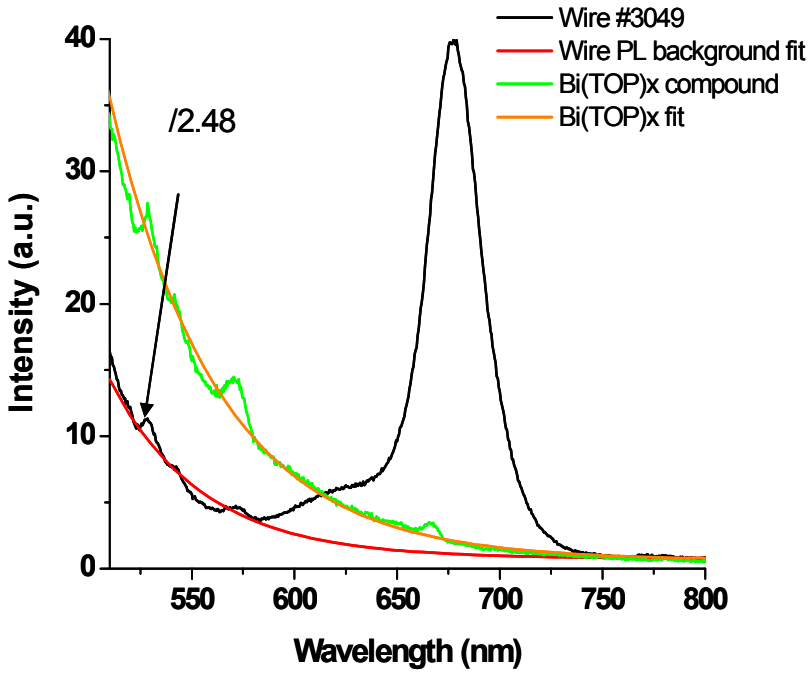

Figure 3-8. Fitting of the $Bi^{3+}(TOP)_m$ feature in the PL spectrum of CdSe quantum wires.

Figure 3-8 shows the fitting of the background "shoulder" in the PL spectrum of a CdSe quantum-wire sample. I first fit the background of the quantum-wire spectrum with an exponential, which is shown as the red curve. A similar fit is shown for the PL spectrum of $Bi^{3+}(TOP)_m$, which is the orange curve. The orange curve was scaled to the red curve by dividing by a constant (2.48). Therefore, the absorbance of $Bi^{3+}(TOP)_m$ at the excitation wavelength (488 nm) was determined by dividing the absorbance in Figure 3-7a by the same constant.

By subtracting this value from the absorbance of the CdSe quantum-wire sample, the absorbance of only the CdSe quantum wires was obtained. After subtracting the fitted green feature from the PL spectrum of the CdSe quantum wires, a reliable PL quantum yield was calculated (Figure 3-9).

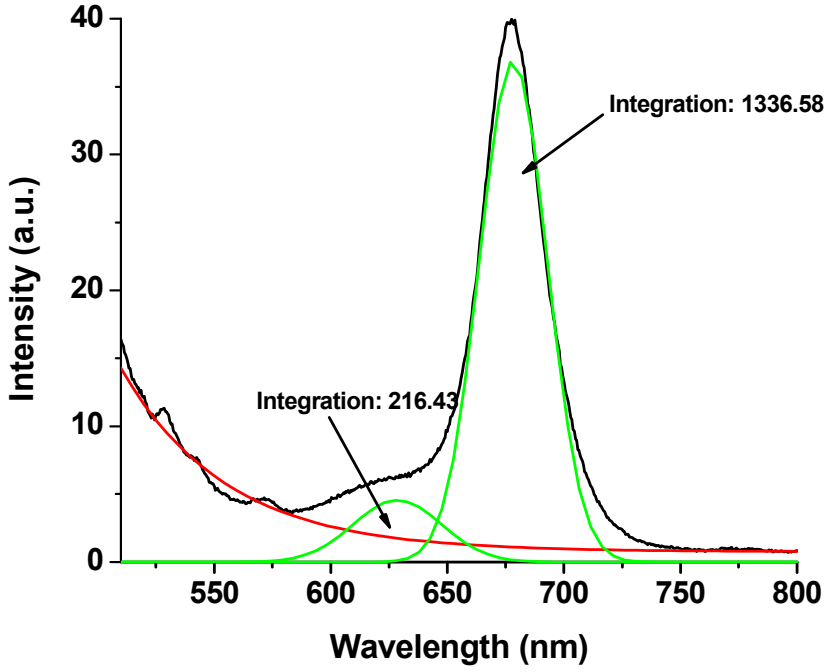

Figure 3-9. The fitting of the PL spectrum of a CdSe quantum-wire sample after subtracting the green material.

The PL quantum yield of the CdSe nanowires was calculated by Eq. 1, where $PL_{wire\_integration}$ and $PL_{freebase\_integration}$ correspond to the integrated PL, and $A_{freebase}$ and A_{wire} respond to the corrected absorption values as described above.

$$QY_{wire} = QY_{freebase} (PL_{wire\_integration}/PL_{freebase\_integration}) / (A_{freebase}/A_{wire}) \quad (1)$$

The role of precursors.

I initially discussed the photoluminescence (PL) effect with CdSe nanowire samples that had been allowed to stand under normal fluorescent lighting in the fume hood. However, not all CdSe nanowires were observed to undergo a photo-induced photo-luminescence enhancement. The behavior of the nanowires depended on the precursors and additives used in their synthesis.

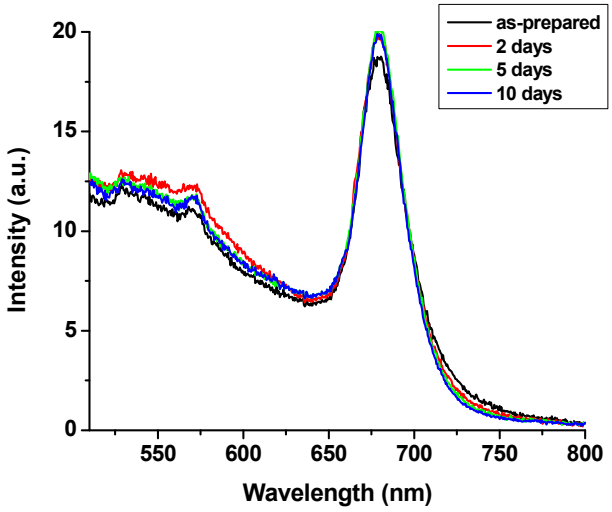

Figure 3-10. Temporal evolution of the photoluminescence spectra of as-prepared and aged CdSe nanowires prepared from $Cd(stearate)_2$. The nanowires were illuminated under fluorescent lamps for various periods.

Nanowires prepared from $Cd(stearate)_2$ exhibited no photo-enhancement. The PL spectra of these CdSe nanowires showed no significant differences upon irradiations (Figure 3-10) for up to 10 days under the fluorescent lamps. The

minor increase in the PL intensity with time was likely due to the loss of a small amount of toluene solvent, which CdSe nanowires were dissolved in. This result indicated that no photo-enhancement occurred for wires made from $Cd(stearate)_2$.

When a toluene solution of CdSe quantum wires made from $Cd(OA)_2$ was subjected to continuous illumination under the fluorescent lamps in the fume hood for several days, the intensity of the PL was found to undergo significant enhancements.[7] Two factors were important to the photoluminescence enhancement in the CdSe quantum dots, one is *oxygen*, and the other one is *light*. These factors were also likely important to the photo-enhancement in the CdSe quantum wires. Four parallel experiments were conducted to investigate these factors. A CdSe nanowire solution in toluene was distributed into 4 different cuvettes. Two of the cuvettes were degassed and bubbled with nitrogen for 2 hours, and sealed to prevent contact with air. The other two cuvettes were septum capped with a syringe needle inserted into each septum to provide air exposure. One of the sealed cuvettes and one of the opened cuvettes were illuminated with the fluorescence lamps. The other two samples were kept in the dark. PL spectra were obtained from the four samples for several days.

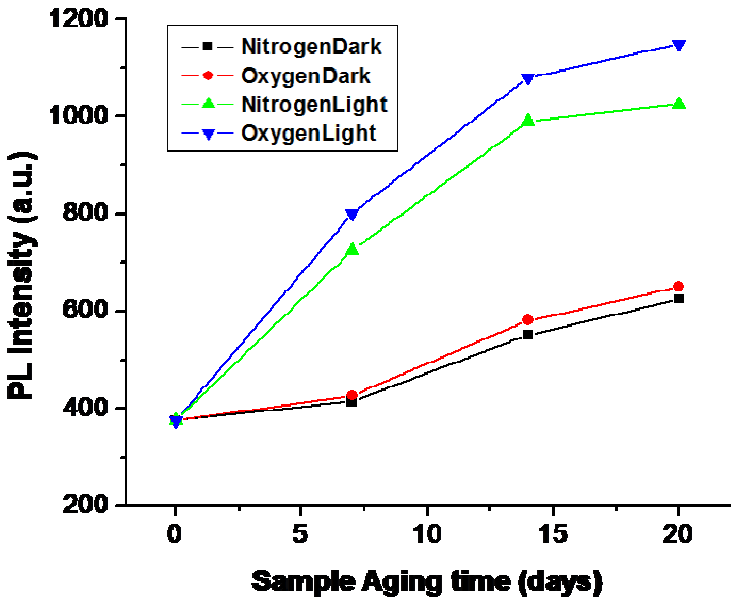

Figure 3-11. Evolution of the PL intensity in a CdSe nanowire sample (~8 nm diamater) under four conditions discussed in the text.

The photoluminescence of the CdSe quantum-wire samples at these four conditions was observed to enhance in all cases (Figure 3-11). The results established that the PL in the samples exposed to light (blue triangles and green triangles in Figure 3-11) enhanced more than in the samples kept in the dark (black squares and red circles in Figure 3-11). Only a slightly difference was observed between the samples in oxygen and inert atmosphere. Therefore, light was determined to be the more important factor than oxygen for the PL enhancement of CdSe nanowires. Oxygen may also have some effect, but not as significant as that of light. Since the quantum-wire purification procedures were conducted in the air, the wires were exposed to oxygen and water, at least briefly

in all cases. Therefore, a possible role for oxygen may not be excluded for the enhancement of PL efficiency upon aging.

The role of light power density.

The PL enhancement of the CdSe quantum wires was observed to occur under different light sources. Different light intensities varied the rate of the photoluminescence enhancement. The light power of the fluorescent lamps in the fume hood is about 0.5 mW/cm^2, under which most of our photo-induced PL enhancement experiments were conducted. I also used a much more intense UV lamp (power density ~ 600 mW/cm^2) to irradiate the wires. The result of the enhancement is shown in Figure 3-12. Note that the photo-induced PL enhancement of CdSe quantum wires under fluorescent lamps usually required several days to achieve a maximum PL efficiency. But under the much stronger UV irradiation, this process was much faster, taking only several minutes. The as-prepared CdSe quantum wires exhibited a weak PL intensity (Figure 3-4, black curve). After 1 - 2 min of irradiation, the PL intensity was significantly increased (red and green curves). After 4 - 5 min, the enhancement of the PL intensity of the CdSe quantum wires reached a maximum, for which the intensity of the excitonic feature is 10 times the original (yellow and indigo curves). However, when ensembles of CdSe quantum wires were irradiated for more than 5 min, the relative PL intensity began to decrease, likely as a result of surface photochemistry that created additional surface traps.

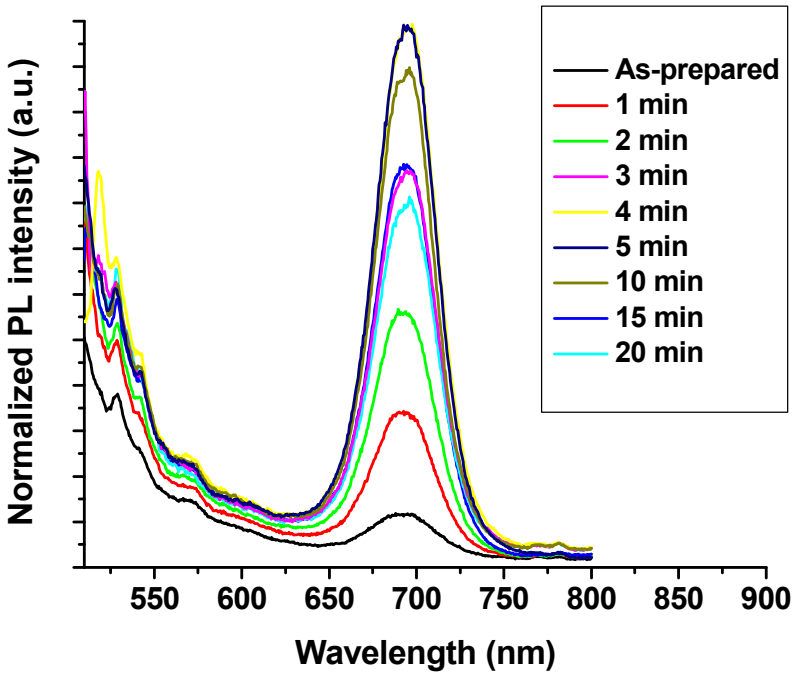

Figure 3-12. Photoluminescence spectra of CdSe quantum wires (~8 nm) irradiated with a UV lamp (600 mW/cm^2) for various periods. The normalization procedure is described in the experimental section.

Solvent effect.

Because the CdSe nanowires were passivated by several kinds of organic surfactants (TOPO, TOP, and oleic acid etc.), they were dispersible in various non-polar solvents. Experiments were conducted to determine if the solvents would affect the photo-induced PL enhancement of the CdSe nanowires.

The photo-enhancement was investigated in toluene, hexane and chloroform. Enhancement was observed in all the solvents, as shown in Figure 3-13.

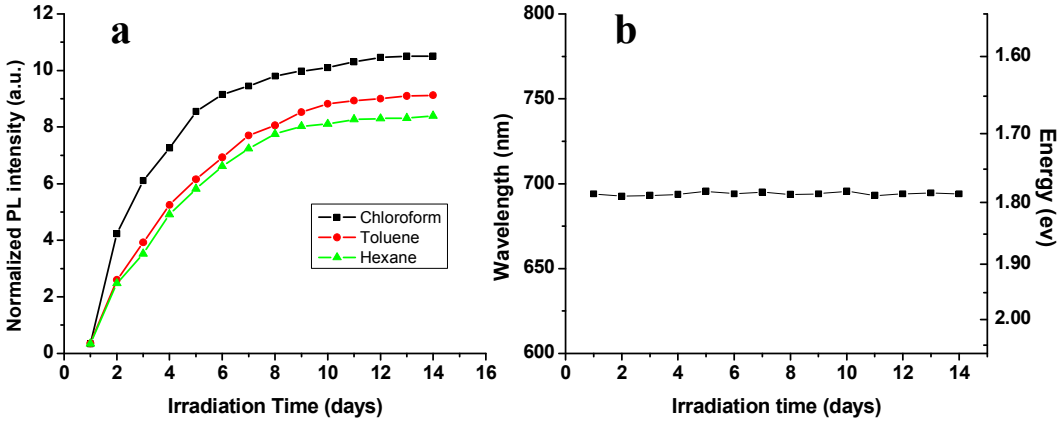

Figure 3-13. (a) Evolution of the PL intensity of a CdSe nanowire sample in various solvents. (b) The peak position evolution over the same time period.

Figure 3-13a shows only a slight enhancement-rate difference in the solvents investigated, which indicated that the PL enhancement of the CdSe quantum wires has no significant solvent effect. The differences in the intensity of the excitonic PL peak observed were most likely caused by the solubility differences of CdSe nanowires in these solvents. After the CdSe quantum-wire dispersions stand for hours or days, depending on the solvent, the nanowires precipitate. The length of the time the quantum wires remain suspended is several hours in hexane, 1 – 2 days in toluene, and several days in chloroform. The precipitated wires do not absorb light as efficiently as suspended wires, which results in slightly different enhancement rates in the three solvents.

Various studies have verified that a blueshift of the emission spectrum often evidences a decrease in particle size during the photo-enhancement studies of quantum dots.[4, 19] Generally, the reason for this observation is the oxidation of the particle surface and subsequent desorption of SeO_2. This process is accompanied by the release of Cd^{2+} from the particle surface. Unlike the observations obtained from the quantum dot studies, our CdSe quantum wires show no peak shift during the photo-induced PL enhancement. Figure 3-13b shows the PL peak position over the enhancement time period. During the photo-induced PL enhancement of the CdSe quantum wires, the diameter of the nanowires does not decrease, as no blue shift was observed during this experiment. Figure 3-14 shows the TEM images of the as-prepared CdSe nanowire sample and the aged sample after irradiation for 2 weeks. The CdSe nanowires after aging were still straight and long. No dissolution or breaking of the CdSe nanowires were evident. Furthermore, no obvious diameter change was observed, which is consistent with the stability of PL peak position over the enhancement period.

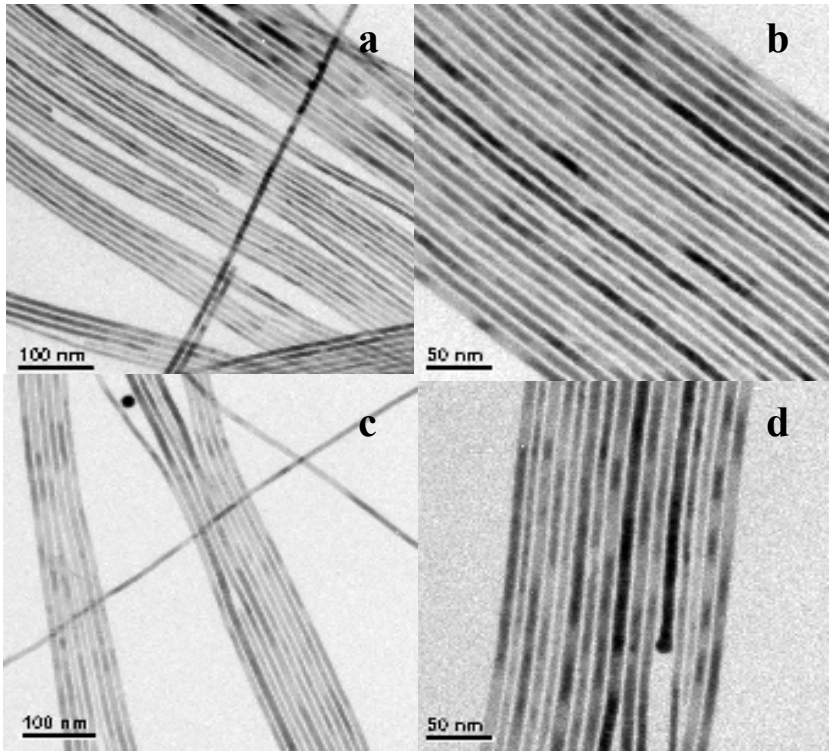

Figure 3-14. Representative TEM images of a CdSe nanowire sample as-prepared (a, b) and after room light exposure for 2 weeks (c, d).

The CdSe nanowires prepared by the earlier method without the addition of phosphonic or phosphinic acid exhibited a better dispersibility in toluene than in chloroform. The dispersibility decreased in the order toluene > chloroform > hexane. However, the new synthesis with additional acids to correct the TOPO problem (Chapter 2) gives nanowires that have better dispersibility in chloroform. The dispersibility of the "new" CdSe nanowires decreases in the order chloroform > toluene > hexane. The additional phosphonic acid or phosphinic acid added into the reaction system increased the polarity of the synthesized CdSe nanowires;

therefore, chloroform becomes a better solvent for suspending CdSe nanowires because of its larger dielectric constant (Table 3-1). Although the newly prepared CdSe quantum wires disperse better in chloroform, chloroform has some disadvantages such as dissolving the carbon film on TEM grid. We still use toluene as the primary solvent for our optical measurements and preparing TEM grids for microscopy.

Table. 3-3 Formula and dielectric constant of toluene, chloroform and hexane.

Solvent	formula	Dielectric Constant
Toluene	C_7H_8	2.38
Chloroform	$CHCl_3$	4.81
Hexane	C_6H_{14}	1.89

The role of stirring.

During the photo-induced photoluminescence enhancement, I observed the aggregation and precipitation of CdSe nanowires out of toluene solution when the concentration of the ensemble nanowire solution was high. The precipitation was expected to decrease photo-enhancement efficiency. A control experiment was performed to compare the difference between keeping the nanowires suspended in solution and allowing them to partially settle. A CdSe wire sample in toluene with a high concentration was divided into two identical cuvettes, and a small stir bar was put into one of the cuvettes. Both cuvettes were capped and wrapped with parafilm to minimize contact with air and water. The temporal evolution of the PL for both samples was recorded (Figure 3-15).

Both of the samples exhibited the photo-induced PL enhancement upon illumination. The signal-to-noise in the spectra from the cuvette containing the stir bar was poor. After removing the stir bar from the cuvette, quality of the PL spectrum was improved (Figure 3-15, a vs. c). The enhancement of the stirred and non-stirred wire samples was about the same within the error of the photoluminescence measurement (Figure 3-15, c).

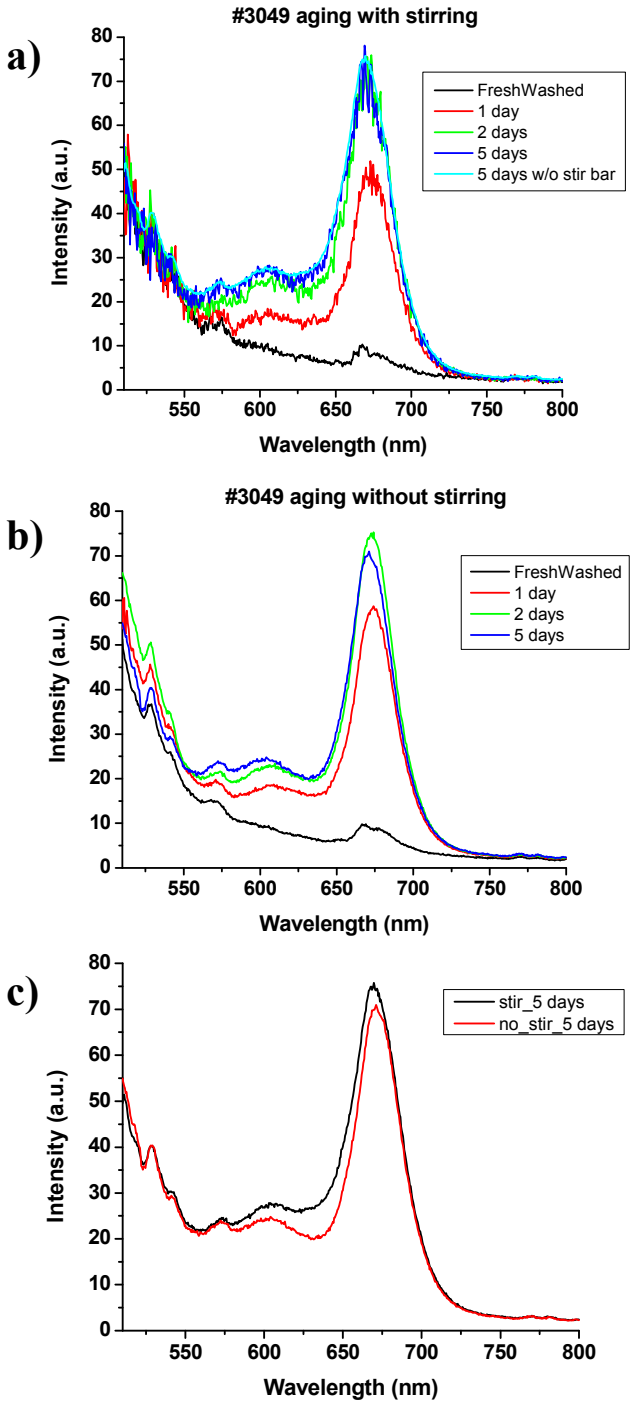

Figure 3-15. The PL evolution of CdSe quantum wire samples (~8 nm) irradiated under fluorescent lamps. (a) stirred to keep wires suspended, (b) without stirring, (c) comparison of the spectra after 5 days.

This result shows that the intensity of the fluorescent light in the fume hood was sufficient to enhance all the quantum wires in the cuvette. Presumably, the slow part of the PL-enhancement process is a surface reconstruction and/or surface-ligand rearrangement which is much slower than the light-absorption process.

Reversibility of the photo-induce PL enhancement.

The PL efficiencies of some organically capped CdSe quantum dots was found to decline significantly upon storage in the dark. Photo-induced recovery of the photoluminescence has been observed in these dots.[5] The dark state, attributed to a surface transformation, was stable for months or until the luminescence was recovered by above-band-gap illumination. The dynamics of the PL recovery were found to follow stretched-exponential kinetics. A similar quasi-reversible photo-enhancement effect in colloidal CdSe and CdSe/ZnS core/shell quantum dots attached to variety of surfactant molecules has also been reported.[7]

The CdSe quantum wires stored in solid form (in solidified TOPO by cooling the synthesis mixture) are very stable. The properties of the nanowires purified from the solid TOPO are as good as the as-prepared CdSe nanowire samples for several months. The purified CdSe quantum wires capped with organic surfactants (TOPO, TOP, OA, and HDA) in toluene solution retain good morphologies and optical properties for several weeks. We observed similar reversible photo-lightening behavior for our CdSe quantum wires as for the quantum dots discussed above when they were alternatively illuminated under fluorescent lights and kept in the dark (Figure 3-16).

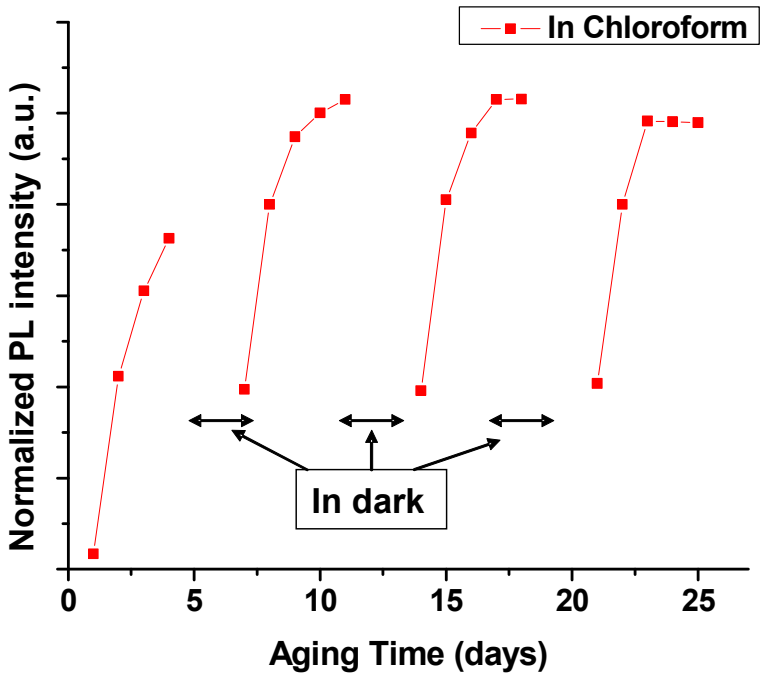

Figure 3-16. The relative PL emission intensities for a CdSe quantum-wire sample (~8 nm) in chloroform illuminated with fluorescent lamps during four illumination periods. The normalization procedure is described in the experimental section.

Typical results from the illumination experiments shown in Figure 3-16 reveal a partially reversible photo-activated photoluminescence enhancement effect. After an initially large PL intensity increase during the first illumination period, the sample was kept in the dark for 2 days, whereupon the PL was observed to partially decay. Subsequent illumination periods (Figure 3-16) resulted in the further PL enhancement of the excition PL intensity followed by repeated diminution in darkness. Chloroform was chosen as the solvent for this experiment because the CdSe quantum wires prepared with DOPA and TDPA have the best dispersibility and stability in chloroform.

The darkening process was not observed when the sample was in the dark for only 1 - 2 hrs. This indicated that the process responsible for the darkening was very slow (usually taking 2 days to achieve). The PL intensities of the CdSe quantum wires immediately after darkening were higher than the original as-prepared sample. Therefore, some irreversible changes to the CdSe quantum wire surface had likely occurred during the illumination. Neither an energy shift of the PL peak nor diameter changes in the CdSe quantum wires were observed during this dark-recovery experiment.

The effect of additional TDPA into the synthesis

In the previous studies of CdSe-nanocrystal growth, alkylphosphonic acids (such as hexylphosphonic acid (HPA)) acted as surfactants that selectively adsorbed to the (001) and (110) faces, shutting down the growth on these faces.[26] This effect speeds up the 1-D growth of the CdSe nanocrystals; therefore, the CdSe system with additional HPA favors the growth of elongated nanostructures, for instance, CdSe nanorods and arrows.[26] Because TDPA (*n*-tetradecylphosphonic acid) and HPA have an identical functional group and differ only by the carbon-chain length, TDPA could be assumed to have the same effect for stabilizing specific facets of wurtzite CdSe nanowires to bind to the dangling bonds on the quantum-wire surface, therefore reduce the surface trap and improve the emission efficiency.

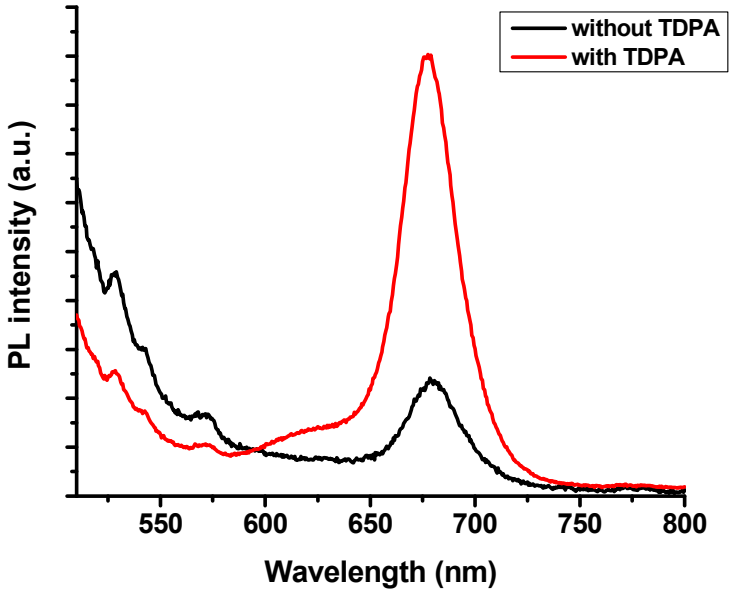

Figure 3-17. Photoluminescence spectra of an as-prepared CdSe quantum wire sample (~8 nm) with added TDPA (5 mg, red curve) and without TDPA (black curve). All the other synthetic conditions were the same. DOPA is present in both syntheses.

Figure 3-17 shows representative PL spectra from well-controlled parallel syntheses of CdSe quantum-wire samples with added TDPA and without TDPA. The sample with 5 mg TDPA in the reaction system showed a significant improvement in the emission efficiency.

The amount of TDPA was varied from 5 mg to 20 mg, but the PL improvement was not significantly affected. Because a large quantity of phosphonic acid added into the reaction system adversely affected the solubility of the CdSe quantum wires, I usually used the least amount (5 mg) of TDPA to improve the photoluminescence efficiency, and retain the solubility of the CdSe nanowires.

The CdSe quantum wires made with different additives show varying degrees of PL enhancement upon illumination. The temporal evolutions of the relative PL intensity of these nanowires are shown in Figure 3-18.

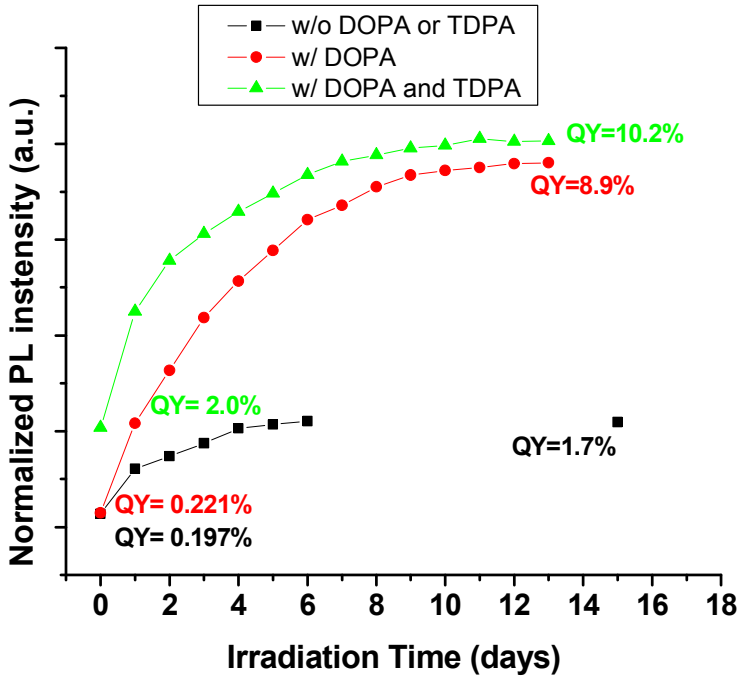

Figure 3-18. Comparison of the photoluminescence enhancement rate of CdSe nanowires synthesized with and without DOPA and TDPA. Black squares (■) are the CdSe nanowires synthesized without DOPA and TDPA. Red circles (●) are CdSe nanowires synthesized with additional DOPA. Green triangles (▲) are CdSe nanowires synthesized with additional DOPA and TDPA. The normalization procedure is described in the experimental section.

All of these CdSe quantum-wire samples were made from $Cd(OA)_2$ as the cadmium precursor. All three samples underwent photo-induced PL enhancement when illuminated under fluorescent lamps. The as-prepared CdSe

quantum wires without TDPA usually have an initially poor quantum yield around 0.2 %. With TDPA in the reaction system, the quantum yield of the as-prepared CdSe nanowires can initially rise to around 2.0 %. The CdSe quantum wires prepared with DOPA (Chapter 2) and TDPA have improved PL intensity after irradiation for several days. These nanowires usually are straighter and have fewer stacking faults and other defects. Presumably they also have better surface-ligand coverage. Photobrightening of these nanowires can achieve much better results compared to the previously synthesized nanowires without DOPA and TDPA.

Additions to the PL enhancement solvent

In both single quantum-dot[27] and quantum-wire[28] studies under a fluorescence microscope, some additional reagents can improve the emission efficiency of the species, such as BME (β-mercaptoethanol),[27] water, and oxygen.

However, for the ensemble CdSe quantum-wire colloids on which I focused, these reagents were difficult to use. Because the CdSe quantum wires are capped with organic ligands and are dispersed in hydrophobic toluene, hydrophilic reagents have failed to enhance the PL of the nanowires. Even a small amount of BME or water caused the irreversible precipitation of CdSe quantum wires from the toluene solution. Bubbling wet air through the CdSe nanowire solution also caused irreversible precipitation in a short time (20 – 30 min).

After synthesis and purification of CdSe nanowires, additional TOP, oleylamine, DOPA and oleic acid were added into the ensemble CdSe quantum-

wire toluene dispersion to explore the effects of these reagents on the photo-induced PL enhancement. All of these additions were in very small amount, otherwise, the CdSe nanowires were dissolved in a few days, or underwent irreversible precipitation. For instance, TOP, olyelamine and oleic acid were added in ~1 mg to 8 ml toluene solution; DOPA is ~ 2 mg in 8 ml toluene solution.

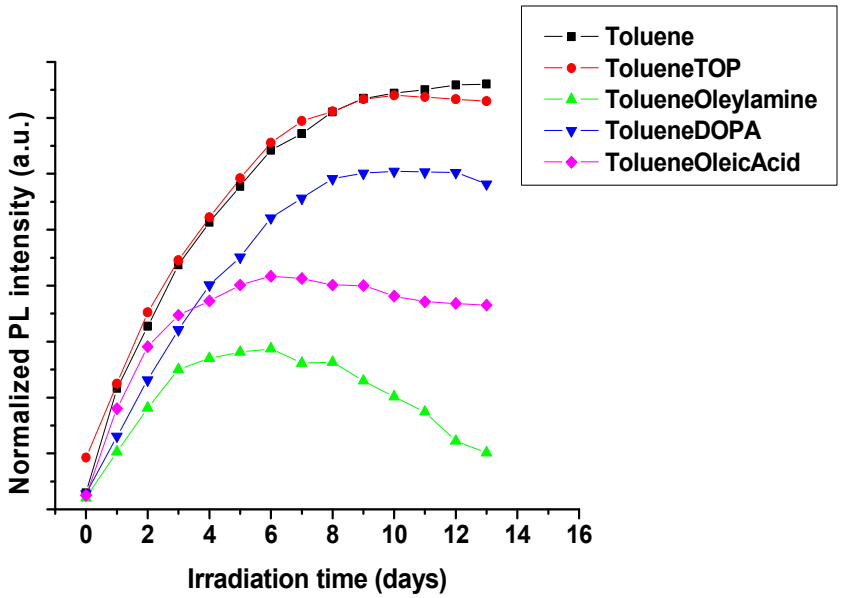

Figure 3-19. Normalized PL intensity profiles of the photo-induced PL enhancement of ensembles of CdSe quantum wires (~8 nm) with additional TOP, oleylamine, DOPA, and oleic acid in the toluene solution. The normalization procedure is described in the experimental section.

From Figure 3-19, most of these additions have no beneficial effect on the photo-induced PL enhancement of CdSe quantum wires except that TOP gave a slightly higher initial PL intensity (red curve of Figure 3-19).

Adding a small amount of TDPA (2 mg into 8 ml solvent, 0.9 mmol/L) into the CdSe quantum wire solution has a significant change to the enhancement rate of this photo-induced process, as shown in Figure 3-20.

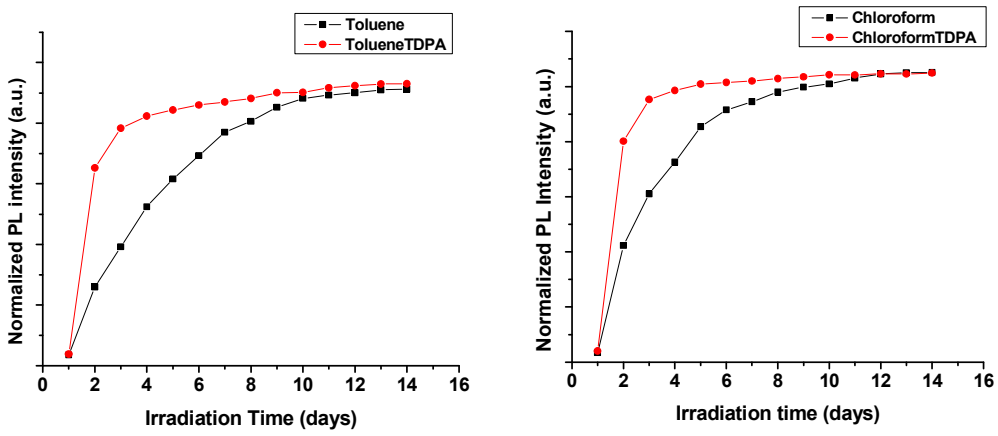

Figure 3-20. Normalized PL intensity profiles of CdSe quantum wire colloids in toluene and chloroform, with and without additional TDPA. The normalization procedure is described in the experimental section.

From the profiles, we can see that adding a small amount of TDPA has no initial effect on the PL intensity of the CdSe quantum wire colloid. However, after 1 - 2 days, the PL intensity of the CdSe nanowires was significantly higher than in the sample without TDPA. After ~10 days, the PL enhancement was about the same as the sample without TDPA. Both the samples reach a similar quantum yield after a period of time (~14 days). TDPA acts as a reagent to speed up the photo-induced PL enhancement rate of the ensemble CdSe quantum wire colloid. Unfortunately, there is no sufficient analytical method to investigate what is

happening to the surface ligands on the CdSe quantum wire with additional TDPA. I suspect TDPA may displace other surface ligands to enhance the surface re-arrangement rate, resulting in higher emission efficiency.

Mechanism of the photo-induced PL enhancement.

Several possible models could explain the photo-induced photoluminescence enhancement of CdSe quantum wires: (1) the dark wires in the ensemble may be induced to start fluorescing; (2) the blinking effect[28] may in some way be inhibited to reduce the amount of the "off" time in the flourescence; or (3) the illumination could cause some chemical change in the luminescent CdSe quantum wires (such as surface-atom reconstruction or surface-ligand rearrangement) that results in higher fluorescence efficiency.

The mechanism of photo-induced PL enhancement of CdSe quantum wires is different from the mechanism of the photoenhancement of CdSe quantum dots. First, the photo-enhancement of CdSe quantum dots can be observed in almost all the CdSe dots system made from various precursors. [2, 4-10, 12, 13] But I only observed photo-induced enhancement from CdSe quantum wires made from $Cd(OA)_2$, not the wires made from $Cd(stearate)_2$. Second, a blue shift of the excitonic PL peak and diameter shrinking were observed during the PL enhancement in most of the CdSe quantum dot studies. But for our CdSe quantum wire system no obvious peak shifting or diameter change occurred during the PL enhancement. Third, the loss of PL intensity of the CdSe quantum wires in the dark was much slower than in the dots, and some irreversible changes occurred

during the photo-enhancement experiment, in contrast to the photon-assisted trap-filling mechanism proposed for the single CdSe quantum-wire study.[28] On the basis of these results, a photo-induced chemistry change on the surface of the CdSe quantum wires is most likely the mechanism of the photo-induced PL enhancement. I propose that the surface atoms of CdSe quantum wires are reconstructed under light illumination, and that surface traps are reduced, such that higher photoluminescence is achieved. Additionally, the unsaturated OA chain and the other surfactants on the CdSe quantum wires may undergo a photo-assisted rearrangement process while illuminated. The rearranged ligands may also reduce the surface traps on the CdSe quantum wires, therefore improving the quantum efficiency of the quantum-wire luminescence.

Conclusion.

The as-prepared CdSe quantum wires dispersed in organic solvents undergo a photo-induced photoluminescence enhancement when illuminated under fluorescent lighting. The proposed mechanism of the phenomenon is photo-induced surface reconstruction and surface-ligand re-arrangement. After irradiation for up to 14 days, the quantum yield of the CdSe quantum wires is enhanced from 0.2 % to ~10 %. We investigated the enhancement procedure with different light power, various additives, and compared the samples with or without stirring during the illumination period. I also observed a partially reversible photobrightening phenomenon, which is similar to the quantum-dot system.

Experimental Section

Chemicals. Cadmium stearate (90%), Cadmium oxide (CdO, 99%), Oleic acid (OA, 90%), tri-*n*-octylphosphine oxide (TOPO, 99%), trioctylphosphine (TOP, 97%) , selenium powder (Se, 100 mesh 99%), poly(1-hexadecene)$_{0.67}$-co-(1-vinylpyrrolidinone)$_{0.33}$, Na[N(SiMe$_3$)$_2$] (1.0M solution in THF) were obtained from Aldrich and used as received. Tetradecylphosphonic acid (TDPA, ~90%) was purchased from Polycarbon Industries Inc. and used as received. Toluene, hexane, and chloroform (analytical grade) were all purchased from Aldrich and used as received. 1,3-diisopropylbenzene (DIPB, from Aldrich) was shaken with concentrated sulfuric acid to remove thiophene, washed with water, and distilled over Na.

Preparation of TOP=Se. A neat mixture of 4 g of elemental Se powder (0.051 mol) and 22 g TOP (0.059 mol) was loaded into a 100 ml storage bottle under dry, O_2-free N_2(g). The Se powder rapidly dissolved into the liquid mixture as heat was evolved. A second portion of 1 g of Se (0.013 mol) was added into the mixture to ensure the conversion of TOP to TOP=Se. The liquid fraction of the mixture was subsequently used.

Preparation of TBP=Se. A neat mixture of 4 g of elemental Se powder (0.051 mol) and 12 g of TBP (0.059 mol) was loaded into a 100 ml storage bottle under dry, O_2-free N_2(g). The Se powder rapidly dissolved into the liquid mixture as heat was evolved. A second potion of 1 g of Se (0.013 mol) was added into the mixture to ensure that all of the TBP had been converted to TBP=Se. The liquid fraction of the mixture was subsequently used.

Preparation of Bi-nanoparticle stock solutions. Monodispersed Bi nanoparticles were grown in DIPB solutions of poly(1-hexadecen) $_{0.67}$-co-(1-vinylpyrrolidinone) $_{0.33}$ and $Na[N(SiMe_3)_2]$ at elevated temperatures (170-210 ^oC), following the procedure previously reported.[29] The diameter of Bi nanoparticles were tuned from 5 to 18 nm (std. deviation = 5-10% of the mean diameter) by varying reaction conditions, and the effective concentration of the dispersions was 0.04 mmol of Bi/g DIPB.

Bi-catalyzed growth of CdSe nanowires. In a typical synthesis of CdSe nanowires, 6 mg of CdO (0.047 mmol), 53 mg of oleic acid (0.19 mmol), 50 mg of hexadecylamine (0.21 mmol), and 5 g of trioctylphosphine oxide (13 mmol) were loaded into a 50 ml reaction tube, which was degassed on a Schlenk line and backfilled with N_2. The reaction mixture was heated at 320 ^oC in a salt bath ($NaNO_3$: KNO_3 ~ 1:1) until a clear solution was generated (~ 10 min). Then, the reaction tube was transferred to a 250 ^oC salt bath for wire growth. At this temperature, a mixed solution of 500 mg of TOP=Se (1.1 mmol), 100 mg of TOP (0.27 mmol) and 23 mg of Bi solution (0.00092 mmol) was rapidly injected into reaction tube.. After 5 min reaction, the reaction mixture was allowed to cool to room temperature.

1 ml aliquot of the reaction mixture was dissolved into 2 ml of toluene, the wires were precipitated with 6 ml of methanol and the sample was centrifuged and the supernatant was decanted. The precipitates were re-dispersed in 2 ml of toluene, precipitated with 6 ml of methanol, followed by centrifugation and

decanting the supernatant again. Then, the precipitates were re-dissolved in toluene for optical measurements.

The diameter of CdSe nanowires grown by this approach were varied by changing the reaction temperature from 240-280 ^{o}C and by choosing different-sized Bi nanoparticles as the catalyst seeds.

Photo-enhancement of CdSe quantum wires. Purified CdSe quantum wires were dispersed in a desired solvent (toluene, chloroform, or hexane) and placed in a quartz cuvette. To minimize the contact with atmosphere and water, the cuvette was sealed with a teflon cap and wrapped with parafilm. For irradiation under fluorescent lamps, the sample was placed on the bench in a fume hood, away from any heat source. For irradiation under a UV lamp (300-W xenon lamp, equipped with a short-pass filter having a cutoff wavelength of 700 nm), the sample was placed in a special lamp box with a cooling system. For measurement of the PL spectrum, the cuvette was removed from the fume hood or lamp box and placed in the fluorometer. Then the cuvette was returned for further illumination. The collection of each spectrum required ~ 15 min. The light power density of the fluorometer at 488nm with 5nm excitation slit is 2.5 $\mu W/cm^2$, which is much lower than the light power of the photo-induced PL enhancement experiment.

Determination of the suitable concentration range for PL quantum-yield measurement.

First, we need to determine the concentration range of our standard free-base TPP. To make sure our ensemble CdSe nanowire PL result was consistent

with the single-wire study, we chose 488 nm as the excitation wavelength. Since the PL quantum yield of freebase TPP is very high, the absorbance at 488 nm is very low. I measured 5 different concentrations of freebase, and took the PL spectra at these different concentrations. The results are shown in Figure 3-21.

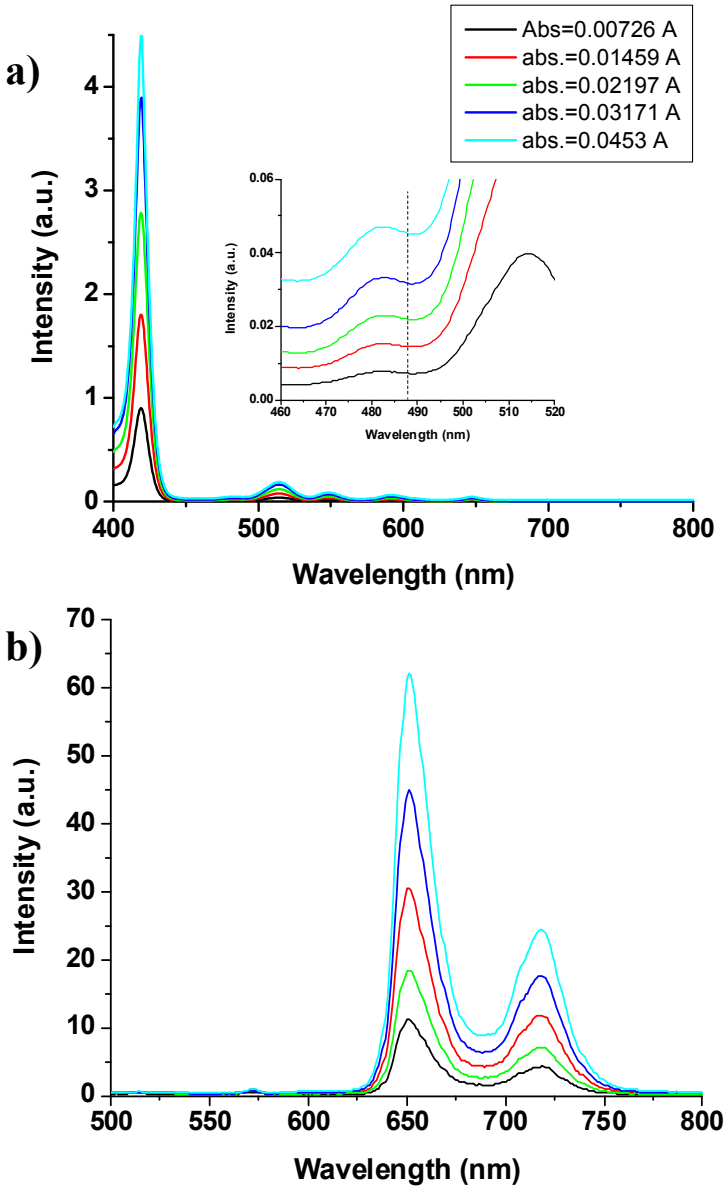

Figure 3-21. The absorption (a) and photoluminescence (b) spectra of freebase TPP at 5 concentrations. The excitation wavelength is 488 nm.

The PL intensity of the freebase increases when the absorbance increases at the excitation wavelength of 488 nm. We calculated the integrations of the PL spectra at different concentrations and plotted them against the absorbance. The table and the plot are shown in Figure 3-22. We found that the integrated PL vs. absorbance is a linear relationship. This result indicated that at this concentration range, freebase TPP shows a linear PL quantum yield increment while increasing the absorbance at excitation wavelength. Thus, this concentration range (from 0.00726 to 0.0453 A) is suitable for PL quantum yield measurement.

Absorbance	Integration
0.00726 A	443.11611
0.01459 A	743.33233
0.02197 A	1201.67459
0.03171 A	1776.34225
0.0453 A	2457.57072

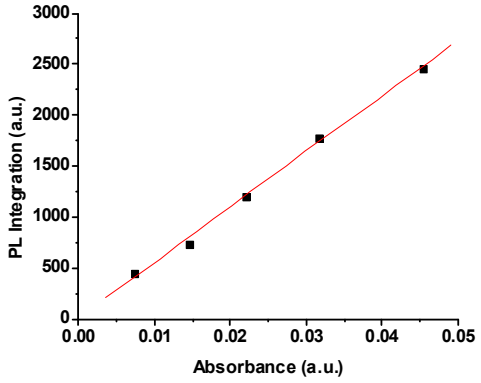

Figure 3-22. The integration of the PL spectra and the plot of integrated PL vs. absorbance for freebase TPP.

To investigate the suitable concentration range for our CdSe quantum-wire solution, the same experiment was conducted. I varied the absorbance of the CdSe quantum wires in toluene at 488 nm over 4 different values, then measured the PL spectrum at each concentration. The results are shown in Figure 3-23.

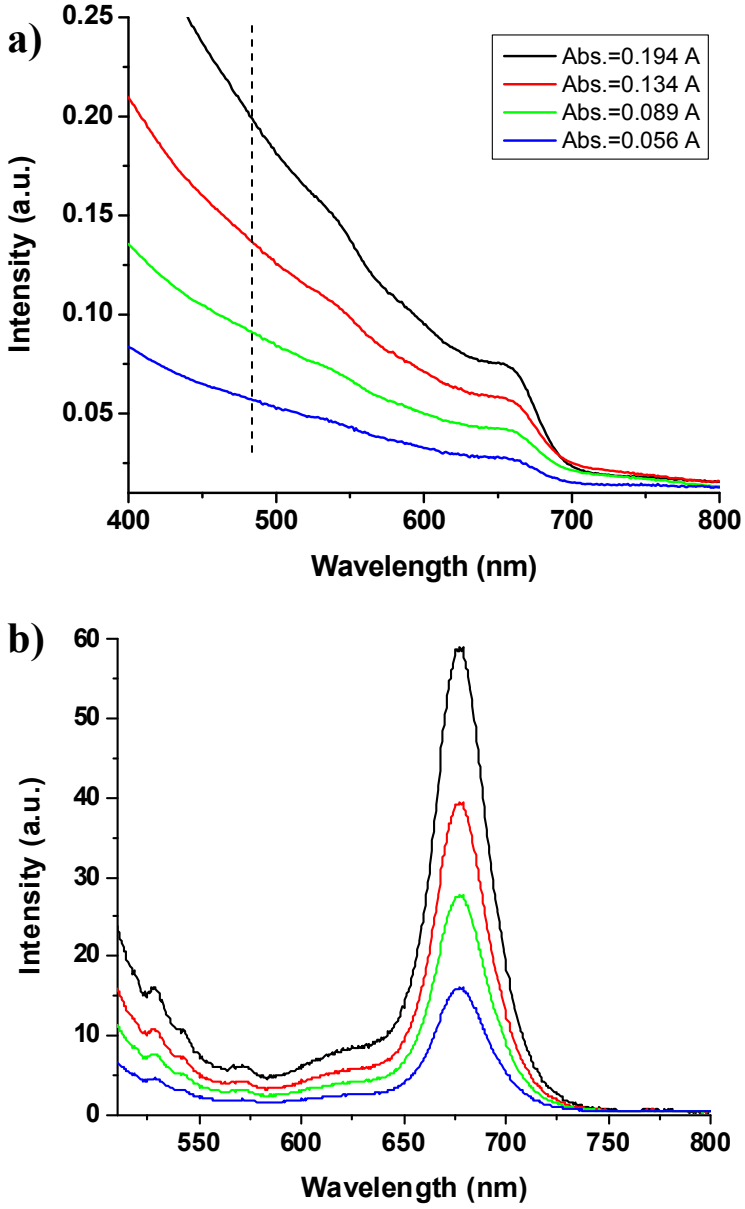

Figure 3-23. The absorption (a) and photoluminescence (b) spectra of CdSe nanowires (~8 nm) at 4 different concentrations. The excitation wavelength is 488 nm.

Similar results were obtained for the CdSe quantum wire samples as for freebase TPP. Calculations and the plot of the integrated PL vs. absorbance are shown in Figure 3-24. The linear relationship between intergrated PL and absorbance showed that this concentration range (from 0.056 to 0.194 A) is appropriate for PL quantum-yield measurements.

Absorbance	Integration
0.194 A	3685.48
0.134 A	2486.99
0.089 A	1770.89
0.056 A	1054.80

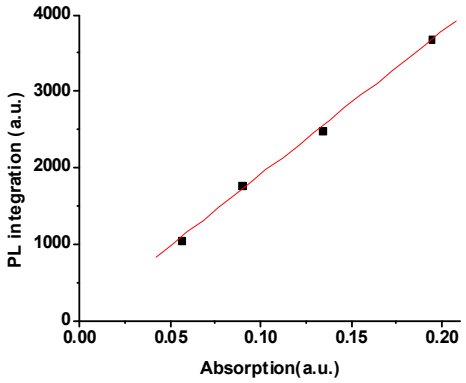

Figure 3-24. The integration of the PL spectra and the plot of integrated PL vs. absorbance for CdSe quantum-wire samples (~8 nm).

Normalization of the PL spectra. An absorption spectrum was recorded prior to each photoluminescence spectrum. A normalization factor was determined for each absorption spectrum to adjust the absorbance at 488 nm to a common value. This normalization factor was subsequently applied to scale the PL intensities in the corresponding PL spectrum.

Characterization. Samples for TEM analysis were prepared by dropping a dilute toluene solution of nanowires onto the 300-mesh carbon-coated copper grids. TEM images were recorded using a JEOL 2000 FX microscope operating at 200 kV. The diameter distribution for each sample was determined using several TEM images at 500K magnification to ensure accurate measurement. The wire diameters were measured and recorded using Image-Pro Express software (version 4.5), and the distribution histograms were constructed from 400-500 diameter measurements for each specimen. Simulations, peak fits and integration calculations were all done via Origin (version 7). UV-visible absorption spectra were recorded on a Varian Cary 100E spectrophotometer at room temperature. The nanowire solution was prepared by diluting the purified nanowire sample with toluene in a 1-cm path-length quartz cuvette, and the baseline correction was performed prior to each measurement. Photoluminescence (PL) spectra were obtained from a Varian Cary Eclipse fluorescence spectro-photometer at room temperature. ^{31}P NMR spectra of CdSe quantum-wire samples were acquired on a Varian Mercury-300 spectrometer with $CDCl_3$ or d_6-acetone as the solvent. MALDI-MS analysis of CdSe nanowires were performed on an ABI 4700 MALDI TOF-TOF on a DHB (2, 5-Dihydroxy benzoic acid) substrate.

References:

1. Manna, L.; Scher, E. C.; Li, L. S.; Alivisatos, A. P. *Journal of the American Chemical Society* **2002,** 124, (24), 7136-7145.

2. Zhelev, Z.; Jose, R.; Nagase, T.; Ohba, H.; Bakalova, R.; Ishikawa, M.; Baba, Y. *Journal of Photochemistry and Photobiology B-Biology* **2004,** 75, (1-2), 99-105.

3. Silver, J.; Ou, W. *Nano Letters* **2005,** 5, (7), 1445-1449.

4. Wang, Y.; Tang, Z. Y.; Correa-Duarte, M. A.; Pastoriza-Santos, I.; Giersig, M.; Kotov, N. A.; Liz-Marzan, L. M. *Journal of Physical Chemistry B* **2004,** 108, (40), 15461-15469.

5. Hess, B. C.; Okhrimenko, I. G.; Davis, R. C.; Stevens, B. C.; Schulzke, Q. A.; Wright, K. C.; Bass, C. D.; Evans, C. D.; Summers, S. L. *Physical Review Letters* **2001,** 86, (14), 3132-3135.

6. Cordero, S. R.; Carson, P. J.; Estabrook, R. A.; Strouse, G. F.; Buratto, S. K. *Journal of Physical Chemistry B* **2000,** 104, (51), 12137-12142.

7. Jones, M.; Nedeljkovic, J.; Ellingson, R. J.; Nozik, A. J.; Rumbles, G. *Journal of Physical Chemistry B* **2003,** 107, (41), 11346-11352.

8. van Sark, W. G. J. H. M.; Frederix, P. L. T. M.; Van den Heuvel, D. J.; Gerritsen, H. C.; Bol, A. A.; van Lingen, J. N. J.; Donega, C. D.; Meijerink, A. *Journal of Physical Chemistry B* **2001,** 105, (35), 8281-8284.

9. Jin, W. J.; Fernandez-Arguelles, M. T.; Costa-Fernandez, J. M.; Pereiro, R.; Sanz-Medel, A. *Chemical Communications* **2005**, (7), 883-885.

10. Biju, V.; Makita, Y.; Sonoda, A.; Yokoyama, H.; Baba, Y.; Ishikawa, M. *Journal of Physical Chemistry B* **2005,** 109, (29), 13899-13905.

11. Korsunska, N. E.; Dybiec, M.; Zhukov, L.; Ostapenko, S.; Zhukov, T. *Semiconductor Science and Technology* **2005,** 20, (8), 876-881.

12. Kimura, J.; Uematsu, T.; Maenosono, S.; Yamaguchi, Y. *Journal of Physical Chemistry B* **2004,** 108, (35), 13258-13264.

13. Uematsu, T.; Maenosono, S.; Yamaguchi, Y. *Journal of Physical Chemistry B* **2005,** 109, (18), 8613-8618.

14. Nazzal, A. Y.; Qu, L. H.; Peng, X. G.; Xiao, M. *Nano Letters* **2003,** 3, (6), 819-822.

15. Simurda, M.; Nemec, P.; Trojanek, F.; Maly, P. *Thin Solid Films* **2004,** 453-54, 300-303.

16. Chon, J. W. M.; Gu, M.; Bullen, C.; Mulvaney, P. *Applied Physics Letters* **2004,** 84, (22), 4472-4474.

17. Oda, M.; Shen, M. Y.; Saito, M.; Goto, T. *Journal of Luminescence* **2000,** 87-9, 469-471.

18. Crooker, S. A.; Hollingsworth, J. A.; Tretiak, S.; Klimov, V. I. *Physical Review Letters* **2002,** 89, (18), -.

19. Derfus, A. M.; Chan, W. C. W.; Bhatia, S. N. *Nano Letters* **2004,** 4, (1), 11-18.

20. Donega, C. D.; Hickey, S. G.; Wuister, S. F.; Vanmaekelbergh, D.; Meijerink, A. *Journal of Physical Chemistry B* **2003,** 107, (2), 489-496.

21. Qu, L. H.; Peng, X. G. *Journal of the American Chemical Society* **2002,** 124, (9), 2049-2055.

22. Yu, W. W.; Qu, L. H.; Guo, W. Z.; Peng, X. G. *Chemistry of Materials* **2003,** 15, (14), 2854-2860.

23. Dhami, S.; Demello, A. J.; Rumbles, G.; Bishop, S. M.; Phillips, D.; Beeby, A. *Photochemistry and Photobiology* **1995,** 61, (4), 341-346.

24. Blasse, G.; Donega, C. D.; Berezovskaya, I.; Dotsenko, V. *Solid State Communications* **1994,** 91, (1), 29-31.

25. deBlank, J.; Blasse, G. *European Journal of Solid State and Inorganic Chemistry* **1996,** 33, (4), 295-307.

26. Manna, L.; Scher, E. C.; Alivisatos, A. P. *Journal of the American Chemical Society* **2000,** 122, (51), 12700-12706.

27. Hohng, S.; Ha, T. *Journal of the American Chemical Society* **2004,** 126, (5), 1324-1325.

28. Glennon, J. J.; Tang, R.; Buhro, W. E.; Loomis, R. A. *Nano Letters* **2007,** 7, (11), 3290-3295.

29. Wang, F. D.; Tang, R.; Yu, H.; Gibbons, P. C.; Buhro, W. E. *Chemistry of Materials* **2008,** 20, (11), 3656-3662.

Chapter 4

Syntheses of CdSe/CdS core/shell nanowires and water-dispersible CdSe nanowires

Introduction

Semiconductor nanocrystals are of great scientific interest because their intrinsic optical and electrical properties make them amenable for uses in photovoltaics,[1] electronics,[2] and sensors.[3] However, the surface of a nanocrystal is made up of atoms that are not fully coordinated; it is highly active and invites the possibility of epitaxial overgrowth of another semiconductor or other inorganic material. Because surface atoms act like defects unless passivated, to remove these defects, high-quality homogeneous II - VI and III – V nanocrystals have been passivated with long-chain organic surfactants.[4, 5] These "capped" nanocrystals have room-temperature photoluminescence quantum yields as high as 50% with a very long fluorescence lifetime. These core-only nanocrystals often have some non-band-edge luminescence.[4, 5] It is generally very difficult to simultaneously passivate both anionic and cationic surface sites by organic ligands; there are always some dangling bonds on the surface. [5, 6]

Nanocomposite materials provide the possibility for enhanced functionality and multifunctional properties in contrast with their more-limited single-component conterparts. One example of a nanocomposite material is the inorganic core-shell structure. In the case where semiconductors comprise the core and shell, the core-shell motif has permitted enhanced photoluminescence,[5-7] improved stability against photochemical oxidation,[8] enhanced processibility,[9] and engineered band structures.[10] Among those core-shell semiconductor nanocrystals, core-shell CdSe structures have been well studied.[5-7,12] The most studied core/shell structure to date is CdSe/ZnS, as evidenced by the number of

publications dealing with this system. Its synthesis was first described by Hines and Guyot-Sionnest, who overcoated 3-nm CdSe nanocrystals with 1~2 monolayers of ZnS, resulting in a quantum yield of 50%.[5] ZnS shell growth has been achieved by the injection of a mixture of the organometallic precursors diethylzinc and hexamethyldisilathiane, also known as bis(trimethylsilyl)sulfide, $S(TMS)_2$, at high temperature (300 ^oC). Using shell-growth temperatures of 140-220 ^oC, a size series of CdSe/ZnS nanocrystals and their in-depth characterization were reported by Bawendi's group.[6, 11, 12]

Core/shell nanocrystals are nanometer-sized inorganic clusters of semiconductor material useful for fluorescent labeling in multicolor biological imaging and detection.[13] These colloidal nanocrystals consist of an inorganic particle and an organic coating that determines their solubility and functionality and influences their photophysics.[14] For these nanocrystals to be biocompatible, they must be water-soluble, non-toxic to the cell, and offer conjugation chemistries for attaching recognition molecules to their surfaces.[14] In addition, they should efficiently target to biomolecules of interest, be chemically stable, and preserve their high photostability.

In this chapter, I will discuss techniques for growing inorganic shells on CdSe quantum wires to improve the photoluminescence quantum efficiency and stability; and for growing various organic shells onto CdSe quantum wires to make them water dispersible, which is potentially useful for bio-applications of these 1-D quantum structures.

Results and Discussion

Classifications of Core/shell systems.

Depending on the bandgaps and the relative positions of electronic energy levels of the involved semiconductors, the shell can have different functions in the core/shell systems. Figure 4-1 shows the band alignment of the three distinct cases of core/shell systems.[15]

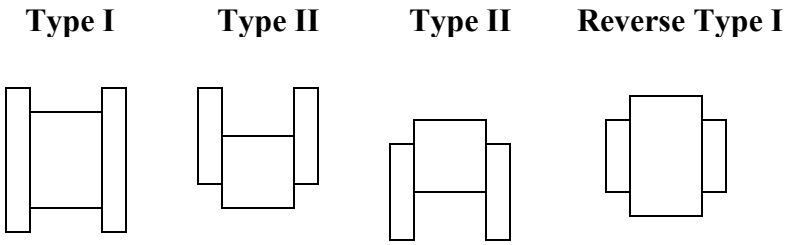

Figure 4-1. Schematic illustration of the energy-level alignment in different core/shell systems realized with semiconductors to date. The upper and lower edges of the rectangles correspond to the positions of the conduction- and valence-band edge of the core (center) and shell (outer) materials, respectively.

In a type-I system, the bandgap of the shell material is larger than that of the core and both electrons and holes are confined in the core. In a type-II system, either the valence-band or the conduction-band edge of the shell material is located in the bandgap of the core. In the reverse type-I system, the bandgap of the shell material is smaller than that of the core, depending of the thickness of the shell, the holes and electrons are partially or completely confined in the shell. Upon excitation of the semiconductor nanocrystals, the resulting staggered band

alignment leads to a spatial separation of the hole and the electron in different regions of the core/shell structure.

To improve the optical properties of semiconductor nanocrystals, the type- I core/shell structure is the most useful and important.[11, 12] The shell is used to physically separate the surface of the optically active core from its surrounding medium. Consequently, the sensitivity of the optical properties to changes in the local environment of the nano-structure surface, induced, for example, by the presence of oxygen or water molecules, is reduced. With respect to core-only nanocrystals, core/shell systems exhibit generally enhanced stability against photodegradation. At the same time, shell growth reduces the number of surface dangling bonds, which can act as trap states for charge carriers and thereby reduce the photoluminescence quantum yield.

Choice of the shell materials.

A general requirement for the shell materials for synthesizing core/shell nanostructures with satisfactory optical properties is epitaxial-type shell growth. Therefore an appropriate band alignment is not the sole criterion for the choice of materials but rather the core and shell materials should crystallize in the same structure and exhibit a small lattice mismatch.[15] In the opposite case, the growth of the shell results in strain and the formation of defect states at the core/shell interface or within the shell.[15] These can act as trap sites for photo-generated

charge carriers and diminish the photoluminescence quantum yield. Table 4-1 lists the material parameters of selected seminconductors.

Table 4-1 . Material parameters of selected bulk semiconductors.[15, 16]

Material	Structure [300K]	Type	E_{gap} [eV]	Lattice parameter [Å]	Band alignment VB/CB (eV)
ZnS	Wurtzite	II-VI	3.91	3.82/6.26	0/3.91
ZnSe	Zinc blende	II-VI	2.69	5.668	0.53/3.75
ZnTe	Zinc blende	II-VI	2.39	6.104	1.26/3.65
CdS	Wurtzite	II-VI	2.49	4.136/6.714	0.18/2.67
CdSe	Zinc blende	II-VI	1.76	5.82	0.60/2.36
CdSe	Wurtzite	II-VI	1.84	4.3/7.01	0.60/2.44
CdTe	Zinc blende	II-VI	1.43	6.482	1.17/2.60
GaN	Wurtzite	III-V	3.44	3.188/5.185	-0.72/2.72
GaP	Zinc-blende	III-V	2.27	5.45	0.99/3.26
GaAs	Zinc blende	III-V	1.42	5.653	1.46/2.88
GaSb	Zinc blende	III-V	0.75	6.096	2.03/2.78
InN	Wurtzite	III-V	0.8	3.545/5.703	-0.46/0.34
InP	Zinc blende	III-V	1.35	5.869	1.10/2.45
InAs	Zinc blende	III-V	0.35	6.058	1.52/1.87
InSb	Zinc blende	III-V	0.23	6.479	2.02/2.25

The table shows that wurtzite CdS and ZnS can be suitable shell materials for wurtzite CdSe core nanowires because of their larger band gap, similar lattice constants, and suitable band offsets for forming type-I core-shell structures to improve the PL quantum efficiency of the quantum wires. The lattice parameters and band alignments for wurtzite CdSe, CdS and ZnS are highlighted in Table 4-1.

Precursors for shell growth.

Appropriate precursors for shell growth should fulfill the criteria of high reactivity and selectivity (no side reactions). For practical reasons and in particular if the scale-up of the production process is sought, additional properties of the precursors come into play. Pyrophoric and highly toxic compounds require special precautions for manipulation, especially in large quantities. An example is the synthesis of cadmium sulfide, one of the most important shell materials used for overcoating numerous II-VI and III-V semiconductor nanocrystals.[17-19] Initially, this synthesis was done with diethylcadmium (pyrophoric) and hexamethyldisilathiane (toxic). Even though widely used in laboratory-scale syntheses, these compounds are not suitable for large-scale production of CdS overcoated nanocrystals. Therefore, a number of alternative precursors were proposed, that are non-pyrophoric and less toxic.[20, 21]

In our shell-growth experiment, cadmium carboxylates and elemental sulfur were used for growing CdS shells; zinc carboxylates and elemental sulfur were used for growing ZnS shells.

Control of the shell thickness.

The control of the shell thickness is a delicate point in the fabrication of core-shell nanocrystals. If the shell is too thin, the passivation of the core nanocrystals is inefficient, resulting in reduced photostability or even the

production of more surface traps, therefore decreasing the photoluminescence quantum efficiency. In the opposite case, if the shell is too thick, the optical property of the nanocrystal generally deteriorates too as a consequence of strain induced by the lattice mismatch of the different core and shell materials, accompanied by the generation of the defect states.[22, 23]

Core/shell systems are typically fabricated in a two-step procedure: initial synthesis of the core materials, followed by a purification step, which is optional, and the subsequent shell-growth reaction. During this final step, a small number of monolayers (typically 1 ~ 5) of the shell materials are deposited on the cores.[17] In order to prevent nucleation of the shell materials and uncontrolled ripening of the core nanocrystals, the temperature of shell growth is usually lower than the temperature of the synthesis of the core structure.[17] Furthermore the shell precursor is added slowly, for example, dropwise injection by means of a syringe. Slow injection of the shell precursor can help the well-distributed growth of the shell materials so that better coverage and controlled thickness of the shell can be achieved.[17]

To calculate the required amount of the shell precursors to obtain the desired shell thickness, it is necessary to know the amount of the core materials in the reaction system. Since the Se precursor is in large excess in our CdSe quantum-wire synthesis, assuming all Cd precursors were converted to the CdSe nanowires (no other morphologies were observed in the TEM images of our CdSe quantum-wire synthesis), the mole amount of the Cd precursor can be roughly calculated to be equal to the moles of the CdSe nanowires formed. The following

calculation procedure shows an example of the amount required to grow a 3-monolayer CdS shell onto 7-nm CdSe nanowires (the core nanowire diameter is obtained from TEM images), where d is the diameter of the nanowire, R is the radius of the nanowire, D is the thickness of the shell, and N_A is Avogadro's number.

For a d = 7 nm (R = 3.5 nm) CdSe nanowire core to grow a 3-monolayer CdS (D = 3*0.35 nm = 1.05 nm) shell:

Lattice parameter of wurtzite CdSe: a = 4.30 Å c = 7.02 Å

Volume of a single CdSe atom pair: $V^0_{CdSe} = \sqrt{3}/4a^2c = 56.2$ Å^3

Lattice parameter of wurtzite CdS: a = 4.136 Å c=6.714 Å

Volume of a single CdS atom pair: $V^0_{CdS} = \sqrt{3}/4a^2c = 49.7$ Å^3

Imagine CdSe nanowires with a cylindrical geometry,

Total atom pairs in the CdSe core nanowires (0.047 mmol, based on the assumption of the complete reaction of Cd and Se precursor):

$0.047E^{-3}$ mol CdSe * N_A =2.83 E^{19}

Total volume in the CdSe core nanowires ~

2.83 E^{19} * 56.2 Å^3 =1.59 E^{21} Å^3 = 1.59 E^{18} nm^3

Total length of CdSe nanowires (d = 7 nm):

L = 1.59 E^{18} nm^3 / πR^2 = 4.13 E^{16} nm

Total volume of 3 monolayers of CdS growing onto 7 nm CdSe nanowires:

$V_{CdS} = 2\pi R^* L * D = 9.36\ E^{17}$ nm^3

Mol of CdS = V_{CdS} / N_A/ V^o_{CdS} = 0.0319 mmol

Both the Cd and S Stock solutions are 0.04 M. The amount of the stock solution needed for shell growth:

0.00319 mmol/0.04 M = 0.80 ml of each Cd and S stock solution.

Characterization of core/shell nanowires.

Most of the basic characterization techniques for core nanowires are also applied to investigate core/shell nanowires, such as UV/vis spectroscopy, PL spectroscopy, powder X-ray diffraction and transmission electron microscopy (TEM). In the case of core/shell systems, however, several experimental difficulties may arise in proving successful shell growth. Optical properties, generally extremely sensitive to nanowire surface modification, can only give indirect information about the possible overcoating with a shell. The increase of the nanowire diameter revealed by TEM or high-resolution TEM is considered to be the most direct proof of successful shell growth. Nevertheless, an accurate determination of the size difference before and after addition of the shell can be severely limited or even impossible by TEM depending on the materials used, the size and size distribution of the core nanowires, and the shell thickness. Advanced microscopy techniques including scanning transmission election microscopy (STEM) coupled with electron energy loss spectroscopy (EELS) or with energy-dispersive X-ray spectroscopy (EDX) can give valuable insight into the obtained core/shell structures.[24]

Epitaxial growth of CdSe/CdS core/shell nanowires.

Two methods were tested for preparing the CdSe core nanowires for CdS shell growth. In the first method, the core CdSe nanowires were first purified by precipitation/decantation.

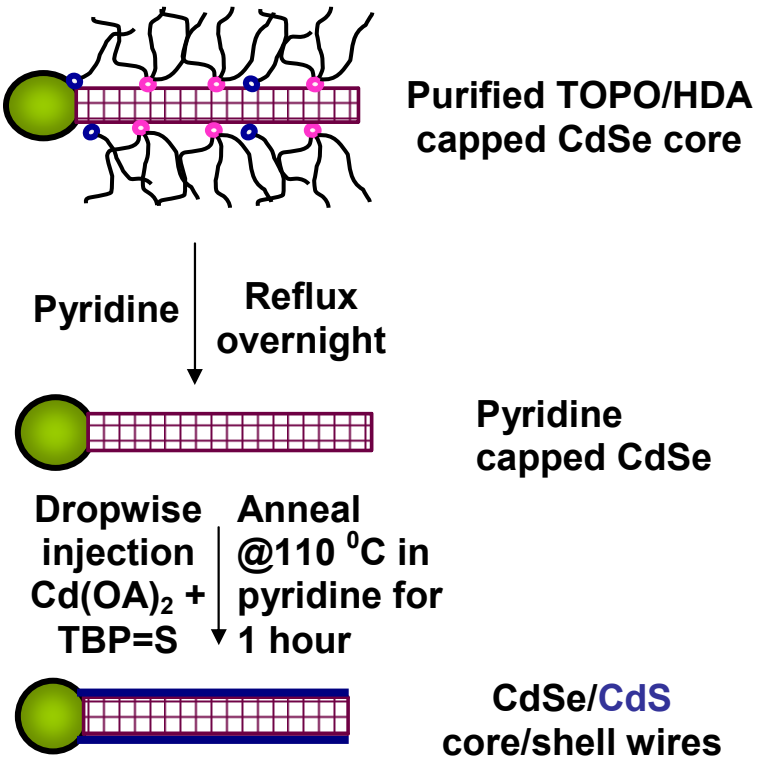

Figure 4-2. Schematic synthesis of CdSe/CdS core/shell nanowires. The CdSe core nanowires were purified before growing the CdS shell followed by refluxing in pyridine overnight.

For this process, pyridine was chosen as a reflux solvent on the basis of prior CdSe/CdS quantum-dot studies.[7, 25] After refluxing CdSe quantum dots in pyridine overnight, TOPO was almost completely removed from the CdSe

quantum dots without affecting their structure. Pyridine displaces TOPO and forms a weak bond to surface atoms of the CdSe quantum dots. Furthermore, NMR studies in the quantum-dot system revealed that pyridine forms a labile bond to the surface Cd atoms of CdSe nanocrystals.[26] Therefore, nanowires refluxed in pyridine should be dynamically capped, providing simultaneous chemical stability and access to the surface. This reaction, schematically shown in Figure 4-2, was conducted at 100 ^{o}C.

The Cd/S precursor molar ratio for shell growth in this process was also very important. Because our core CdSe quantum wires were synthesized under Se-rich conditions, the surface of the CdSe quantum wires was Se rich. For trials using S:Cd > 1.5:1 for shell growth, the formation of CdS-only nanocrystals (having a high-energy exciton peak in the absorption spectrum) was observed. When the Cd:S precursor ration was more than 1:1, the formation of the CdS-only nanocrystals was prevented at the 100 ^{o}C reaction temperature; only shell growth occurred. By checking the absorption spectra of aliquots, it was found that Cd/S precursors participated only in shell growth. No CdS-only features were observed.

Plots of the absorption spectra for well-controlled CdSe/CdS core/shell nanowire synthesis via this approach are given in Figure 4-3. From the spectra, the original purified CdSe core nanowires have a first excitonic peak around 680 nm, which is shown as the black curve. But after refluxing the nanowires in pyridine overnight, the first excitonic feature shifted to around 660 nm. This blue shift indicated a decrease in the diameter of the CdSe nanowires during the refluxing process. At the same time as pyridine replaced the TOPO/TOP as the

surfactant of the CdSe core nanowires, some of the surface Cd and Se atoms were apparently also removed. The loss of the surface atoms caused the reduction in the diameter of the CdSe quantum wires and the blue-shift of the absorption spectrum. The green curve shows the absorption spectrum of the CdSe/CdS core/shell nanowires, which exhibited a first excitonic feature around 660 nm. This is similar to the core nanowires after refluxing.

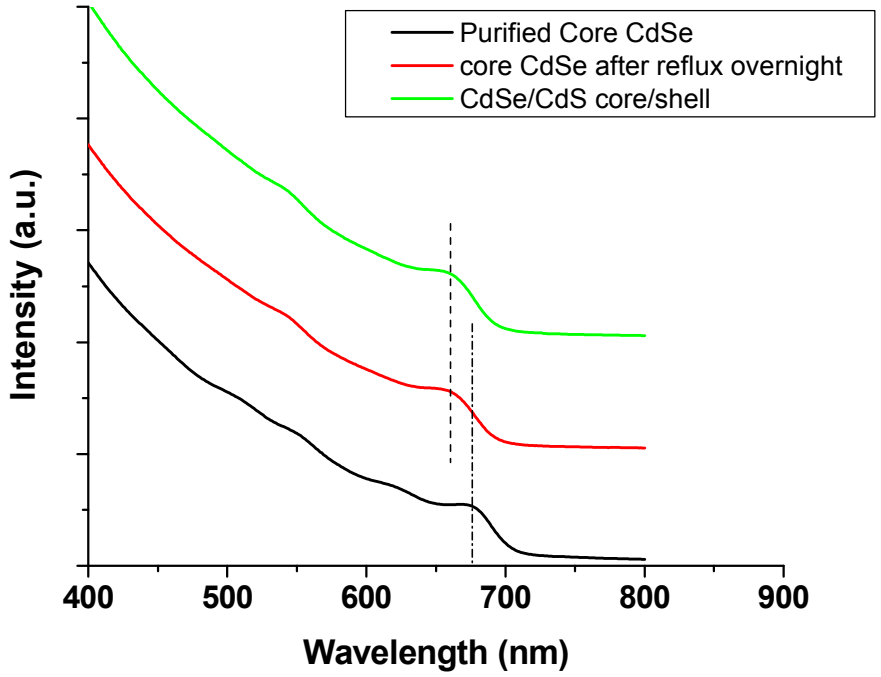

Figure 4-3. Absorption spectra of the core CdSe nanowires (black curve), refluxed, pyridine-capped CdSe core nanowires (red curve), and core/shell CdSe/CdS nanowires (green curve).

The TEM images of the CdSe core and the CdSe/CdS core/shell structures are shown in Figure 4-4. Although the TEM images did not directly confirm the

shell growth, a large population of CdS nanocrystals was absent. The quality of the core/shell nanowires was reduced compared to the CdSe core wires, presumably due to the reflux procedure in pyridine.

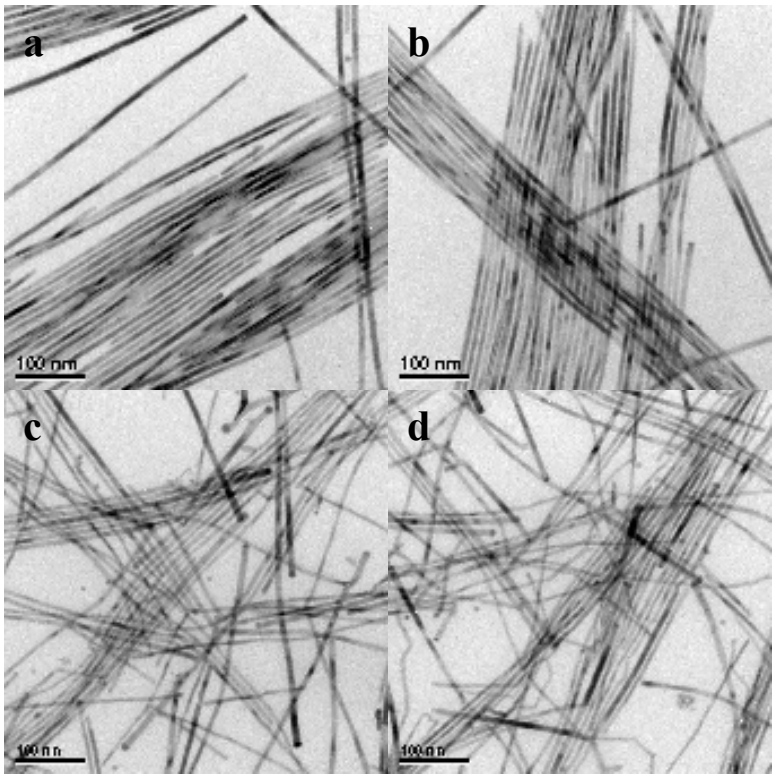

Figure 4-4. TEM images of CdSe core nanowires (a, b) and CdSe/CdS core/shell nanowires.

The photoluminescence spectra of the ensemble CdSe core-only nanowires and CdSe/CdS core/shell nanowires are shown in Figure 4-5. There was a significant enhancement of the photoluminescence efficiency for the CdSe/CdS core/shell nanowires compared to the core-only nanowires, indicating the

successful formation of a type-I core/shell nanostructure. Both electrons and holes were more efficiently confined in the CdSe core; therefore an improved quantum yield was achieved. The blue shift was calculated from the guidelines in the plot to be ~ 20 nm, which is consistent with the blue shift in the absorption spectra of the two samples.

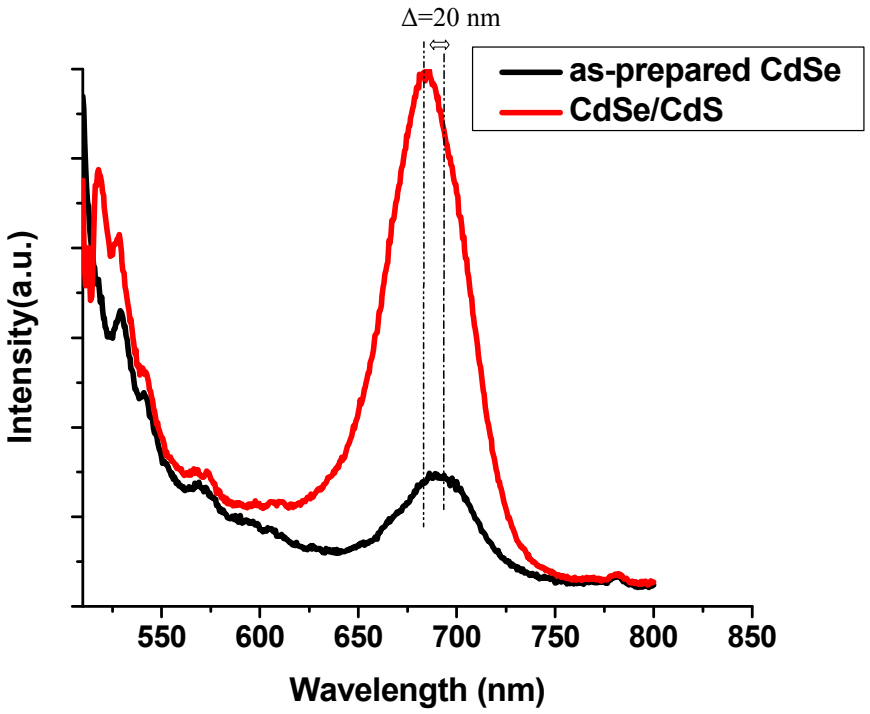

Figure 4-5. Photoluminescence spectra of CdSe core nanowires and CdSe/CdS core/shell nanowires made from pyridine-reflux preparation method.

The diameter of the core CdSe nanowires was 8.48 nm (± 11.1%), and the diameter of the CdSe/CdS core/shell nanowires prepared by the first method was

8.60 nm (± 17.5%). The histograms of the measurement of the diameter of the core and core/shell wires are shown in Figure 4-6. The similar diameter of the core CdSe nanowires and the CdSe/CdS core/shell nanowires resulted from the diameter shrinking during the reflux procedure and the shell growth.

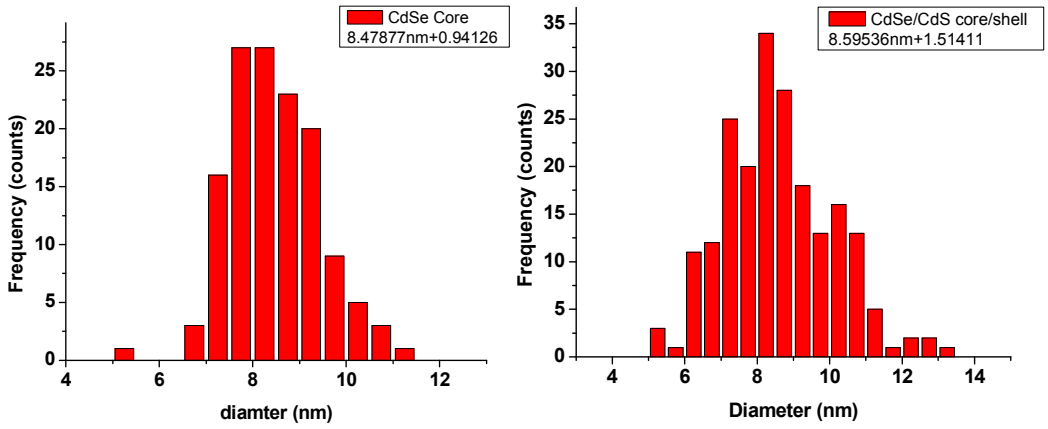

Figure 4-6. Histograms of the diameters of CdSe core nanowires and CdSe/CdS core/shell nanowires made via the pyridine-reflux method.

In the second prepration method, the CdSe nanowires were never precipitated out of solution; they were retained as a dispersion in toluene. The purification of the core nanowires was performed by an extraction method, which was adapted from the synthesis of the core/shell quantum dots[17, 27, 28](see Experimental section).

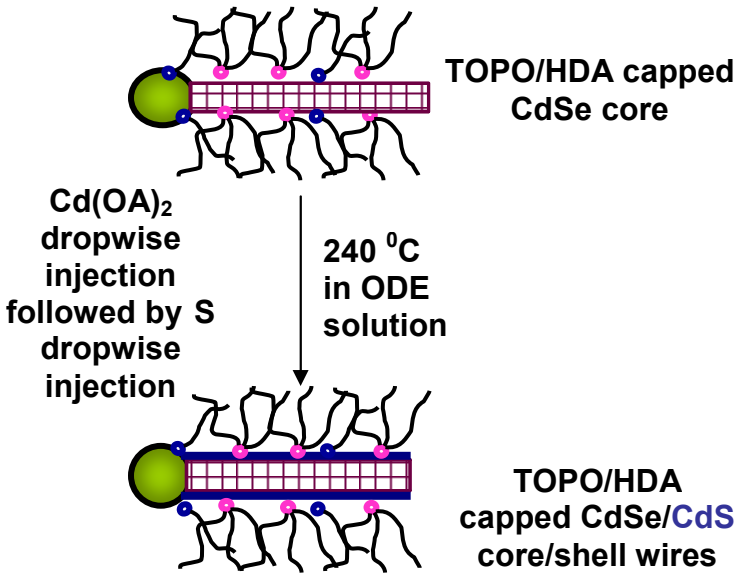

Figure 4-7. Schematic synthesis of CdSe/CdS core/shell nanowires. The nanowires were purified via an extraction method and the shell growth was performed in ODE (octadecene) solution.

The shell growth was conducted by the so called Successive Ion Layer Absorption and Reaction (SILAR) which was originally developed for the deposition of thin films on solid substrates from solution baths.[29, 30] This technique was successfully used in the CdSe/CdS core/shell semiconductor quantum-dot synthesis.[17] Here I applied the SILAR concept to the growth of CdSe/CdS core/shell quantum wires in the non-coordinating solvent ODE (1-octadecene). The scheme of this preparation method is shown in Figure 4-7.

The reaction temperature played an important role for the shell growth of CdS onto the CdSe quantum wires through SILAR in ODE solution. Reactions conducted at less than 200 ^{o}C resulted in the growth of CdS nanocrystals instead

of CdSe/CdS core/shell structure; this indicated that the SILAR method only works at high temperature. At high temperatures, the Cd precursors were largely consumed by epitaxial growth prior to the addition of the S precursors, while for S precursors, next added into the system, the only possibility was to grow onto the core/shell nanowire surface. Although there were still some free CdS nanocrystals formed during this process, they were easily removed from the samples via a precipitation purification procedure.

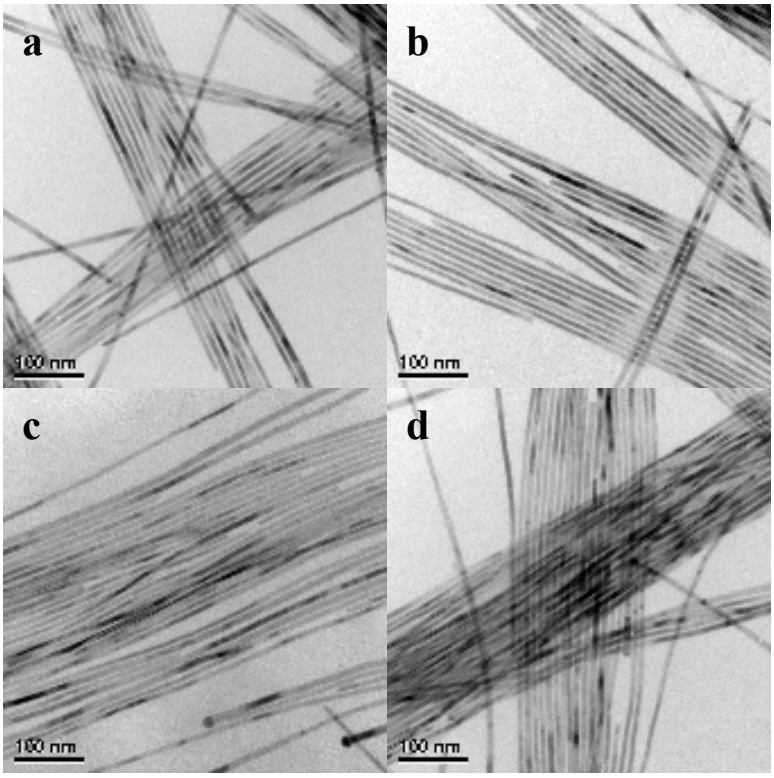

Figure 4-8. TEM images of CdSe core nanowire (a, b) and CdSe/CdS core/shell nanowire (c,d) made via SILAR method.

The TEM images of the core CdSe nanowires and the CdSe/CdS core/shell nanowires made via the SILAR method are shown in Figure 4-8. The diameter histograms of the core and core/shell samples are shown in Figure 4-9. Although an obvious difference in the diameters of the core sample and core/shell samples cannot be distinguished from TEM images, the diameter increment of the CdSe/CdS core/shell sample is evident from the statistical results. No CdS nanocrystals were observed in the purified CdSe/CdS sample (Figure 4-8 c and d) , indicating their successful removal by the precipitation/re-disperse procedure.

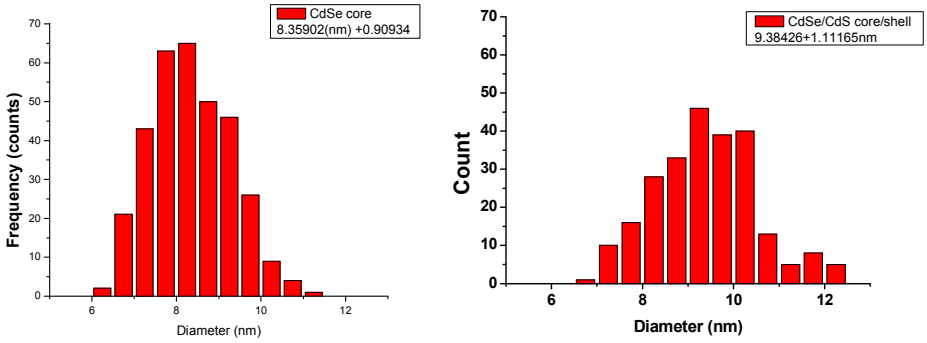

Figure 4-9. Histograms of the diameters of CdSe core nanowires and CdSe/CdS core/shell nanowires made via the SILAR method.

The absorption spectra of the CdSe core sample, core sample after extraction, and the CdSe/CdS core/shell sample are shown in Figure 4-10. The excitonic features are quite similar in the three spectra. Importantly, the excitonic feature of the core CdSe nanowires did not show a noticeable shift after the extraction procedure and shell growth, which is shown in Figure 4-10 by the guideline. This contrasts with the results of the pyridine-reflux preparation. In the

second method, the CdSe core is better protected from surface-atom loss during the extraction procedure.

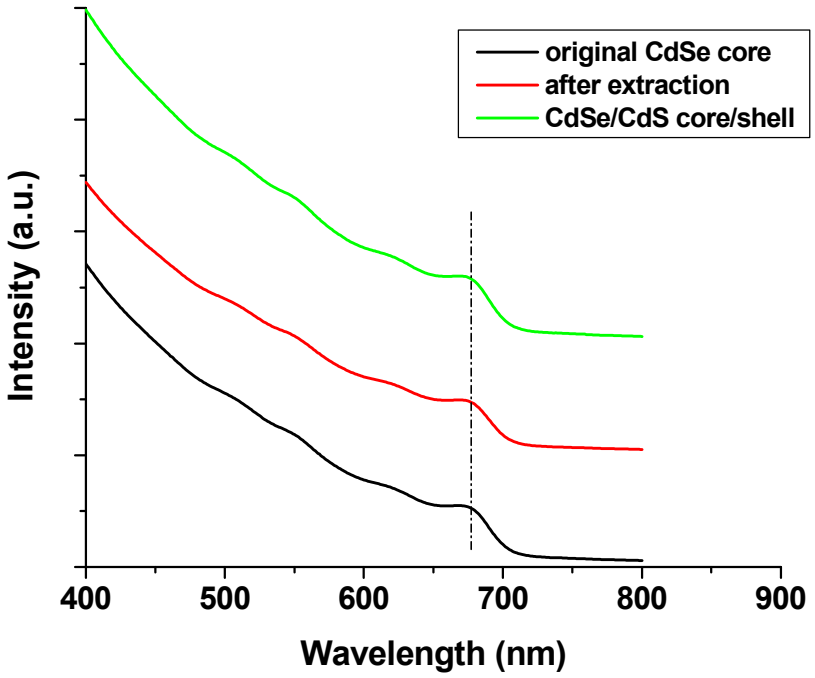

Figure 4-10. Absorption spectra of the core CdSe nanowires (black curve), CdSe core after the extraction procedure (red curve), and core/shell CdSe/CdS nanowires (green curve).

The photoluminescence spectra of the core and core/shell samples are shown in Figure 4-11. The large enhancement of the emission efficiency proved the successful formation of the CdSe/CdS type-I core/shell nanostructure. Note the absence of a blue shift for the PL peak in the core and core/shell nanowires, which is consistent with the absorption spectra. This result further proved that the CdSe core nanowires were well protected by the extraction method; there was no

surface-atom loss upon transfer of the wires into the shell growth solvent. The PL quantum yield of the CdSe/CdS core/shell structure was improved to 11%, from the original value of 2% for the core CdSe quantum wires.

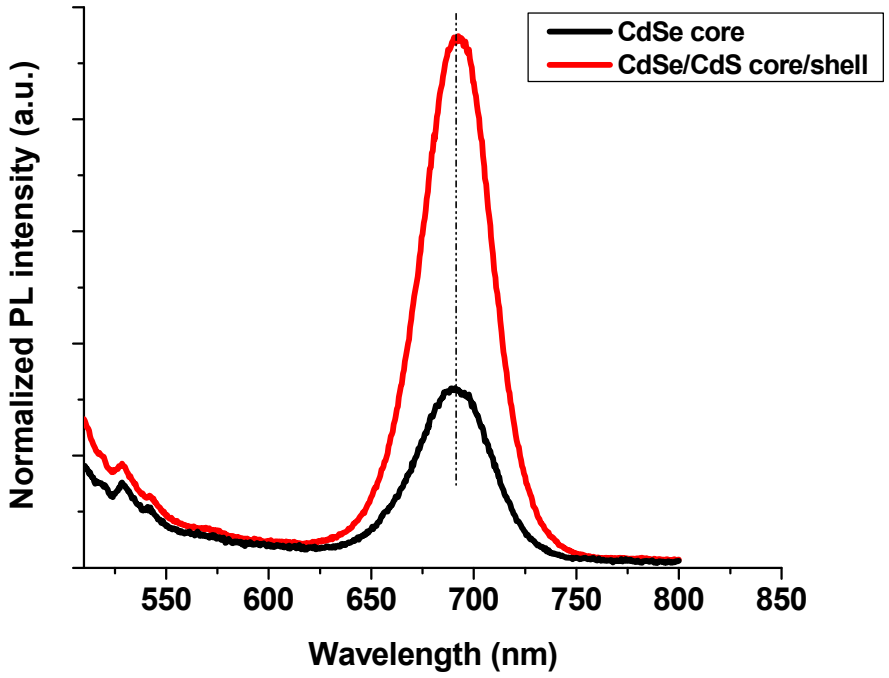

Figure 4-11. Photoluminescence spectra of CdSe core nanowires and CdSe/CdS core/shell nanowires made via SILAR method.

Using the same SILAR reaction conditions, by changing the shell precursors to $Zn(stearate)_2$ and elemental S, CdSe/ZnS core/shell nanowires were also obtained with improved photoluminescence efficiency. The PL quantum yield of CdSe/ZnS was improved to 8%, from the original 2% for the core-only CdSe quantum wires.

Destruction of mismatch-strained core/shell nanowire structure.

Further enhancement of the PL efficiency for the CdSe/CdS core/shell nanowires by illuminating the sample under fluorescent light as described in Chapter 3 was not successful. The PL quantum yield of the CdSe/CdS core/shell wires did not show noticeable change upon the illumination for the first 1 - 5 days. After 5 days, the PL intensity of the CdSe/CdS core/shell nanowires showed a slight decay. Along with the PL decay, the destruction of the core/shell nanowires was observed. The TEM images of the CdSe/CdS core/shell nanowires illuminated for 10 days are shown in Figure 4-12.

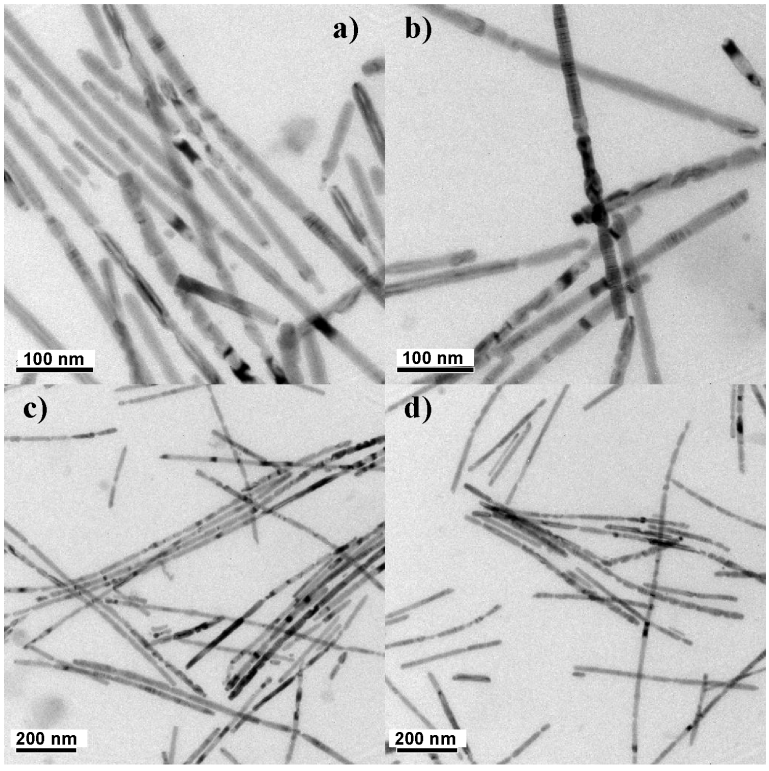

Figure 4-12. Representative TEM images of CdSe/CdS core/shell nanowires illuminated under fluorescent light for 10 days in toluene.

There was no evidence for the dissolution of the core/shell nanowires. The destruction of the core/shell nanowires resulted from the lattice mismatch of the core material (CdSe) and shell material (CdS). The core/shell system tends to relax the mismatch strain by either developing a modulation of the surface, potentially leading to the creation of island or notches on the surface, or by forming misfit dislocations.[23, 31] The CdS shell of the CdSe/CdS core/shell nanostructure developed irregular diameter fluctuations on the nanostructure surface, which was caused by the strain force from the lattice mismatch between wurtzite CdSe and CdS (4%, Table 4-1). The schematic illustration of this process is shown in Figure 4-13.

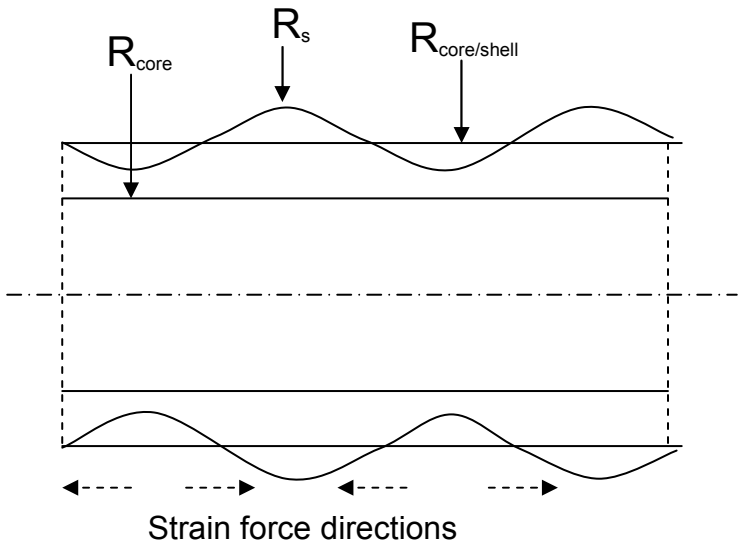

Figure 4-13. Schematic side view of a core-shell nanowire with a perturbation of the radius of the surface; R_{core} and $R_{core/shell}$ are the initial core and core/shell structure radii, and R_s is the surface radius caused by strain force, respectively.

For the extreme cases, this force broke the CdSe/CdS core/shell nanostructures into short nanorod sections, which were also observed in the TEM images (Figure 4-12). The average length of the nanowires was significantly decreased by this process; from >1 μm to ~ 400 nm. The PL quantum yield of the CdSe/CdS sample after this process was decreased to ~ 5% from the 11% for the as-prepared core/shell structure, indicating surface-trap creation during this process.

Water-dispersible CdSe quantum wires.

Nanostructures dispersed in water are useful for many applications. As examples, semiconductor quantum dots are used as fluorescent tags in biology, magnetic Fe_2O_3 nanoparticles are used as contrast agents in magnetic resonance imaging (MRI), and Pd nanoparticles are used as green catalysts.[32-34] If CdSe quantum wires can be dispersed into water, the unique optical properties, suitable optical window, and 1-D morphology of CdSe quantum wires may have promising applications in biology or medical areas. For quantum dots, the easiest method to disperse nanoparticles in water is to prepare them directly in water using water-soluble surfactants or polymers.[35-38] But for our CdSe quantum-wire system, the preparation of good quality nanowires requires high temperatures with a coordinating organic solvent to achieve; the direct synthesis of CdSe nanowires in water is not yet possible.

The applications of CdSe semiconductor quantum wires require narrow diameter distributions to produce uniform physical and optical properties. The conditions to prepare these kinds of quantum wires render them insoluble in water and preclude their use in biological applications, without further processing. A variety of strategies have been developed for the hydrophilization of quantum-dot surfaces. One approach is the replacement of the hydrophobic ligands with more hydrophilic ones.[39-41] In this case, a decay of the photoluminescence (PL) is usually observed after transfer of the functionalized nanoparticles into biological systems.[39, 41] The reason for this observation is partial degradation of the quantum dots caused by reactions of the semiconductor materials with oxygen as well as the aqueous environment.[39, 40] One possibility for a more effective protection of quantum dots in biological systems is coating of the particles with silica or a polymer shell.[35, 42] Alternatively, multiple quantum dots have been embedded into silica colloids.[43] In this way, the decrease of PL after transfer of the semiconductor nanoparticles into biological environments is minimized or even completely avoided.[44-47] No water-soluble CdSe quantum wires have been reported to date. Both approaches taken in the quantum-dot studies could potentially be adapted to water-dispersible quantum-wire research. Here I report achieving success with the ligand-exchange strategy.

PEI-coated CdSe quantum wires.

Since PEI (hyperbranched polyethylenimine, 600 D) is insoluble in toluene, which is normally used for dissolving our CdSe quantum wires, another non-polar solvent must be chosen to perform the ligand-exchange reaction. PEI is soluble in many polar solvents and sufficiently soluble in chloroform and dichloromethane.[48] Chloroform is one of the best solvents for our CdSe quantum wires. Quantum wires with PEI in chloroform form a very stable colloid, which cannot be centrifuged with a common laboratory centrifuge. The displacement of the original surface ligands of the CdSe quantum wires (TOPO, TOP, and HDA) with PEI was therefore conducted in chloroform.

The subsequent phase-transfer was performed in two ways. The first was direct extraction of the CdSe quantum wires from the chloroform solution with water. The second was precipitation of the PEI-derivatized quantum wires with toluene and subsequent redispersion in water. The direct extraction usually occured over several hours and the product yield was somewhat low because the water/chloroform boundary was not very clear and many quantum wires remained in the phase-boundary zone. The precipitation method was preferred; it was fast and efficient to separate the water-soluble CdSe quantum wires from the chloroform.

After precipitation of the PEI-coated CdSe quantum wires with toluene, the precipitates were dispersible in water or methanol and insoluble in chloroform or less polar solvents (such as toluene and hexane). This is strange because the CdSe quantum wires were precipitated from chloroform. This observation is similar to

those in the water-dispersible quantum-dot study.[48] The PEI facilitates steric stabilization in chloroform and electrostatic stabilization in protic solvents.[48] The electrostatic stabilization process is irreversible once the solvent has been deprotonated by the PEI, which is in consequence positively charged. The schematic mechanism is shown in Figure 4-14.

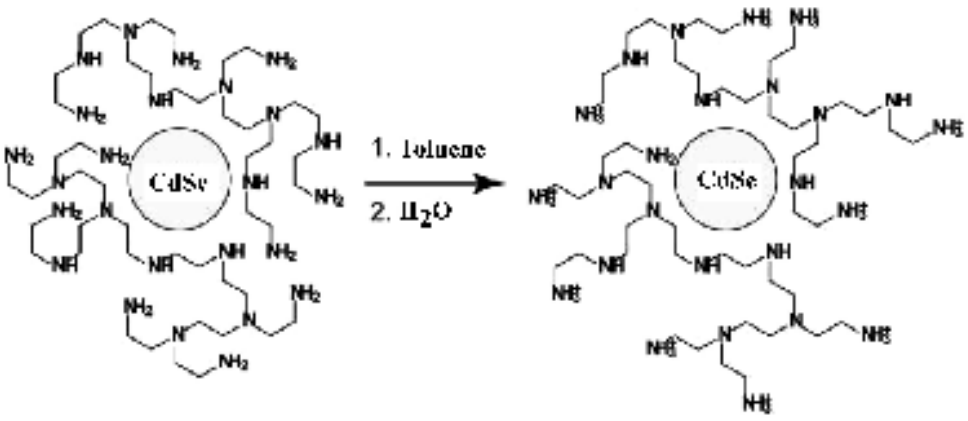

Figure 4-14. Schematic illustration of the switching of amphiphilic PEI from fairly lipophilic to hydrophilic.[48]

Figure 4-15a shows the comparison of the absorption spectra of the CdSe quantum wires (diameter ~ 8 nm) before and after the ligand-exchange reaction with PEI.

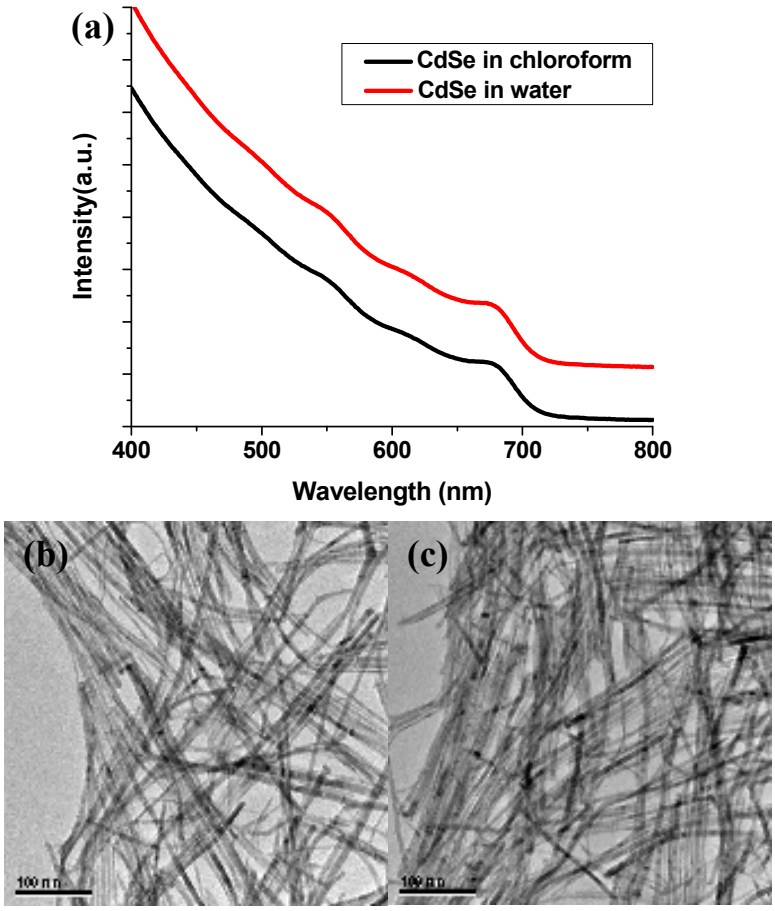

Figure 4-15. The absorption spectra of CdSe quantum wires before ligand exchange and after ligand exchange with PEI (a). TEM images of the CdSe quantum wires after dispersing in water via ligand-exchange with PEI (b and c).

The absorption spectra and TEM image show that the morphology of the CdSe quantum wires remained after ligand exchange, and no significant excitonic peak shift in the absorption spectrum was observed. But unfortunately, the photoluminescence of the CdSe quantum wires disappeared after this ligand-exchange reaction. Heating or adding ligands generally beneficial to PL did not restore the PL of the CdSe wires. The PL loss of the CdSe quantum wires was

irrecoverable. Apparently, many surface traps were created during the ligand exchange from the well-passivated TOPO/TOP surface, which quenched the PL.

PEG-Phosphine oxide polymer-coated CdSe quantum wires.

Although the CdSe quantum wires were successfully transferred into water via exchange of the surface ligands with PEI (hyperbranched polyethylenimine), the photoluminescence of the CdSe nanowires was quenched. This limited applications of the quantum wires in biological systems. A better ligand was necessary to induce aqueous dispersibility while retaining the PL efficiency.

Our CdSe quantum wires were well passivated by TOPO/TOP ligands. Consequently, phosphine-oxide passivation might be retained with a polymer that also contains hydrophilic groups to support water dispersibility. In this way, the CdSe quantum wires may retain their optical properties upon transfer into water via ligand-exchange. An easily synthesized polymer consisting of phosphine oxide and PEG [poly(ethylene glycol)] was introduced in the quantum-dot study.[49] There are two major steps for the synthesis of the polymer: (1) polymerization of 1,2-bis(dichlorophosphino)ethane and poly(ethylene glycol) and (2) neutralization of the HCl-phosphine salts that formed during (1).[49] The phosphines are oxidized to phosphine oxides during step (2). A scheme for the synthesis of this polymer is shown in Figure 4-16.

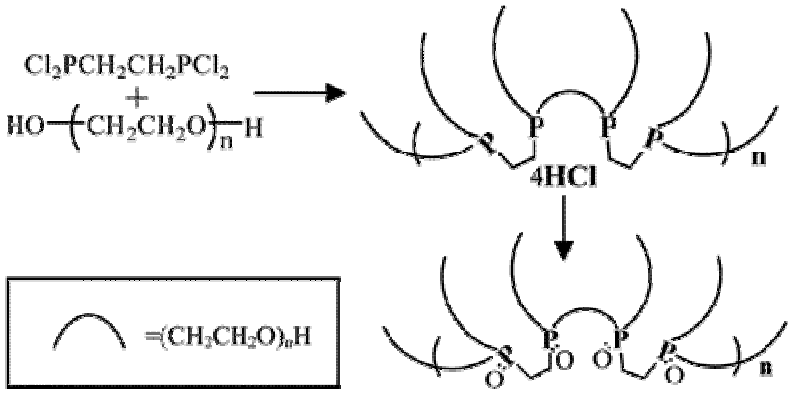

Figure 4-16. Schematic illustration of the synthesis of PEG-phosphine oxide polymer.[49]

The structure of this PEG-phosphine oxide polymer, includes phosphine-oxide groups very similar to TOPO, which is proven to be a good surfactant for passivating the CdSe quantum-wire surface. The other component of the polymer is the PEG group, which is hydrophilic, and can serve the purpose of transferring our CdSe quantum wires into aqueous systems.

A CdSe quantum-wire solution in chloroform was heated at 60 ^{o}C with stirring for 1 h after the addition of the PEG-phosphine oxide polymer. Toluene was added into the solution to precipitate the CdSe nanowires. The brown precipitates so obtained were dissolved into water. A TEM image of the CdSe nanowires after ligand exchange is shown in Figure 4-17 (right). The morphology of the CdSe quantum wires didn't show a significant change after the ligand-exchange reaction.

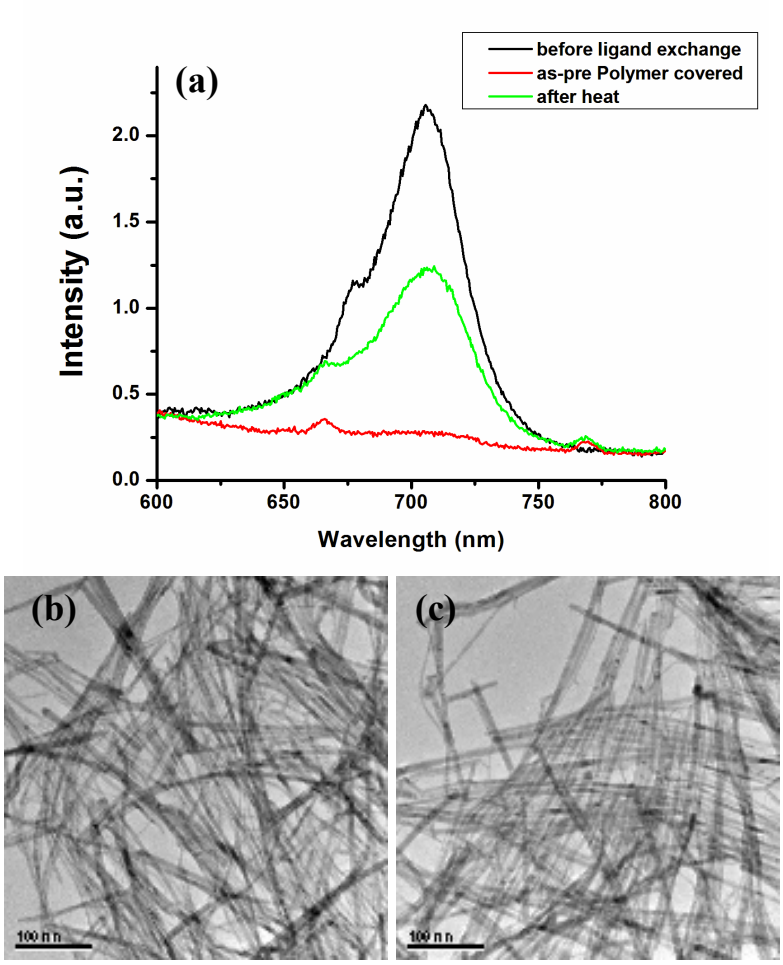

Figure 4-17. Photoluminescence spectra of the CdSe quantum wires at different stages of the ligand-exchange reaction with PEG-phosphine oxide polymer (a) and TEM images of the CdSe quantum wires from aqueous dispersion after ligand exchange (b and c).

Figure 4-17 also shows the photoluminescence spectra of the CdSe quantum wires before ligand exchange (black curve), immediately after ligand-exchange (red curve), and after heating at 60 ^{o}C in water for 1 h after ligand exchange (green curve). The results establish that the as-prepared water-dispersible CdSe quantum wires also lost their PL feature due to the damage

caused to the nanowire surface during the ligand exchange. But after annealing the dispersion, the emission of the CdSe quantum wires was partially restored. The possible mechanism of this recovery of PL may due to the surface phosphine/phosphine oxide ligand surface reconstruction upon heating. These water-dispersible CdSe quantum wires have spectroscopic properties comparable to those in organic dispersions, which is suitable for potential biological applications.

CdSe/SiO_2 core/shell nanowires.

Because CdSe is harmful for *in vivo* study due to the toxicity of the material,[50] a non-toxic shell that can retain the morphology and physical properties of the semiconductor quantum nanostructures could enable biological applications.

SiO_2 is an excellent shell material to solve problems of toxicity, biocompatibility, and water solubility of CdSe quantum wires. Because SiO_2 is hydrophilic, it cannot be directly grown as a coating shell in the organic solvent in which the CdSe quantum wires are typically dispersed. It is necessary to functionalize the CdSe quantum-wire surface to make it water soluble in order to grow the SiO_2 shell. Therefore, the orginal hydrophobic CdSe quantum wires were coated with PEI or PEG-phosphine oxide polymer via ligand-exchange reaction to make the nanowires water soluble, as discussed above. The polymer-coated water soluble CdSe quantum wires were then dissolved in methanol, into

which tetraethyl orthosilicate (TEOS) and a small amount of water were added with stirring. The subsequent addition of a small amount of ammonium hydroxide (NH_4OH) induced the hydrolysis reaction and condensation of TEOS to produce SiO_2 shells on the CdSe quantum wire surface.

Figure 4-18 shows the TEM images of CdSe/SiO_2 core/shell nanowires, which were made from CdSe quantum wires after the ligand-exchange reaction with PEG-phosphine oxide polymer. The CdSe quantum wires were annealed for 1 h at 60 ^oC to restore the photoluminescence before coating with SiO_2. These TEM images show that all the CdSe quantum wires were successfully coated by SiO_2 shells. A control experiment of directly coating SiO_2 onto hydrophobic CdSe quantum wires under the same reaction conditions failed to produce the CdSe/SiO_2 core/shell structures, indicating the ligand-exchange procedure is necessary and important for the successful growth of SiO_2 shells.

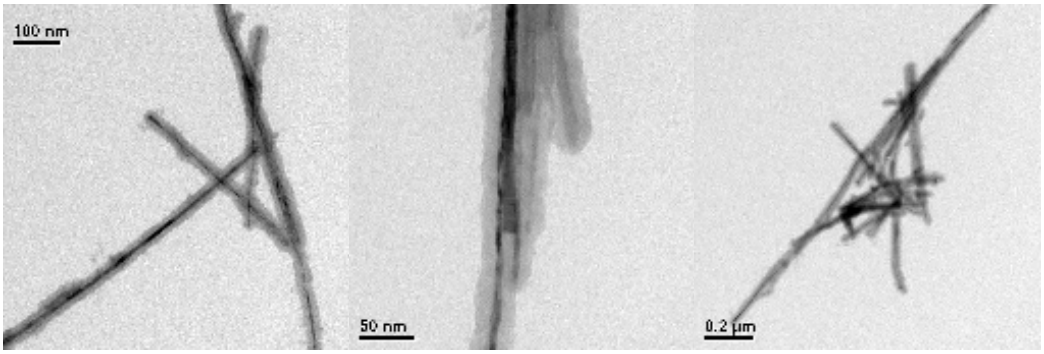

Figure 4-18. TEM images showing successful growth CdSe/SiO_2 core-shell quantum wires.

The absorption and photoluminescence spectra are shown in Figure 4-19. The excitonic feature of the CdSe quantum wires was preserved in the CdSe/SiO_2 core/shell structures. There was no obvious change in the absorption spectra before and after coating. The PL spectrum of the CdSe/SiO_2 core/shell structure exhibited a larger high-energy rise, which may come from the SiO_2 shell. Although the emission efficiency of the CdSe/SiO_2 was reduced compared to the original CdSe quantum wires in organic solvent, the advantages of the lower toxicity and water dispersibility show that the luminescent CdSe/SiO_2 core/shell structure is still promising for the biomedical applications.

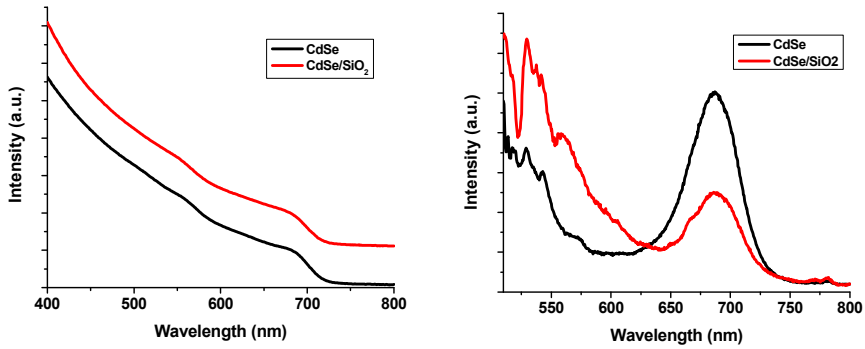

Figure 4-19. Absorption and photoluminescence spectra of CdSe core quantum wires and CdSe/SiO_2 core/shell structures.

Conclusion:

I successfully synthesized the Type-I CdSe/CdS core/shell nanowires using the optimized CdSe quantum wires as the core structures. The CdSe/CdS core/shell nanowires exhibited improved photoluminescence efficiency, comparable to that achieved in photoenhanced CdSe core-only nanowires (Chapter 3). The destruction of the core/shell CdSe/CdS nanowires resulting from lattice mismatch of the core material and shell material was also observed.

Water-dispersible CdSe quantum wires were also made via coating PEI and PEG-phosphine oxide polymers onto the nanowire surfaces. CdSe/SiO_2 core/shell structures were also made from the hydrolysis reaction of TEOS in aqueous solution containing polymer-coated CdSe quantum wires. These water-dispersible nanowires preserved the morphologies and optical properties of 1-D semiconductor quantum nanostructures, which is promising for applications due to their lower toxicity and biomedical compatibility.

Experimental Section

Chemicals. Cadmium stearate (90%), Cadmium oxide (CdO, 99%), Oleic acid (OA, 90%), tri-n-octylphosphine oxide (TOPO, 99%), trioctylphosphine (TOP, 97%) , selenium powder (Se, 100 mesh 99%), poly(1-hexadecene)$_{0.67}$-co-(1-vinylpyrrolidinone)$_{0.33}$, Na[N(SiMe$_3$)$_2$] (1.0 M solution in THF), anhydrous pyridine, 1-octadecene (ODE), polyethylenimine (PEI, M_n = 600) polyethylene glycol (PEG, M_n = 600), 1,2-bis(dichlorophosphino)ethane, tetraethyl orthosilicate (TEOS, 98%), ammonium hydroxide solution (NH_4OH, 27%) and dioctylamine (DOA, 98%) were obtained from Aldrich and used as received. Tetradecylphosphonic acid (TDPA, ~90%) was purchased from Polycarbon Industries Inc. and used as received. Toluene, hexane and chloroform (analytical grade) were all purchased from Aldrich and used as received. 1,3-diisopropylbenzene (DIPB, from Aldrich) was shaken with concentrated sulfuric acid to remove thiophene, washed with water, and distilled over Na.

Preparation of TOP=Se. A neat mixture of 4 g of elemental Se powder (0.051 mol) and 22 g TOP (0.059 mol) was loaded into a 100 ml storage bottle under dry, O_2-free N_2(g). The Se powder rapidly dissolved into the liquid mixture as heat was evolved. A second portion of 1 g of Se (0.013 mol) was added into the mixture to ensure the conversion of TOP to TOP=Se. The liquid fraction of the mixture was subsequently used.

Preparation of TBP=Se. A neat mixture of 4 g of elemental Se powder (0.051 mol) and 12 g of TBP (0.059 mol) was loaded into a 100 ml storage bottle under dry, O_2-free N_2(g). The Se powder rapidly dissolved into the liquid mixture as heat was evolved. A second potion of 1 g of Se (0.013 mol) was added into the mixture to ensure that all of the TBP had been converted to TBP=Se. The liquid fraction of the mixture was subsequently used.

Preparation of Bi-nanoparticle stock solutions. Monodispersed Bi nanoparticles were grown in DIPB solutions of poly(1-hexadecen) $_{0.67}$-co-(1-vinylpyrrolidinone) $_{0.33}$ and Na[N(SiMe$_3$)$_2$] at elevated temperatures (170-210 ^{o}C), following the procedure previously reported.[51] The diameter of Bi nanoparticles were tuned from 5 to 18 nm (std. deviation = 5-10% of the mean diameter) by varying reaction conditions, and the effective concentration of the dispersions was 0.04 mmol of Bi/g DIPB.

Bi-catalyzed growth of CdSe nanowires. In a typical synthesis of CdSe nanowires, 6 mg of CdO (0.047 mmol), 53 mg of oleic acid (0.19 mmol), 50 mg of hexadecylamine (0.21 mmol), and 5 g of trioctylphosphine oxide (13 mmol) were loaded into a 50 ml reaction tube, which was degassed on a Schlenk line and backfilled with N_2. The reaction mixture was heated at 320 ^{o}C in a salt bath ($NaNO_3$: KNO_3 ~ 1:1) until a clear solution was generated (~ 10 min). Then, the reaction tube was transferred to a 250 ^{o}C salt bath for wire growth. At this temperature, a mixed solution of 500 mg of TOP=Se (1.1 mmol), 100 mg of TOP

(0.27 mmol) and 23 mg of Bi solution (0.00092 mmol) was rapidly injected into reaction tube. After 5 min reaction, the reaction mixture was allowed to cool to room temperature.

1 ml aliquot of the reaction mixture was dissolved into 2 ml of toluene, the wires were precipitated with 6 ml of methanol and the sample was centrifuged and the supernatant was decanted. The precipitates were re-dispersed in 2 ml of toluene, precipitated with 6 ml of methanol, followed by centrifugation and decanting the supernatant again. Then, the precipitates were re-dissolved in toluene for optical measurements.

The diameter of CdSe nanowires grown by this approach can be varied by changing the reaction temperature from 240 ^{o}C to 280 ^{o}C and by choosing different sized Bi nanoparticles as the catalyst seeds.

Synthesis of CdSe/CdS core/shell structure via the first method.

Injection solution. The cadmium injection solution (0.04 M) was prepared by heating CdO (0.062 g, 0.48 mmol) in oleic acid (1.08 g, 3.8 mmol) at 280 ^{o}C until clear, then TBP (10.8 ml, 43.3 mmol) was added. The sulfur injection solution (0.04 M) was prepared by dissolving sulfur powder (0.013 g, 0.40 mmol) in TBP (10.0 ml, 40.1 mmol) at 120 ^{o}C. Both injection solutions were made under N_2 flow and allowed to cool to room temperature for future use.

Procedure for CdS shell growth. TOPO-capped CdSe nanowires (0.047 mol, based on the assumption of complete reaction between Cd precursor and Se precursor) were transferred to a 50 ml three necked flask, degassed, and backfilled with N_2 on a Schlenk line. To this was added 30 ml of anhydrous pyridine. The CdSe nanowires dissolved readily, and the solution was allowed to reflux overnight under N_2. The amount of the injection solution needed was calculated using the method described in the Results. 1 mL each of $Cd(OA)_2$ (0.04 M) and TBP=Se (0.04 M) were loaded into 2 syringes. They were alternately added dropwise (1 drop per second) to the reaction solution at 110 ^oC. After the injection of the stock solution was complete, the reaction mixture was allowed to heat at 100 ^oC for 20 min to complete the shell growth. Methanol (3 ml) was added into reaction mixture at room temperature to precipitate the CdSe/CdS core/shell nanowires. The precipitates were dissolved in toluene or chloroform for optical measurements.

Synthesis of CdSe/CdS core/shell structure via the second method (SILAR)

Injection solution. The cadmium injection solution (0.04 M) was prepared by dissolving CdO (0.615 g, 4.8 mmol) in oleic acid (10.83 g, 38.3 mmol) and ODE (108 mL, 337 mmol) at 240 ^oC. The sulfur injection solution (0.04 M) was prepared by dissolving sulfur (0.13 g, 4 mmol) in ODE (100 mL, 312 mmol) at 200 ^oC. Both injection solutions were made under N_2. After clear solutions were obtained, the Cd injection solution and sulfur injection solution were allowed to cool to room temperature. The Cd injection solution required heating using a heat

gun with shaking to produce a clear solution before each use. For each injection, a calculated amount of a given injection solution was taken with a syringe using standard air-free procedures.

Procedure for SILAR CdS shell growth. CdSe nanowires (0.047 mmol, based on the assumption of complete reaction between Cd precursor and Se precursor) were dissolved in 2.5 g of toluene were mixed with 3.0 g of HDA and 10.0 g of ODE in a 50 ml three-neck flask. The flask was evacuated at room temperature and then at 110 ^{o}C for 1 h to remove the toluene and any residual air from the system. Subsequently, the system was backfilled with N_2 and the reaction mixture was further heated to 240 ^{o}C for the shell growth. The first injection was 0.30 ml of the Cd injection solution (0.04 M), and the amounts of the subsequent injection solutions were calculated using the method described in the Results. The second injection was 0.30 ml of Se injection solution (0.04 M). Then 2 injection cycles of Cd and S were alternately executed. The reaction was terminated by allowing the reaction mixture to cool to room temperature. The final product (CdSe/CdS core/shell nanowires) was diluted by toluene followed by methanol precipitation (toluene : methanol = 7 : 3). The precipitates were re-dissolved in toluene for characterization.

Synthesis of water soluble CdSe nanowires with PEI. In a typical experiment, PEI (M_n = 600, ~0.2 ml, 0.00036 mmol) was added to the chloroform solution (~4 ml) of the purified CdSe nanowires (0.02 mmol of CdSe). The resulting solution mixture was sonicated in a cleaning bath at room temperature for 30 min to ensure

completion of the PEI coating. Toluene (~1 ml) was added to precipitate the CdSe nanowires, and the precipitates were collected by centrifugation and re-dissolved in methanol or water for characterization.

Synthesis of water soluble CdSe nanowires with PEG-phosphine oxide.

Synthesis of PEG-phospine oxide polymer.[49] Degassed 7.75 g (12.92 mmol) poly(ethylene glycol) (M_n = 600) was dissolved in 20.0 g of DMF for 1 h and then 1.0 g (4.31 mmol) 1,2-bis(dichlorophosphino)ethane was added dropwise slowly while the solution was under N_2 and vigorously stirred. The reaction solution was stirred at room temperature for 24 h after the addition. K_2CO_3 (2.38 g, 17.24 mmol) and 10 mL of methanol were then added and stirred vigorously. The solution was stirred for another 48 h until the pH reached 7~8. The solution was centrifuged and the precipitates were removed. The solvent was removed at a reduced pressure and the remaining solid was dissolved in 50 ml of chloroform. The solution was centrifuged again and the precipitates were removed, leaving the product in the solution.

Ligand-exchange procedure. CdSe nanowires (0.047 mmol, based on the assumption of complete reaction between Cd precursor and Se precursor) were precipitated using methanol and dispersed in 10 mL chloroform. 10 mL of a chloroform solution containing the PEG-phosphine oxide polymer was mixed with the CdSe nanowire solution. The solution was vigorously stirred at 50 ^oC for 1 h and then allowed to cool to room temperature. Toluene (~2 ml) was added to

precipitate the CdSe nanowires. The precipitates were collected and re-dissolved into methanol or water for characterization and further experiments.

Synthesis of water soluble $CdSe/SiO_2$ core/shell nanowires. In a typical synthesis, the PEG-phosphine-oxide-polymer-coated CdSe nanowires were dissolved in a mixture of methanol (~ 1 mL) and H_2O (~ 0.2 mL) into which TEOS (~ 0.06 mL, 0.27 mmol) and DOA (~ 0.2 mL, 0.66 mmol) were added. The obtained solution was stirred for 20 min at room temperature. After that, one drop of NH_4OH solution was injected by syringe to adjust the pH of the solution to ~ 8. The reaction mixture was stirred for another 20 min to induce the hydrolysis and condensation of TEOS. The $CdSe/SiO_2$ core/shell wires were collected by centrifugation and re-dispersed in methanol or water for characterization.

Characterization. Samples for TEM analysis were prepared by dropping a dilute toluene solutions of NWs onto 300-mesh carbon-coated copper grids. TEM images were recorded using a JEOL 2000 FX microscope operating at 200 kV. The diameter distribution for each sample was determined using several TEM images at 500K magnification to ensure accurate measurement. The wire diameters were measured and recorded using Image-Pro Express software (version 4.5), and the distribution histograms were constructed from 400-500 diameter measurements for each specimen. Simulations, peak fits, and integration calculations were all done using Origin (version 7). UV-visible absorption spectra were recorded on a Varian Cary 100E spectrophotometer at room temperature.

The nanowire solutions were prepared by diluting the purified nanowire samples with a certain amount of toluene in a 1-cm path-length quartz cuvette, and a baseline correction was performed prior to each measurement. Photoluminescence (PL) spectra were taken on a Varian Cary Eclipse fluorescence spectro-photometer at room temperature.

References:

1. Tian, B.; Kempa, T. J.; Lieber, C. M. *Chemical Society Reviews* **2009,** 38, (1), 16-24.

2. Ma, R. M.; Dai, L.; Qin, G. G. *Nano Letters* **2007,** 7, (4), 868-873.

3. Patolsky, F.; Timko, B. P.; Yu, G. H.; Fang, Y.; Greytak, A. B.; Zheng, G. F.; Lieber, C. M. *Science* **2006,** 313, (5790), 1100-1104.

4. Qu, L. H.; Peng, X. G. *Journal of the American Chemical Society* **2002,** 124, (9), 2049-2055.

5. Hines, M. A.; Guyot-Sionnest, P. *Journal of Physical Chemistry* **1996,** 100, (2), 468-471.

6. Dabbousi, B. O.; RodriguezViejo, J.; Mikulec, F. V.; Heine, J. R.; Mattoussi, H.; Ober, R.; Jensen, K. F.; Bawendi, M. G. *Journal of Physical Chemistry B* **1997,** 101, (46), 9463-9475.

7. Peng, X. G.; Schlamp, M. C.; Kadavanich, A. V.; Alivisatos, A. P. *Journal of the American Chemical Society* **1997,** 119, (30), 7019-7029.

8. Correa-Duarte, M. A.; Giersig, M.; Liz-Marzan, L. M. *Chemical Physics Letters* **1998,** 286, (5-6), 497-501.

9. Danek, M.; Jensen, K. F.; Murray, C. B.; Bawendi, M. G. *Chemistry of Materials* **1996,** 8, (1), 173-180.

10. Kim, S.; Bawendi, M. G. *Journal of the American Chemical Society* **2003,** 125, (48), 14652-14653.

11. RodriguezViejo, J.; Jensen, K. F.; Mattoussi, H.; Michel, J.; Dabbousi, B. O.; Bawendi, M. G. *Applied Physics Letters* **1997,** 70, (16), 2132-2134.

12. Rodriguez-Viejo, J.; Mattoussi, H.; Heine, J. R.; Kuno, M. K.; Michel, J.; Bawendi, M. G.; Jensen, K. F. *Journal of Applied Physics* **2000,** 87, (12), 8526-8534.

13. Alivisatos, P. *Nature Biotechnology* **2004,** 22, (1), 47-52.

14. Tsay, J. M.; Doose, S.; Pinaud, F.; Weiss, S. *Journal of Physical Chemistry B* **2005,** 109, (5), 1669-1674.

15. Reiss, P.; Protiere, M.; Li, L. *Small* **2009,** 5, (2), 154-168.

16. Wei, S. H.; Zunger, A. *Applied Physics Letters* **1998,** 72, (16), 2011-2013.

17. Li, J. J.; Wang, Y. A.; Guo, W. Z.; Keay, J. C.; Mishima, T. D.; Johnson, M. B.; Peng, X. G. *Journal of the American Chemical Society* **2003,** 125, (41), 12567-12575.

18. Talapin, D. V.; Nelson, J. H.; Shevchenko, E. V.; Aloni, S.; Sadtler, B.; Alivisatos, A. P. *Nano Letters* **2007,** 7, (10), 2951-2959.

19. Mauser, C.; Limmer, T.; Da Como, E.; Becker, K.; Rogach, A. L.; Feldmann, J.; Talapin, D. V. *Physical Review B* **2008,** 77, (15), -.

20. Guo, W. H.; Li, J. J.; Wang, Y. A.; Peng, X. G. *Journal of the American Chemical Society* **2003,** 125, (13), 3901-3909.

21. Talapin, D. V.; Koeppe, R.; Gotzinger, S.; Kornowski, A.; Lupton, J. M.; Rogach, A. L.; Benson, O.; Feldmann, J.; Weller, H. *Nano Letters* **2003,** 3, (12), 1677-1681.

22. Trammell, T. E.; Zhang, X.; Li, Y. L.; Chen, L. Q.; Dickey, E. C. *Journal of Crystal Growth* **2008,** 310, (12), 3084-3092.

23. Schmidt, V.; McIntyre, P. C.; Gosele, U. *Physical Review B* **2008,** 77, (23).

24. Yu, Z. H.; Guo, L.; Du, H.; Krauss, T.; Silcox, J. *Nano Letters* **2005,** 5, (4), 565-570.

25. Katari, J. E. B.; Colvin, V. L.; Alivisatos, A. P. *Journal of Physical Chemistry* **1994,** 98, (15), 4109-4117.

26. Sachleben, J. R.; Wooten, E. W.; Emsley, L.; Pines, A.; Colvin, V. L.; Alivisatos, A. P. *Chemical Physics Letters* **1992,** 198, (5), 431-436.

27. Yu, W. W.; Peng, X. G. *Angewandte Chemie-International Edition* **2002,** 41, (13), 2368-2371.

28. Yu, W. W.; Qu, L. H.; Guo, W. Z.; Peng, X. G. *Chemistry of Materials* **2003,** 15, (14), 2854-2860.

29. Ristov, M.; Sinadinovski, G.; Grozdanov, I.; Mitreski, M. *Thin Solid Films* **1989,** 173, (1), 53-58.

30. Park, S.; Clark, B. L.; Keszler, D. A.; Bender, J. P.; Wager, J. F.; Reynolds, T. A.; Herman, G. S. *Science* **2002,** 297, (5578), 65-65.

31. Wang, H. L.; Upmanyu, M.; Ciobanu, C. V. *Nano Letters* **2008,** 8, (12), 4305-4311.

32. Dubertret, B.; Skourides, P.; Norris, D. J.; Noireaux, V.; Brivanlou, A. H.; Libchaber, A. *Science* **2002,** 298, (5599), 1759-1762.

33. Perez, J. M.; Josephson, L.; O'Loughlin, T.; Hogemann, D.; Weissleder, R. *Nature Biotechnology* **2002,** 20, (8), 816-820.

34. Li, Y.; Hong, X. M.; Collard, D. M.; El-Sayed, M. A. *Organic Letters* **2000,** 2, (15), 2385-2388.

35. Gerion, D.; Pinaud, F.; Williams, S. C.; Parak, W. J.; Zanchet, D.; Weiss, S.; Alivisatos, A. P. *Journal of Physical Chemistry B* **2001,** 105, (37), 8861-8871.

36. Xie, Y.; Xu, J. J.; Yu, J. S.; Chen, H. Y. *Chinese Journal of Inorganic Chemistry* **2004,** 20, (6), 663-667.

37. Lee, J.; Yang, B. C.; Li, R. F.; Seery, T. A. P.; Papadimitrakopoulos, F. *Journal of Physical Chemistry B* **2007,** 111, (1), 81-87.

38. Dif, A.; Henry, E.; Artzner, F.; Baudy-Floc'h, M.; Schmutz, M.; Dahan, M.; Marchi-Artzner, V. *Journal of the American Chemical Society* **2008,** 130, (26), 8289-8296.

39. Wang, X. Q.; Wu, J. F.; Li, F. Y.; Li, H. B. *Nanotechnology* **2008,** 19, (20).

40. Palaniappan, K.; Xue, C. H.; Arumugam, G.; Hackney, S. A.; Liu, J. *Chemistry of Materials* **2006,** 18, (5), 1275-1280.

41. Breus, V. V.; Heyes, C. D.; Nienhaus, G. U. *Journal of Physical Chemistry C* **2007,** 111, (50), 18589-18594.

42. Wang, M. F.; Felorzabihi, N.; Guerin, G.; Haley, J. C.; Scholes, G. D.; Winnik, M. A. *Macromolecules* **2007,** 40, (17), 6377-6384.

43. Lu, C. H.; Bhattacharjee, B.; Hsu, C. H.; Chen, S. Y.; Ruaan, R. C.; Chang, W. H. *Journal of Electroceramics* **2006,** 17, (1), 21-29.

44. Bruchez, M.; Moronne, M.; Gin, P.; Weiss, S.; Alivisatos, A. P. *Science* **1998,** 281, (5385), 2013-2016.

45. Chan, W. C. W.; Nie, S. M. *Science* **1998,** 281, (5385), 2016-2018.

46. Mattoussi, H.; Mauro, J. M.; Goldman, E. R.; Anderson, G. P.; Sundar, V. C.; Mikulec, F. V.; Bawendi, M. G. *Journal of the American Chemical Society* **2000,** 122, (49), 12142-12150.

47. Wang, Y. A.; Li, J. J.; Chen, H. Y.; Peng, X. G. *Journal of the American Chemical Society* **2002,** 124, (10), 2293-2298.

48. Nann, T. *Chemical Communications* **2005**, (13), 1735-1736.

49. Kim, S. W.; Kim, S.; Tracy, J. B.; Jasanoff, A.; Bawendi, M. G. *Journal of the American Chemical Society* **2005,** 127, (13), 4556-4557.

50. Qian, L.; Bera, D.; Tseng, T. K.; Holloway, P. H. *Applied Physics Letters* **2009,** 94, (7).

51. Wang, F. D.; Tang, R.; Yu, H.; Gibbons, P. C.; Buhro, W. E. *Chemistry of Materials* **2008,** 20, (11), 3656-3662.